長岡技術科学大学
Nagaoka University of Technology

Doctoral Dissertation

Upgrade Recycling Cast Iron Scrap Chips towards Iron-based Thermoelectric Materials

（熱電材料へ向けた鋳鉄切削屑のアップグレードリサイクル）

Assayidatul Laila Binti Nor Hairin

12701187

Academic Advisor

Assoc. Prof. Makoto Nanko

March, 2016

Graduate School of Engineering

Materials Science and Engineering

Nagaoka University of Technology, Japan

Abstract

As fossil energy resources are running out and their environmental concerns are increasing, clean and sustainable energy resources and related technologies are receiving more and more spot lighting. Among the leading technologies to overcome the situations, thermoelectric materials are gaining new attention because their potential to resolve the matters in waste heat recovery systems without any harmful emission. Thermoelectric materials consist of abundant and cheap elements which are required for the widespread use of devices. On the other hand, cast iron is an iron alloy that contains more than 2 mass% carbon, and 1-3 mass% silicon. In order to fabricate their mechanical part made from cast iron scrap chips, machining processes are essentially applied. As a result, the cast iron scrap chips were generated. Recycling of cast iron scrap chips is an interesting subject because it can be utilized as a starting material for preparing iron-based alloys and compounds. Some Fe-based intermetallic compounds such as β-$FeSi_2$ and Fe_2VAl are promising candidates for power generation with good thermoelectric properties, low cost and low toxicity.

In this work, the upgrade recycling of cast iron scrap chips into β-$FeSi_2$ thermoelectric materials was proposed as an eco-friendly and cost-effective production process. The thermoelectric properties of undoped, p- and n-type β-$FeSi_2$, prepared utilizing cast iron scrap chips, have been characterized by measuring the Seebeck coefficient, electrical conductivity and thermal conductivity at temperatures ranging from room temperatures to 800°C. By doping with different substitution concentrations of Co, Mn and Al, the conduction type and properties of β-$FeSi_2$ can be modified and improved using cast iron scrap chips as a starting material. The effects of the doping elements are discussed for preparing β-$FeSi_2$ utilizing cast iron scrap chips. Cast iron scrap chips could be preferable as a starting material to replace pure Fe for n-type and p-type β-$FeSi_2$ thermoelectric materials. The optimum value of *ZT* obtained in the present study is preferable for use as a starting material to produce β-$FeSi_2$ thermoelectric materials and showed promise as an eco-friendly and cost-effective production process for thermoelectric materials. As well as the fabrication of the module of n-type and p-type β-$FeSi_2$ was developed and coefficient thermal expansion was evaluated. In this study, the isothermal oxidation tests were carried out at 800°C in air for 14 d by using an

electric furnace and the oxidation behavior of β-$FeSi_2$ prepared from cast iron scrap chips was reported. Based on the results, β-$FeSi_2$ prepared from cast iron scrap chips has probably a long lifetime at high temperature around 800°C in air and has excellent potential in high temperature stability for high temperature thermoelectric devices even when using cast iron scrap chips as a starting material.

Furthermore, the development of eco-friendly Heusler alloy Fe_2VAl made from cast iron scrap chips is investigated, in which the microstructure and the thermoelectric performance of the product were mainly examined. The power factor value, *PF* value for the undoped Fe_2VAl made from cast iron scrap chips was prevailed approximately twice improved and p-type Fe_2VAl prepared using cast iron scrap chips was about 10% smaller as compared than those previously reported. However, the n-type Fe_2VAl specimen made from cast iron scrap chips could not possible to fabricate due to the small difference in the off-stoichiometry since the compositions of cast iron scrap chips contain some impurities. Based on the XRD results and thermoelectric performance of n-type Fe_2VAl made from pure Fe added with 2, 4, 6 mass% C, the results showed that samples have similar behavior with the 2C.I-V-0.9Al-0.1Si sample. It means the C contains in cast iron scrap chips has influence in conduction type. Hence, it is further necessary to investigate the effect of impurities contains in cast iron scrap chips on the development of n-type Fe_2VAl alloy and further improvements in the thermoelectric performance are desired.

Ultimately, the general guidelines to highly valued intermetallic compounds toward the upgrade recycling of cast iron scrap chips is discussed to achieve better upgrade recycling process. In the future study, the guideline could be applied to fabricate another intermetallic compound made from cast iron scrap chips. From the above statements we can conclude that iron-based thermoelectric β-$FeSi_2$ and Fe_2VAl are successfully fabricated by using cast iron scrap chips. This upgrade recycling material is considerable effort to reducing the abundant waste towards eco-friendly and cost effective production process. Thus, this present study revealed that the cast iron scrap chips can be optimum utilize as a starting material for fabricating iron based materials and prevailed comparable thermoelectric performance to that previously reported.

OUTLINE PAGE

List of Tables

List of Figures

List of Abbreviations

CTE	Coefficient of thermal expansion
E_c	Conduction band
E_g	Energy gap
E_v	Valence band
E_f	Fermi level
EDXS	Energy-dispersive x-ray spectroscopy
EPMA	Electron probe micro-analysis
GDMS	Glow discharge mass spectrometry
k	Thermal conductivity ($Wm^{-1}K^{-1}$)
k_{lat}	Lattice thermal conductivity
k_{el}	Electron thermal conductivity
PECS	Pulsed electric current sintering
PF	Power factor ($\mu Wm^{-1}K^{-2}$)
U_{hot}	Electrical potential at hot region
U_{cold}	Electrical potential at cold region
T_{hot}	Temperature at hot region
T_{cold}	Temperature at cold region
SEM	Scanning electron microscope
XRD	X-ray diffraction
XRF	X-ray fluorescence
XPS	X-ray photoelectron spectroscopy
ZT	Figure of merit
α	Seebeck coefficient ($\mu V/K$)
σ	Electrical conductivity (Sm^{-1})
α^2	Thermopower
ΔT	Temperature different
ΔV	Electrical potential different

Chapter 1: Introduction

1.1 Energy Harvesting Devices

An energy harvesting device generates electric energy from its surroundings using scientific process or referring to Direct Energy Conversion techniques [1]. The energy harvesting devices do not consume any fuel or resources. Thus, steel, glass, or cement manufacturing industries reject large quantities of waste heat at temperature below 400-500°C, which are useful in heat harvesting solutions. Since the majority of energy subject to conversion is lost as heat, it would be advantageous to develop some technique that can harvest the waste heat directly into some other useful forms of energy such as electricity. Thermoelectric materials can harvest a huge amount of fuel energy lost as waste heat in the combustion engines. Besides, thermoelectric materials also can harvest 42% of solar energy in the infrared spectrum lost as heat in photovoltaic conversion. According to the IDTechEx report, the market for the harvesting devices is expected to rise $605 million in 2010 to $4.4 billion by 2020 [2]. The sophisticated of this device has created a huge interest among the industry and academic sectors. Between 2000 and 2010, the number of papers published each year regarding thermoelectric materials research that is used in the thermoelectric devices, and development has increased 2.5 fold [2].

Thermoelectric materials display a significant coupling between the thermal and electrical transfer. This coupling of thermal and electrical energy can be exploited to serve as a solid-state heat pump or heat engine. Unlike conventional heat engines and pumps, the thermoelectric devices require no traditional working fluids, mechanical components, and moving parts. During the operation, the thermoelectric materials produce zero vibrations, noise, or torque; making them an ideal power source for precise scientific equipment. Driven by the need to improve the fuel economy, the automotive industry is investigating the thermoelectric devices for both refrigeration and power generation. Thermoelectric devices in the exhaust system can recover some of the 40% of energy wasted as hot exhaust gas and reduce the direct engine load on the alternator. Also, it will result in less pollution to the air such as reduction of CO_2 emission from the fossil energy resources.

1.2 Thermoelectric Materials

1.2.1 Seebeck Effects

The Seebeck effect is named after the Thomson Johann Seebeck, who first observed this phenomenon in 1821 [3]. Figure 1.1 illustrates the experiment performed by Seebeck. A bimetallic loop of copper and bismuth wires was connected first. When a burner was employed to heat one of the joints, deflections in a magnetic needle placed close to the loop were observed. This phenomenon was first explained, albeit incorrectly as magnetic polarization produced by a temperature difference in metals. After years of experiments and debate, it was concluded that what Seebeck observed was actually due to an electrical current induced by disturbing the equilibrium of temperature [3].

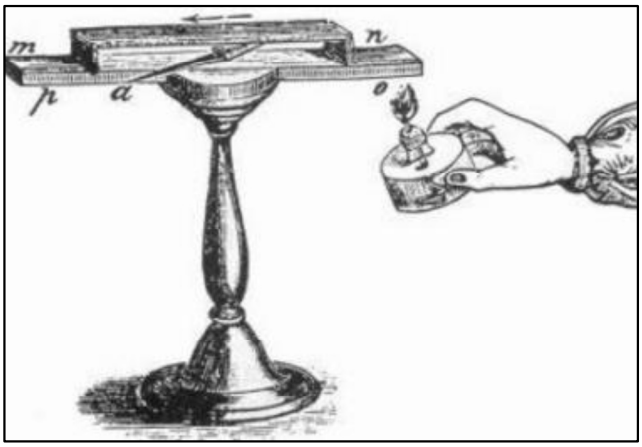

Figure 1.1 Illustration of Seebeck's experiment [3].

Figure 1.2 shows the chemically homogenous conductor subjected to a small thermal gradient in a single crystal. The charge carriers at the hot end of the materials are more energetic and thus, they tend to flow to the cold end. Consequently, the colder region has more charge carriers per volume than the hot end, resulting in the establishment of an internal electrical potential that repels charge carriers arriving from the hot region. At the equilibrium, there will be a stable electrical potential difference $\Delta V = U_{hot} - U_{cold}$ between the two ends along with a temperature difference of $\Delta T = T_{hot} - T_{cold}$ to balance the thermal driving force.

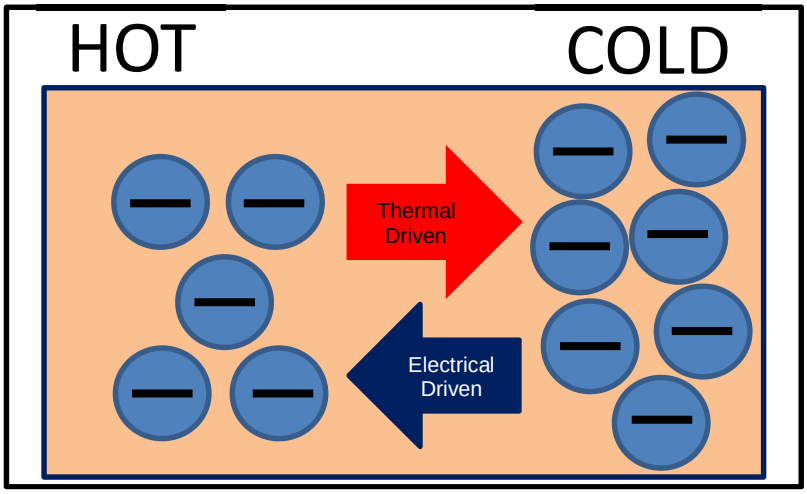

Figure 1.2 (a) A simple microscopic schematic of the Seebeck effect.

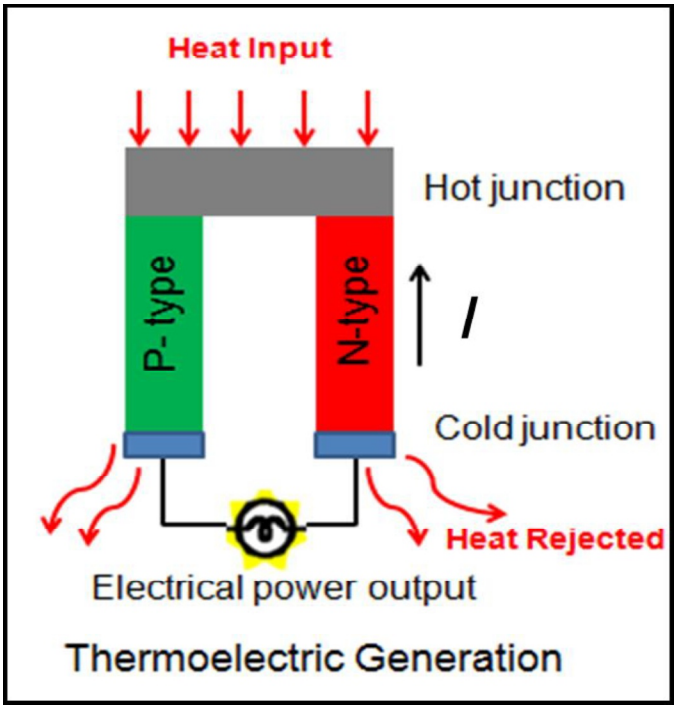

Figure 1.2 (b) Schematic diagram showing a thermoelectric p-n junction comprising each semiconductor type, one p-type and other p-type.

At the same ΔT, the generated electrical potential, ΔV could vary depending on the properties of the materials or average temperature. The Seebeck coefficient $\alpha_x(T)$ is then used to quantify the relationship between $\Delta V \; and \; \Delta T$ in a certain material at a fixed average temperature $T = (T_{hot} + T_{cold}) / 2$.

$$\alpha_x\,(T) = -\lim_{\Delta T \to 0} \frac{\Delta V}{\Delta T} \qquad (1\text{-}1)$$

The negative sign in Eq. 1-1 arises due to the sign convention employed for the Seebeck coefficient. According to this convection, a negative Seebeck coefficient is assigned to n-type materials that have negative charge carrier, such as electrons as their major charge carrier. In reference to Figure 1.2 (a), cold end of the materials at equilibrium has more negative charge carriers and thus, a lower electrical potential than the hot end. Therefore, $\Delta V \; / \; \Delta T$ is positive and a negative sign is needed to fulfill the proposed sign convection.

Themoelectric generators can be operated by placing a temperature gradient across the junction of two dissimilar conductors, for example, two different metals or semiconductors, causing diffusion of charge carriers (electrons or holes) through the conductor from the warmer side to the cooler side resulting in a voltage or electrical current. This is known as Seebeck effect and is illustrated in Figure 1.2 (b), which shows a p-n semiconductor junction.

1.2.2 Semiconductor and Dopants

Modern thermoelectric materials are composed from semiconductors rather than metals, owing to their higher energy conversion efficiency and capacity for doping [4]. Semiconductors can be described as materials that exhibit properties between those of conductors and insulators [5]. In semiconductors and insulators, the valence band, which is almost fully occupied, and the conduction band, the occupancy of which is dependent on the temperature, are separated by a band gap. When electrons are excited across the conduction band, for example, by thermal energy, current can flow in the material, which is the reason for the high dependence

of the conductivity of the semiconductor on temperature. Semiconductors exhibit small to moderate band gaps, for example germanium (0.67 eV) [5] and silicon (1.11 eV) [6], whilst those of insulators such as undoped diamond (5.5 eV) [6], are much larger, resulting in a very high electrical resistivity (up to $10^{18}\Omega$m) [7].

For an intrinsic semiconductor as shown in Figure 1.3 (a), at 0 K, the Fermi level lies at the center of the band gap to represent the probability of finding an electron in the valence band or the conduction band. When the electron is excited, a hole is created, which can be treated as an equally, but oppositely, charged carrier to the electron. These holes migrate towards the p-n junction in the n-type semiconductor or away from the junction in the p-type semiconductor. Extrinsic semiconductors are those, which have been doped in order to change the chemical or electrical properties of the material as demonstrated in Figure 1.3 (b) and (c) [8]. N-type semiconductors have dopants from the VA group, such as P^{+5}. These donor impurity atoms are in substitutional solid solution. The extra valence electron not needed for the sp^3 tetrahedral bonding is only loosely bound to the P atom in a donor energy level, E_d. The energy of this donor energy level is close to the lowest energy level of the conduction band (in Si it is 0.4 eV) and so it is easy to promote an electron from the donor level to the conduction band. These promoted electrons become charge carriers that contribute to the material's conductivity. Since they are negative, the result is called an n-type semiconductor. P-type semiconductors have dopants from the IIIA group such as B^{+3}. These donor impurity atoms in substitutional solid solution. The lack of an electron needed for sp^3 tetrahedral bonding is easily filled by a neighboring Si atom into an acceptor energy level, E_a of the dopant atom. The energy of this acceptor level is only slightly above the valence band and so it is easy to promote an electron from the valence band into it. For each promotion of an electron into one of these acceptor levels, a hole is left in the valence band. It is these holes that become the charge carriers and contribute to the conductivity of the semiconductor. Since these holes are positive, the result is called a p-type semiconductor.

Doping of materials generally can be achieved by introducing specific atoms as substitution impurities into the crystal lattice. This can affect the physical

properties such as the electrical conductivity of the materials, depending on the electronegativity or the number of valence electrons of elements being introduced. Amphoteric doping is where the element being introduced acts as either an electron or donor or refer as acceptor, depending on which lattice site it occupies. Varying the temperature during the doping process can encourage selective occupant of the new atoms. Isoelectric doping involves the substitution lattice atoms with atoms from the same group, for example, nitrogen substituting a phosphorus atom. This method should not change the carrier concentration, but the recombination behavior of the electron-hole pair. This produces a huge difference in the ironic part of the binding in the crystal lattice and therefore, create the local differences. However, the alloying of compound with isoelectric cations and anions is different from the doping semiconductors. For example, when alloying bismuth telluride with antimony telluride or with bismuth selenide could create defects in the crystal structure [9,10]. These may include substitution defects or vacancies and can induce a greater extent of phonon scattering within the crystal structure leading to lower thermal conductivity. Thus, other properties, including the charge carrier concentration and charge carrier mobility can also be affected, leading to the changes in the p- or n-type behavior of materials.

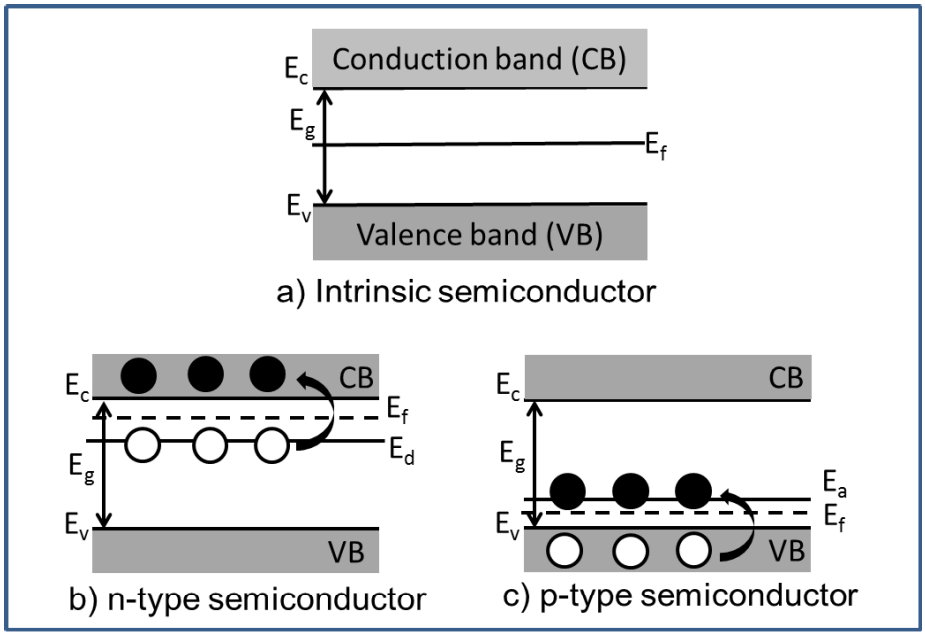

Figure 1.3. The three types of semiconductors; a) Intrinsic semiconductor, b) n-type semiconductor and c) p-type semiconductor [8].

1.2.3 Applications of Thermoelectric Devices

The reason thermoelectric materials are receiving so much renewed attention is due to their extensive applications. Firstly, a thermoelectric device can serve as a power generator using the waste heat energy. Many energy and automobile companies are carrying research to extract energy from these waste heat streams and to enhance its efficiency. Thermoelectric devices also can be served as a solid refrigerator, which includes various cooling applications such as air-conditioners and water cooler. During refrigeration, it also reduces harmful coolant gases such as chlorofluorocarbons (CFCs). Figure 1.4 shows some examples of applications, including a car with thermoelectric generator and radiator, biomedicine applications using the temperature difference between the human body and the ambient air, and solid-state refrigerator. Due to its simplicity and reliability, a large potential market for thermoelectric devices beyond the applications described above is coming around the corner [11].

Figure 1.4 Thermoelectric applications; shows a car with thermoelectric generator and radiator, solid-state refrigerator and biomedicine applications using the human body temperature [11].

1.2.4 Thermoelectric Performance

Recently, thermoelectric materials have gain significant attention due to the potential applications in waste heat recovery systems. In order to utilize the low temperature, small scale, and widely scattered waste heat effectively, thermoelectric generation plays a vital role. This methodology has a conversion efficiency that is independent of the energy scale and is capable of converting thermal energy to electricity. The efficiency of a thermoelectric device is simply defined by the ratio of the voltage difference created across the device against the temperature difference across the device. Thermoelectric material properties are typically evaluated using a dimensionless figure of merit, *ZT*, which can be expressed as:

$$ZT = \alpha^2 \sigma / k\,(T) \qquad (1\text{-}2)$$

where α (VK^{-1}) is defined as the magnitude of an induced thermoelectric voltage in response to the temperature difference applied across the materials [12], σ (Sm^{-1}) is the electrical conductivity, k ($Wm^{-1}K^{-1}$) is the thermal conductivity, and T (K) is the absolute temperature [13-16]. It is evident that a large Seebeck coefficient, α, a high electrical conductivity, σ, and a low thermal conductivity, k, are required to obtain a high dimensionless thermoelectric figure of merit, *ZT*, and it is essential for thermoelectric materials to have high values of *ZT*.

As can be seen, both electronic and phononic contributions are contributed to the conductivity of the material. A phonon is a quantum mechanical description for the vibrational modes of atoms or molecules in solids or liquids. They can contribute to the physical properties of materials such as thermal conductivity and electrical conductivity. $\alpha^2 \sigma$ ($mW\ m^{-1}K^{-2}$) is often referred as the power factor and quoted against the temperature of measurement.

1.3 Iron-based Thermoelectric Materials

1.3.1. β-$FeSi_2$ Thermoelectric Materials

Thermoelectric materials convert temperature differences into electricity and vice versa. In the Seebeck effect, a temperature gradient across a material causes the diffusion of charge carriers across the gradient, thus creating a voltage difference between the hot and cold ends of the materials. A number of materials have been tested for utilization in a thermoelectric generator. Semiconducting β-$FeSi_2$ has been considered as one of the promising thermoelectric materials for energy conversion in the temperature range from 200 to 900°C. The material has low toxicity, low cost, excellent oxidation resistance up to 800°C, and exhibits high electrical conductivity and large thermoelectric power [17-19]. The sintered β-$FeSi_2$ has higher mechanical strength and heat resistance than chalcogenides, and it is chemically stable at high temperature. Therefore, it has a great potential to be used in the high temperature atmosphere without any protection.

Figure 1.5 shows the equilibrium phase diagram of the FeSi-Si system and the crystal structure of β-$FeSi_2$, α-$FeSi_2$, and ε-FeSi. FeSi melts congruently at 1683 K and shows homogeneity region extending from 49.0 to 50.8 at 1400 K. Stoichiometric iron silicides, β-$FeSi_2$ possesses stable semiconductor properties below 1255 K. Above this temperature, however, it transits to the metallic phase [20-23], which is eutectic alloy composed ε-FeSi [24] and α-$FeSi_2$ [25,26]. The high temperature α-$FeSi_2$ phase deviates from the stoichiometric composition, has a tetragonal structure with about 13% Fe vacancies. As shown in the phase diagram of Figure 1.5 (a) [27], the silicon content in the eutectic alloy at the eutectic point corresponds to that of $FeSi_2$, and the semiconducting phase is obtained by annealing the eutectic alloy below 1255 K. The crystal structure of β-$FeSi_2$, α-$FeSi_2$, and ε-FeSi are shown in Figure 1.5 (b). ε-FeSi consist of a cubic structure with 8 atoms in a unit cell [24], α-$FeSi_2$ is a tetragonal structure with 2.87 atoms in a unit cell [25,26], and β-$FeSi_2$ presents an orthorhombic structure with 48 atoms in a unit cell [20].

It is possible to dope β-$FeSi_2$ resulting in both n and p-type semiconductor [16]. The replacement of iron with an element (left hand side of the periodic table) such

as Mn [28-31], Cr [32,33], V [32], Ti, or other elements of this group, produces p-type material whereby n-type material will be produced if iron is replaced with an element (right hand side of the periodic table) such as Co [16,30,33-37], Ni [32,38], or other elements from this group. Substitution of a Group 3 element in silicon produces p-type material. Of a wide range of doping elements investigated, the optimization of the thermoelectric were formed using Co [31,39,40] for n-type doping and Al or Mn [31,41,42] for p-type respectively. Except for Al, these doping elements are substituted in Fe. In the case of Al-doped β-$FeSi_2$, Al is a p-type dopant and is substituted in Si. The conduction mechanism of β-$FeSi_2$ doped with Al or Co was investigated by Birkholtz and Schelm [33] who concluded that p-type and n-type β-$FeSi_2$ were governed by band and polaron conduction respectively. Moreover, it was noted that the thermoelectric power of p-type β-$FeSi_2$ doped with Mn is rather high, and its conductivity is interesting, especially near the semiconductor-to-metal transition temperature [43,44]. Therefore, both thermocouples can be prepared from the same basic materials, thus eliminating problems of different thermal expansion.

In previous studies, the starting materials used to fabricate β-$FeSi_2$ were typically pure Fe with 99.99% purity and Si with 99.9% purity [45-47]. The arc-melting method based on ingot metallurgy [40,44], mechanical alloying [47], sintering [40,42], and the combinations of them are the conventional processes to fabricate β-$FeSi_2$.

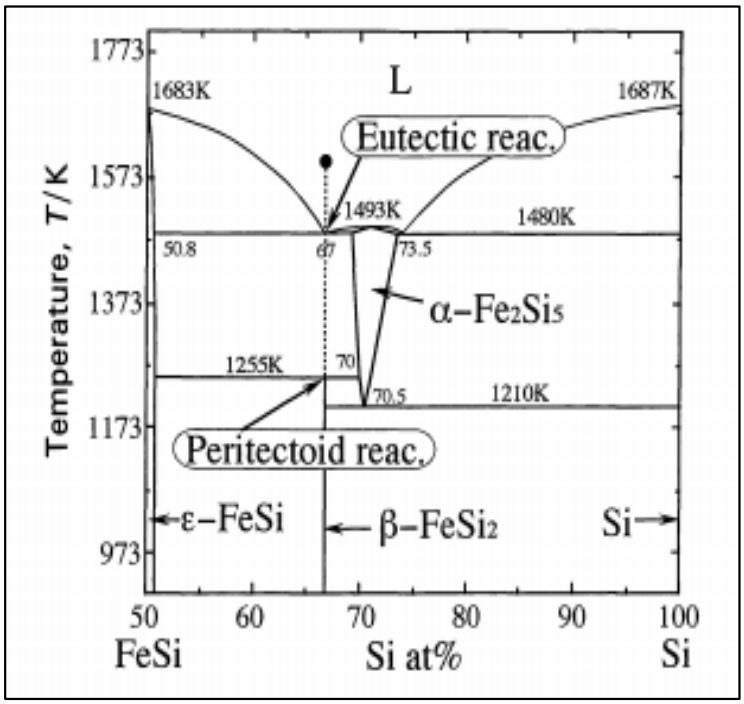

(a) Equilibrium phase diagram of the FeSi-Si system [27]

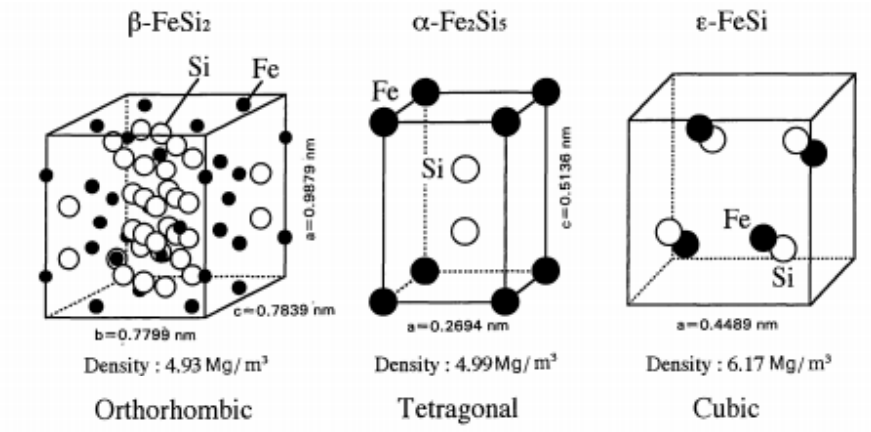

(b) Crystal structure of β-$FeSi_2$, α-$FeSi_2$ and ε-FeSi [20,24-26]

Figure 1.5. a) Equilibrium phase diagram of the FeSi-Si system and b) crystal structure of β-$FeSi_2$, α-$FeSi_2$ and ε-FeSi.

1.3.2. Fe_2VAl Thermoelectric Materials

Intermetallic compounds based on the Fe_3Al system have shown the greatest interest, because they show high temperature strength, excellent oxidation, and corrosion resistance. These compounds have the Heusler type structure, which was discovered by Heusler [48]. The Heusler type structure is described as $(T_{1-x}\,M_x)_3X$, whereby T and M are generally transition metals [49-56], and many compounds have this type of structure. The most spectacular feature of the resistance anomaly has been found for $(Fe_{1-x}\,V_x)_3Al$ [57], as well as for $(Fe_{1-x}\,V_x)_3Si$ [58] and $(Fe_{1-x}\,V_x)_3Ga$ [59]. Among them, the $(Fe_{1-x}\,V_x)_3Al$ system has been remained a greater interest because a single phase $D0_3$ structure remains stable over a wide V composition range [60-62]. Figure 1.6 (a) shows the crystal structure of $(Fe_{1-x}\,V_x)_3Al$ [63]. It has three kinds of site Fe_I, Fe_{II}, and Al. The Fe_I site has eight nearest Fe_{II} neighbors in an octahedral configuration, as the Al site does. $(Fe_{1-x}\,V_x)_3Al$ is able to exist between X=0 and X=1 and the crystal structure changes from $L2_1$ to $D0_3$ [64-66], with increasing vanadium concentration. Figure 1.6 (b) shows the equilibrium phase diagram of the Fe-Al system ($D0_3$) [67].

Especially, during the change from Fe_3Al to Fe_2VAl, only the Fe_I site is replaced by vanadium [64][66]. Figure 1.6 (c) shows the partial Al-Fe-V isothermal section at 500°C [68,69]. As compared to the other substituents such as Ti, Cr, and Mn, the vanadium shows an optimum property since a narrow pseudogap in the density of states is the characteristics of the Fe_2VAl compound, as shown in Figure 1.6 (d) [70-72]. The Fermi level is located in this narrow pseudogap and the electric resistivity shows semi-conductive behavior. Because the electron density near this Fermi level change sharply, the Seebeck coefficient becomes larger [73]. The reason for this selective replacement of vanadium is also well discussed in the literature [74]. As compared to the density of state for $L2_1$ type, Fe_2TiAl phase was calculated in the Figure 1.6 (d) [70,71], which is a little different than Fe_2VAl. The Fermi level is located at a lower energy than the pseudogap. Therefore, it is required to introduce more valence electrons in Fe_2TiAl in order to shift the Fermi level to higher state of energy.

In particular, the Heusler-type intermetallic compound Fe_2VAl has received intense attention because of the occurrence of a semiconductor-like temperature

dependence of electrical resistivity over a wide temperature range up to 1200 K and above [61]. So far, the band structure calculations have [75,76] consistently predicted the presence of a deep pseudogap at the Fermi level due to the hybridization effects, which has been clearly manifested by optical conductivity [77] and photoemission spectroscopy [78] measurements. Because of the possessions of a sharp pseudogap across the Fermi level, Fe_2VAl based alloys have attracted a great deal of interest as a potential candidate in the thermoelectric materials [79,80]. In metallic systems, the Seebeck coefficient, α at a temperature T is often discussed using the well-known formula [81]. Since the density of states (DOS) of Fe_2VAl sharply changes in both valence and conduction band sides of the pseudogap, the Seebeck coefficient enhances significantly when the Fermi level is shifted due to doping. For the n-type material, the doping was carried out into one of the iron, vanadium, and aluminum sites [82,83]. For the p-type materials, the doping was carried into the iron or vanadium site [84,85].

From the practical point of view, because of its high mechanical strength and excellent resistance to oxidation and corrosion, a durable thermo-electric module can be fabricated using the alloy Fe_2VAl [86]. Moreover, the Heusler alloy is comprised predominantly from the abundant elements such as Fe and Al and contains no toxic elements. The high durability and abundance of this material could be advantageous, which can be implemented as a thermoelectric generator system. Fe_2VAl has thermoelectric power generation near the room temperature because of its high power factor compared to the conventional thermoelectric materials, such as Bi-Te and Pb-Te [87]. Fe_2VAl is a semimetal with a narrow pseudogap at the Fermi level [88,89]. Thus, small stoichiometric deviations could cause large changes in the transport properties [90]. The methods for controlling the pseudogap in Fe_2VAl have been reported by several researchers, such as change its composition from stoichiometric to nonstoichiometric [91-92] and substitution of the fourth element [93,94]. These proposed methods increase the absolute values of the Seebeck coefficient and reduce the electrical resistivity of Fe_2Val. However, the thermal conductivity is comparatively large. As a result, the small ZT will be obtained. It is essential to decrease the thermal conductivity to obtain the high performance of Fe_2VAl. Furthermore, in a Fe_2VAl system, the enhancement of the PF value and the control of conduction type can be

realized simultaneously by the partial element substitution, such as Si in the Al site for n-type and Ti in V site for p-type [95]. The arc-melting methods based on ingot metallurgy [90-93], mechanical alloying [96-98], and the combination of them [94] are the conventional processes to fabricate bulk Fe_2VAl.

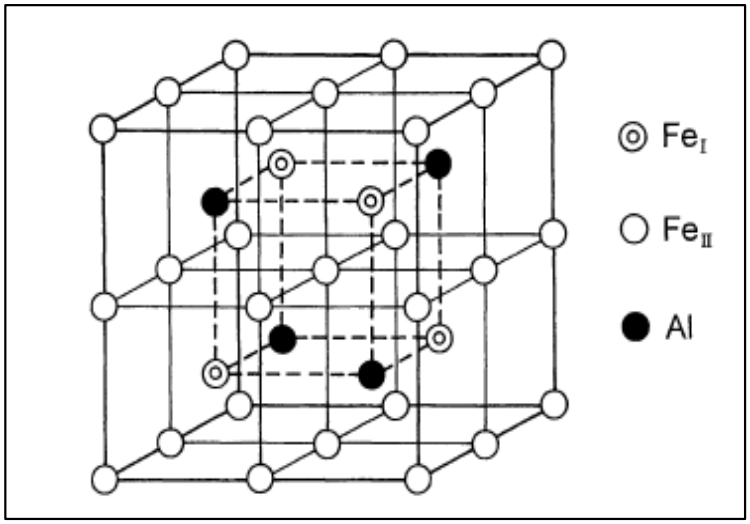

(a) Crystal structure of Heusler type compound [63]

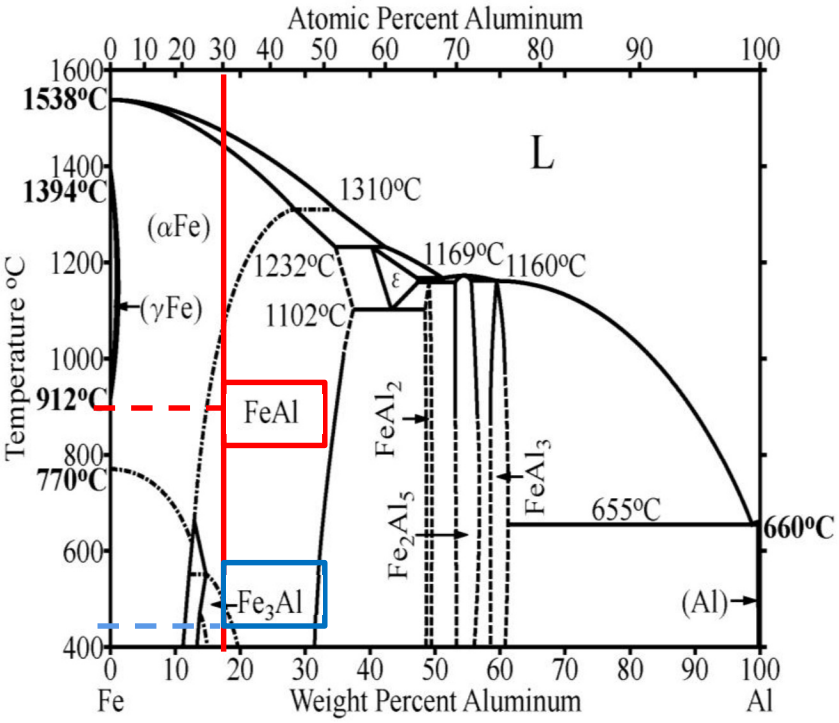

(b) Equilibrium phase diagram of the Fe-Al system [67]

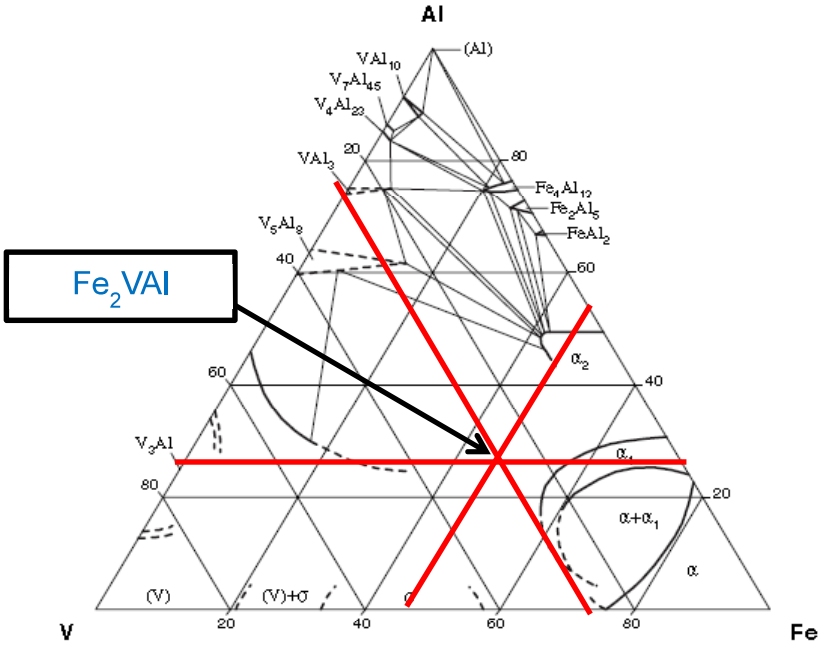

(c) Ternary system of Fe_2VAl [68,69]

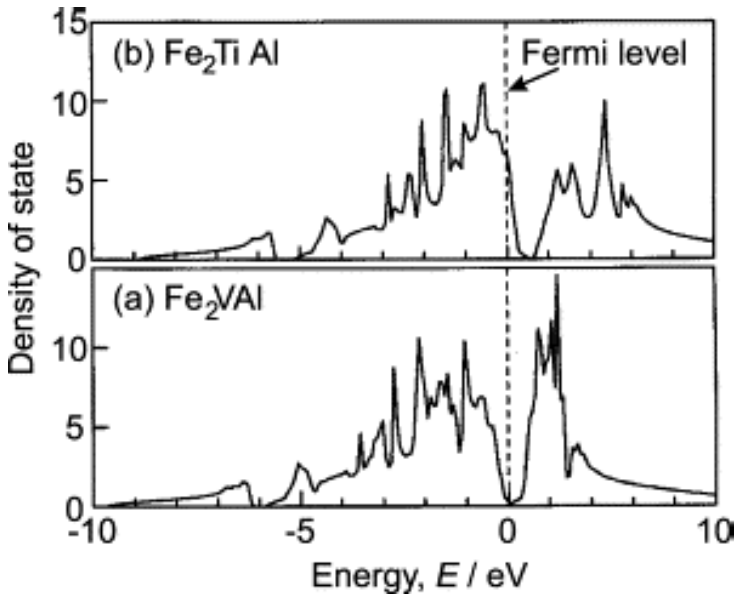

(d) Total density of state (DOS) for Fe2VAl: the Fermi level at 0 eV [70,71]

Figure 1.6 a) Crystal structure of Heusler type compound, b) Equilibrium phase diagram of the Fe-Al system, c) Ternary system of Fe_2VAl and d) Total density of state (DOS) for Fe_2VAl.

1.4 Properties and Applications of Cast Iron

Alloys of Fe with carbon, silicon and other elements after going through solidification and crystallization graphite precipitates from the melt, are called cast irons. The foundry alloys are the basic structural materials, and they form 75% of the world of production of castings. Depending on the shape of graphite precipitated from the melt during the crystallization, there are three basic kinds of cast iron (marked with an abbreviation in accordance with the European standard [99,100]; cast iron with lamellar graphite, cast irons with vermicular graphite and cast irons with spheroidal graphite).

The term of cast iron refers to those iron-carbon-silicon alloys which contain 2.5 – 4 mass% carbon and usually 1-3 mass% silicon. Cast iron is an important engineering material with a number of advantages, mainly good castability and machinability and moderate mechanical properties. Because of its economical advantages, cast iron is used for many applications in the automotive and engineering industry as shown in Figure 1.7 [101]. In addition, specific cast irons are the material of choice for sea water pump housings, rolling mill rolls, and parts for earth moving equipment. As the morphology of graphite has a major influence on the mechanical properties of cast iron, metallographies quality control of gray iron is an integral part of its production process. Using standard reference comparison charts, image analysis techniques, or combination of both, the morphology, size and distribution of the graphite can be determined on an unetched, polished sample. Depending on the specification, the sample is then etched to check the structure of the matrix. Scrap chips of cast-iron were produced from the cutting and milling processes of cast-iron products, which consist of primarily iron with 2.1–4 mass% of carbon and 1–3 mass% of silicon. Thus, cast-iron scrap chips may become a suitable starting material for preparing the iron-based material.

(a)

(b)

Figure 1.7 Applications of cast iron; a) Cast iron pan and b) Crankshaft ductile iron [101].

1.5 Scope of The Thesis

Based on the mentioned above, the main objective of this thesis is the upgrade recycling of cast iron scrap chips toward iron based thermoelectric materials as an eco-friendly and cost-effective production process. Due to the large quantities of waste heat rejected from manufacturing industries, thermoelectric materials can harvest a huge amount of fuel energy lost as waste heat directly into electricity. On the other hand, scrap chips of cast-iron were produced from the machining processes of cast-iron products, which consist primarily of iron with carbon and silicon may be a suitable starting material for preparing iron-based thermoelectric materials. In chapter 2, the physical characterization and chemical analysis of cast iron scrap chips as a starting material for fabrication of iron based alloys were discussed. Chapter 3 shows the upgrade recycling cast iron scrap chips toward β-$FeSi_2$ thermoelectric materials. The thermoelectric properties of undoped, p- and n-type β-$FeSi_2$, prepared utilizing cast iron scrap chips were characterized by measuring the Seebeck coefficient, electrical

conductivity, and thermal conductivity at temperature ranging from room temperature to 800°C. By doping with different substitution concentrations of Co, Mn, and Al, the conduction type and properties of β-$FeSi_2$ can be modified and improved using the cast iron scrap chips as a starting material. The effects of the doping elements for preparing β-$FeSi_2$ utilizing cast iron scrap chips were discussed. Besides, the fabrication of the module of n-type and p-type β-$FeSi_2$ was developed and the respective coefficient thermal expansion was evaluated. Furthermore, the isothermal oxidation tests were carried out at 800°C in the air for 14 days by using an electric furnace. The oxidation behavior of β-$FeSi_2$ prepared from cast iron scrap chips was reported. In chapter 4, the development of eco-friendly Fe_2Val thermoelectric materials prepared using cast iron scrap chips was discussed, in which the microstructure and the thermoelectric performance of the product were examined. Finally, chapter 5 discussed the general guidelines to valued the intermetallic compounds toward upgrade recycling of cast iron scrap chips. In all the chapters, characterizations of the samples were carried out and discussed using different techniques such as x-ray diffraction, x-ray photoelectron spectroscopy, scanning electron microscopy, standard 4 probes method, and laser flash method. Finally, general conclusions are made in chapter 6, which represents the main contribution of this thesis. Fig. 1.8 shows the schematic illustration of the content of the thesis as mentioned above.

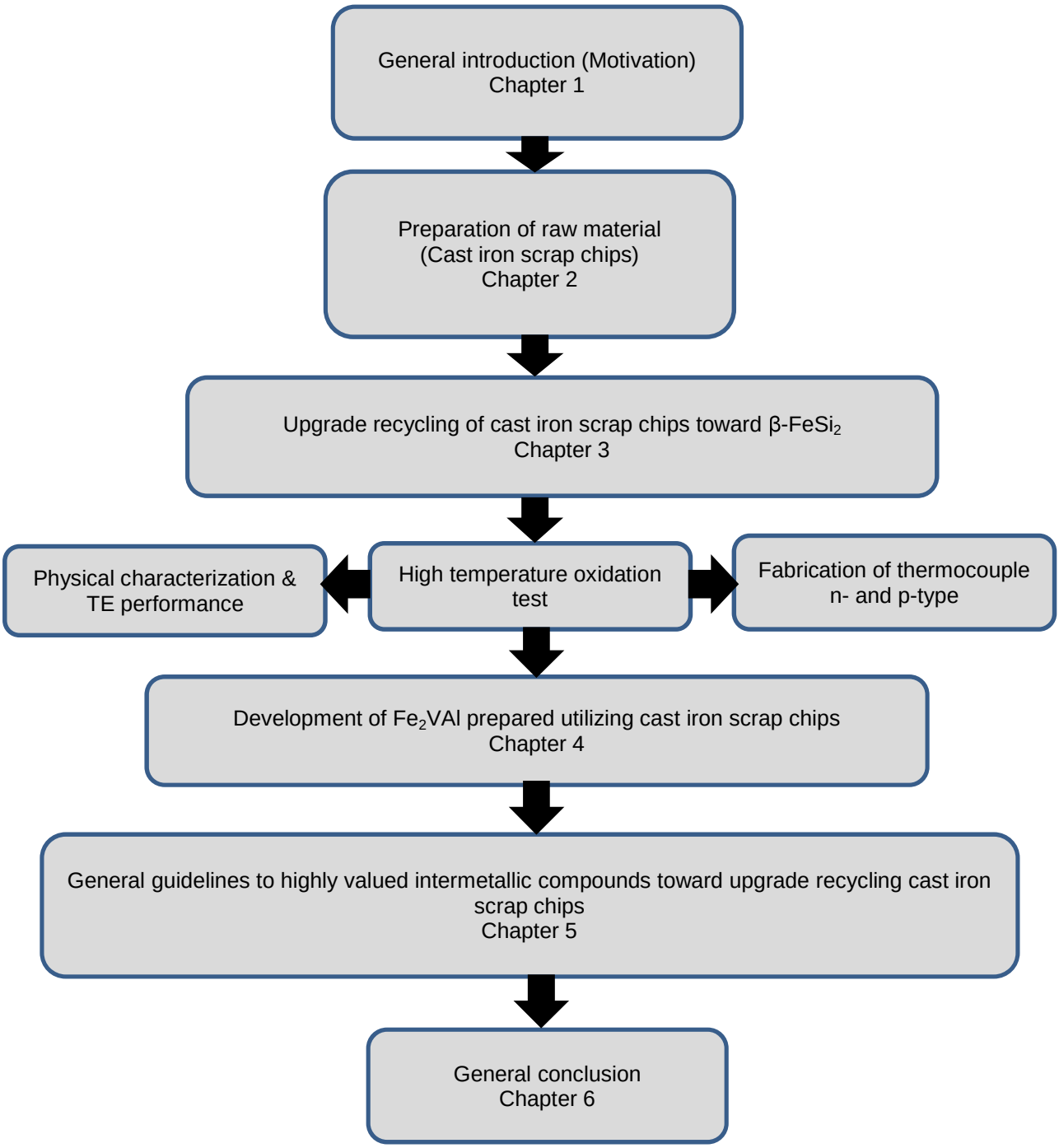

Figure 1.8 Schematic illustration of the structure of this thesis.

1.6 References

1. Billinghurst, M., & Starner, T. (1999). Wearable devices new ways to manage information. *IEEE Computer, 32*, 57–64.
2. *IDTechEx. Energy Harvesting and Storage for Electronic Devices 2010-2020*. (2010). Retrieved 11, November, 2015, from http://www.idtechex.com/research/reports/energy_harvesting_and_storage_for_electronic_devices_2010_2020_000243.asp.
3. Seebeck, T.J. (1823). Magnetische polarisation der metalle und erze durck temperatur-differenz. *Abh. K. Akad. Wiss*., 265.
4. Xiao, F., Handgarter, C., Yoo, B., Rheem, Y., Lee, K., & Myung, N. (2008). Recent progress in electrodeposition of thermoelectric thin films and nanostructures. *Electrochimica Acta., 53* (28), 8103–8117.
5. Kittel, C. (1976). *Introduction to Solid State Physics*. London: Wiley.
6. Streetman, B., G., & Banerjee, S., K. (2010). *Solid State Electronic Devices*. Pearson/Prentice Hall.
7. Pierson, H. O. (1993). *Handbook of Carbon, Graphite, Diamond, and Fullerenes: Properties, Processing, and Applications.* Noyes Publications.
8. Nave, C., R. (2008). HyperPhysics: Band Theory for Solids. 2012. URL http:// hyperphysics.phy-astr.gsu.edu/hbase/solids/band.html#c1. Accessed 2013- 08-21Snyder G J and Toberer E S, Complex thermoelectric materials. *Nature Materials., 7 (2)*, 105–14.
9. Wright, D. A. (1958). Thermoelectric properties of bismuth telluride and its alloys. *Nature.,181* (4612), 834–834.
10. Tritt, T. M., Boettner, H., & Chen, L. (2008). Thermoelectrics: Direct solar thermal energy conversion. *Mrs Bulletin, 33* (4), 366-368.
11. Jeffrey, S. G. (2008). *The Electrochemical Society Interface*, 54-56.
12. Dialvo, F. J. (1999). Thermoelectric cooling and power generation. *Science., 285* (5428), 703–706.
13. Rowe, D. M. (1995). *CRC Handbook of Thermoelectrics*. Boca Raton: CRC Press.
14. Rowe, D. M., & Bhandari, C. M. (1983). *Modern Thermoelectrics*. London: Holt, Rinehart and Winston Limited.
15. Rowe, D. M. (2006). *Thermoelectrics Handbook: Macro to Nano.* CRC Press.

16. Ware, R. M., & McNeil, D. J. (1964). Iron disilicide as a thermoelectric generator material*. Proc. Inst. Electr. Eng., 111*, 178–182.
17. Zao, X. B., Zhu, T. J., Hu, S. H., Zhou, B. C., & Wu, Z. T. (2000). Transport properties of rapid solidified Fe-Si-Mn-Cu thermoelectric alloys. *J. Alloy. Comp., 306*, 303–306.
18. Nishida, I., (1973). Study of semiconductor to metal transition in Mn doped $FeSi_2$. *Phys. Rev., B7*, 2710.
19. Ito, M., Nagai, H., Katsuyama, S., & Majima, K. (2001). Effects of Ti, Nb and Zr doping on thermoelectric performance of β-$FeSi_2$. *J. Alloy. Compd., 315*, 251–258.
20. Dusausoy, P. Y., Protas, J,, Wandji, R., & Roques, B. (1971). *Acta Cryst., B27*, 1209.
21. Bucksch, R. (1967). *Naturf, 22a*, 2124.
22. Wandji, R. C. R. (1968). *Acad. Sci., C267,* 1587.
23. Wandji, R. C. R. (1968). *Acad. Sci, C269*, 907.
24. Pauling, L., & Soldate, A. M. (1948). *Acta Cryst., 1*, 212.
25. Sidorenko, F. A., Geld, P. V., & Dubrovskaya, L. B. (1959). *Fiz. Metal Metalloved, 8*, 735.
26. Samsonove, G. V. (1955). *Refractory Transition Metal Compounds (pp.*178). New York/ London: Academic Press.
27. Kubaschewski, O. (1982). *Iron-Binary Phase Diagram* (pp. 136). New York: Springer-Verlag.
28. Tani, J., & Kido, H. (1999). *J. Appl. Phys., 86*, 464.
29. Nishida, I., (1973). *Phys. Rev., B7*, 2710.
30. Kojima, T., Okamoto, M., & Nishida, I. (1984). *Proc. 5th Int. Conf.Thermoelectric Energy Conversion, ed. By Rao K R, Arlington*, 56.
31. Umemoto, M.(1995). *Mater. Trans., 36*, 373.
32. Kombayashi, M., Hijikita, K., & Ido, S. (1991). *Jpn. J. Appl. Phys., Part 1, 30,* 331.
33. Birkholz, U., & Schelm, J. (1968). Mechanism of electrical conduction in β-$FeSi_2$. *Phys. Status Solidi, B27*, 413–425.
34. Hesse, J., & Bucksh, R. (1970). *J. Mater. Sci., 5*, 272.

35. Wandji, R., Le, Corre, C., Genin, J. M., & Roques, B. (1971). *Phys. Status Solidi, B45,* K123.
36. Kojima, T., Masumoto, M., Okamoto, M. A., & Nishida, I. (1990). *J. Less-Common Met., 159,* 299.
37. Waldecker, G., Meinhold, H., & Birkholz, U. (1973). *Phys. Status Solidi, A 15*, 143.
38. Nagai, H., Maeda, I., Katsuyama, S., & Majima, K. (1994). *J. Japan Society of Powder and Powder Metallurgy, 41*, 560.
39. Tokiai, T., & Usegi, T. (1995). Improvement in thermoelectric characteristics of n-type iron disilicide by local composition modification. *J. Ceram. Soc., 78*, 1089–1092.
40. Nanko, M., Chang, S., Matsumaru, K., Ishizaki, K., & Takeda, M. (2006). Isothermal oxidation of sintered β-$FeSi_2$ in air. *Mat. Sci. Forum, 522*, 641–648.
41. Ohta, Y., Miura, S., & Mishima, Y. (1999). Thermoelectric semiconductor iron disilicides produced by sintering elemental powder. *Intermetallic, 7*, 1203–1210.
42. Tani, J. I., & Kido, H. (1999). Electrical properties of Cr-doped β-$FeSi_2$. *J. Appl. Phys., 38,* 2717.
43. Birkholtz, U., & Schelm, J. (1969). *Phys. Stat. Sol., K177*, 34.
44. Kojima, T. (1989). *Phys. Stat. Sol., 111*, 233.
45. Kato, H., Kato, M., Nishino, Y., Mizutani, U., & Asano, S. (2001). *J. Jpn. Inst. Metals, 65,* 652-656.
46. Tani, J. I., & Kido, H. (1999). Mechanism of electrical conduction of Mn-doped $FeSi_2$. *J. Appl. Phys., 86*, 464.
47. Ur, S. C. (2003). *Twenty Second Int. Conf. on Thermoelectric IEE*, 149.
48. Heusler, Fr. (1903). *Verhandlungen der Deutschen Physikalischen Gesellschaft 5*, 219.
49. Ishikawa, K., Kainuma, R., Ohnuma, I., Aoki, K., Ishida, K. (2002). *Acta Materialia, 50*, 2233–2243.
50. Soda, K., Mizutani, T., Yoshimoto, O., Yagi, S., Mizutani, U., Sumi, H., Nishino, Y., Yamada, Y., Yokoya, T., Shin, S., Sekiyama, A., Suga, S. (2002). *J. Synchrotron Radiation, 9,* 233–236.
51. Suga, S., Imada, S., Yamasaki. A., Ueda, S., Muro, T., Saitho, Y. (2001). *J. Mag. Mater., 233,* 60–64.

52. Mitamura, H., Takeshita, N., Uwatoko, Y., Mori, H., Yamaguchi, A., Tomita, T., Wada, H., Mori, N., Ishimoto, H., Goto, T. (2000). *Physica, B 284–288*, 1341–1342.
53. Mitamura, H., Takeshita, N., Uwatoko, Y., Mori, H., Yamaguchi, A., Tomita, T., Wada, H., Mori, N., Ishimoto, H., Goto, T. (2000). *Physica, B 281/282*, 150–151.
54. Dordevii, S. V., Basov, D. N., Slebarski, A., Maple, M. B., Degiorgi, L. (2002). *Phys. Rev., B 66*, 75122–75125.
55. Fraga, G. L. F., Pureur, P., Brandao, D. E. (2002). *Solid State Commun., 124,* 7–10.
56. Dong, J. W., Lu, J., Xie, J. Q., Chen, L. C., James, R. D., Mckernan, S., Palmstrom, C. J. (2001). *Physica, E 10*, 428–432.
57. Nishino, Y., Kumada, C., & Asano, S. (1997). *Science. Mater., 36*, 461.
58. Nishino, Y., Inoue, S., Asano, S., & Kawamiya, N. (1993). *Phys. Rev., B 48* (13), 13607.
59. Kawamiya, N., Nishino, Y., Matsuo, M., & Asano, S. (1991). *Phys. Rev., B 44* (12), 406.
60. Popiel, E., Tuszynski, M., Zarek, W., & Rendecki, T. (1989). *J. Less-Common Met., 146,*127.
61. Nishino, Y., Kato, M., Asano, S., Soda, K., Hayasaki, M., Mizutani, U. (1997). *Phys. Rev. Lett., 79* (10), 1909–1912.
62. Nishino, Y. (2000). *Intermetallics, 8*,1233.
63. Kawaharada, Y., Kurosaki, K., & Yamanaka, S. (2003). *J. Alloy Comp., 352*, 48.
64. Okpalugo, D. E., Booth, J. G., & Faunce, C. A. (1985). *J. Phys., F 15*, 681–692.
65. Webster, P. J., & Ziebeck, K. R. A. (1983). *Phys. Lett., A 98*, 51.
66. Nishino, Y., Kumada, C., & Asano, S. (1997). *Script. Mater., 36*, 461.
67. Kubaschewski, O. (1982). *Iron-Binary Phase Diagram* (pp. 6). Berlin: Springer Science and Business Media, LLC .
68. Sokolovskaya, E. M., Badalova, L. M., & Kazakova, E. F. (1987). Phase composition of rapidly quenched alloys of the system Al-Fe-V. *Izv. Akad. Nauk SSSR. Met., 5*, 212.
69. Sokolovskaya, E. M., Badalova, L. M., Kazakova, E. F., & Stroeva, N. V. (1988). Interactions of Intermetallic Compounds in the ternary system aluminum-iron-vanadium (in Russian). *Vestn. Mosk. Univ., Ser. 2: Khim 29*, 303.

70. Botton, G. A., Nishino, Y., & Humphreys, C. J. (2000). *Intermetallics, 8*, 1209–1214.
71. Guo, G. Y., Botton, G. A., & Nishino, Y. (1998). *J. Phys. Condens. Matter., 10,* L119–L126.
72. Bansil, A., Kaprzyk, S., Mijnarends, P. E., & Toboła, J. (1999). *Phys. Rev., B60,* 13396–13412.
73. Hanada, Y., Suzuki, R. O., & Ono, K. (2001). *J. Alloy Comp., 329*, 63–68.
74. Ishida, S., Ishida, J., Asano S., & Yamashita, J. (1976). *J. Phys. Soc. Jpn., 41,* 1570.
75. Singh, D. J.,& Mazin, I. I., (1998). *Phys. Rev., B57*, 14352.
76. Weht, R., & Pickett, W. E., (1998). *Phys. Rev., B58*, 6855.
77. Feng, Y., Rhee, J. Y., Wiener, T. A., Lynch, D. W., Hubbard, B. E., Sievers, A. J., Schlagel, D. L., Lograsso, T. A., & Miller, L. L. (2001). *Phys. Rev., B63*, 165109.
78. Soda, K., Murayama, H., Shimba, K., Yagi, S., Yuhara, J., Takeuchu, T., Mizutani, U., Sumi, H., Kato, M., Kato, H., Nishino, Y., Sekiyama, A., Suga, S., Matsushita, T.,& Saito, Y.(2005). *Phys. Rev., B 71*, 245112.
79. Nishino, Y. (2005). *The Science of Complex Alloy Phases* (T. B. Massalski and P. E. Turchi, Ed.). Warrendale: TMS.
80. Nishino, Y. (2011). IOP Conf. Ser. *Mater. Sci. Eng., 18*, 142001.
81. Mott, N. F., & Jones, H. (1936). *The Theory of the Properties of Metals*. Oxford: Clarendon Press.
82. Lu, W., Zhang, W., & Chen, L. (2009). *J. Alloys Compd., 484*, 812.
83. Mikami, M., Kinemuchi, Y., Ozaki, K., Terazawa, Y., & Takeuchi, T. (2012). *J. Appl. Phys., 111*, 093710.
84. Matsuura, H., Nishino, Y., Mizutani, U., & Asano, S. (2002). *J. Jpn. Inst. Met., 66*, 767.
85. Kobayashi, F., Ide, N., & Nishino, Y. (2007). *J. Jpn. Inst. Met., 71*, 208.
86. Nishino, Y. (2001). *Mater. Trans., 42*, 902-910.
87. Nishino, Y., Deguchi, S., & Mizutani U. (2006). *Phys. Rev., B74*, 115115.
88. Weht, R., & Pickett, W. E. (1998*). Phys. Rev., B58*, 6855–6861.
89. Nishino, Y., Kato, H., Kato, M., & Mizutani, U. (2001). *Phys. Rev., B63*, 1-4.
90. Hanada, Y., Suzuki, R. O., & Ono, K. (2001). *J. Alloy Comp., 329*, 63–68.
91. Lue, C. S., & Kuo, K. (2002). *Phys. Rev., B66*, 085121/1-5.

92. Kato, H., Kato, M., Nishino, Y., Mizutani, U., & Asano, S. (2001). *J. Jpn. Inst. Metal., 65*, 652–656.
93. Lu, W., Zhang, W., & Chen, L. (2009). *J. Alloy Comp., 484*, 812–815.
94. Nakayama, H., Ide, N., & Nishino, Y. (2008). *Mater. Trans., 49*, 1858–1862.
95. Nishino, Y., Inoue, S., Asano, S., & Kawamiya, N. (1993). *Phys. Rev., B48*, 13607.
96. Mikami, M., Matsumoto, A., & Kobayashi, K. (2008). *J. Alloy Comp., 461*, 423–426.
97. Mikami, M., & Kobayashi, K. (2008). *J. Alloy Comp., (2008) 466*, 530–534.
98. Mikami, M., Tanaka, S.,& Kobayashi, K. (2009). *J. Alloy Comp., 484*, 444–448.
99. Macnaughtan, M. (2006). Cast Iron Materials Standards for a new Millenium. *Proceedings of the 67th World Foundry Congress ICME 2006, Harrogate*, 146/1-146/10.
100. Elbel, T., Senberger, J., Zadera, A., & Hampl, J. (2008). Behaviour of oxygen in cast irons. *International Scientific Journal, 33*, 111–116.
101. Kazumichi, S., Yaer, X., Masahito, T., & Hideki S. (2009). Mechanical Properties of Spheroidal Graphite Cast Iron Made by Reduced Pressure Frozen Mold Casting Process. *Materials. Transactions.*, 50 (5), 1128-1134.

Chapter 2: Characterization of cast iron scrap chips

2.1. Introduction

Cast-iron is one of the most popular metallic materials used for mechanical components in pipes, machines and automotive parts, such as cylinder heads (declining usage) and block gearbox cases (declining usage) [1-2]. It has become an engineering material with a wide range of applications. Scrap chips of cast-iron were produced from the cutting and milling processes of cast-iron products, which consist primarily of iron with 2.1–4 mass% of carbon and 1–3 mass% of silicon. Thus, cast-iron scrap chips may be a suitable starting material for preparing iron-based materials.

The starting materials used to fabricate β-$FeSi_2$ were typically pure Fe with 99.99% purity and Si with 99.9% purity [3]. The process of recycling cast-iron scrap chips for β-$FeSi_2$, which is an eco-friendly and cost-effective production process, is known as “upgrade recycling”. This is the process of producing high value materials from scraps of low value materials [4,5]. The material cost is reduced when β-$FeSi_2$ is fabricated from the waste of the manufacturing process of cast-iron components. It is evident from the equation (1-1) that a large Seebeck coefficient, α, a high electrical conductivity, σ, and a low thermal conductivity, k, are required to obtain a high dimensionless thermoelectric figure of merit, ZT [6]. In this chapter, the cast iron scrap chips (C.I.) is synthesized and discussed in terms of cleaning process of the cast iron scrap chips and optimum numerical chemical composition of Si in the cast iron chips.

2.2 Experimental Procedure

The cast iron scrap chips were prepared by drilling operation of cast iron block in our laboratory. Figure 2.1 shows the image of cast iron scrap chips after drilling operation process. After collecting the cast iron scrap chips in a beaker, it was cleaned using ethanol in an ultrasonic bath over 4 cycles of 20 min and then dried in a fume chamber (Yamato Scientific Co. Ltd, Japan). The specimens were then characterized using X-ray fluorescence (XRF) (Rigaku, Japan) and energy dispersion X-ray spectroscopy (EDXS) (EDAX INC., USA) for elemental and chemical analysis.

Furthermore, for reconfirmation of chemical analysis, the concentration of impurities in the cast iron scrap chips was analyzed using glow discharge mass spectrometry (GDMS). For GDMS synthesis, the evaluation of the cast iron scrap chip powders was performed by consolidation using a pulsed electric current sintering (PECS) technique.

Figure 2.1 Images of cast iron scrap chips generated by the drilling process.

In order to make sure the capability of cast iron scrap chips as a starting material, β-$FeSi_2$ was prepared with this scrap chips. The starting materials for the undoped β-$FeSi_2$; C.I.-Si1.86 and C.I.-Si2 samples were prepared using the solid-state reaction technique with cast iron scrap chips (the prefix "C.I." stands for "cast iron scrap chips"), along with silicon grains (purity: 99.99%). The chemical composition of the material was cast iron: Si= C.I.: (1.86<Si<2.00). The powder mixture was prepared using rotary dry ball milling for 1 d. The powder mixture was placed directly in a die and consolidated using the PECS technique at 950°C for 10 min in a vacuum at a uni-axial pressure of 80 MPa. The sintered specimens were annealed at 900°C for 6 d in a vacuum. The constituent phase and microstructure of the specimens was observed using a scanning electron microscope (SEM) and energy dispersion X-ray spectroscopy (EDXS) for elemental and chemical analyses.

2.3. Results

2.3.1. Physical characterization and chemical analysis

Figure 2.2 presents the XRD patterns of the cast iron scrap chips and cast iron bulk. These results identified the predominant peak of α-Fe and indicated the graphite peak in both samples. Figure 2.3 (a) presents the SEM images that reveal the lamellar graphite structure distributed over the α-Fe structure of the cast iron bulk sample. As shown in Figure 2.3, the particle size of cast iron scrap chips was approximately 100-150 µm. The XRF and GDSM analysis of the cast iron bulk in Table 2.1 indicated that the sample consisted primarily of iron with 6.0 mass% of carbon, 2.1 mass% of silicon and minor elements, such as magnesium, manganese, phosphorus and sulfur.

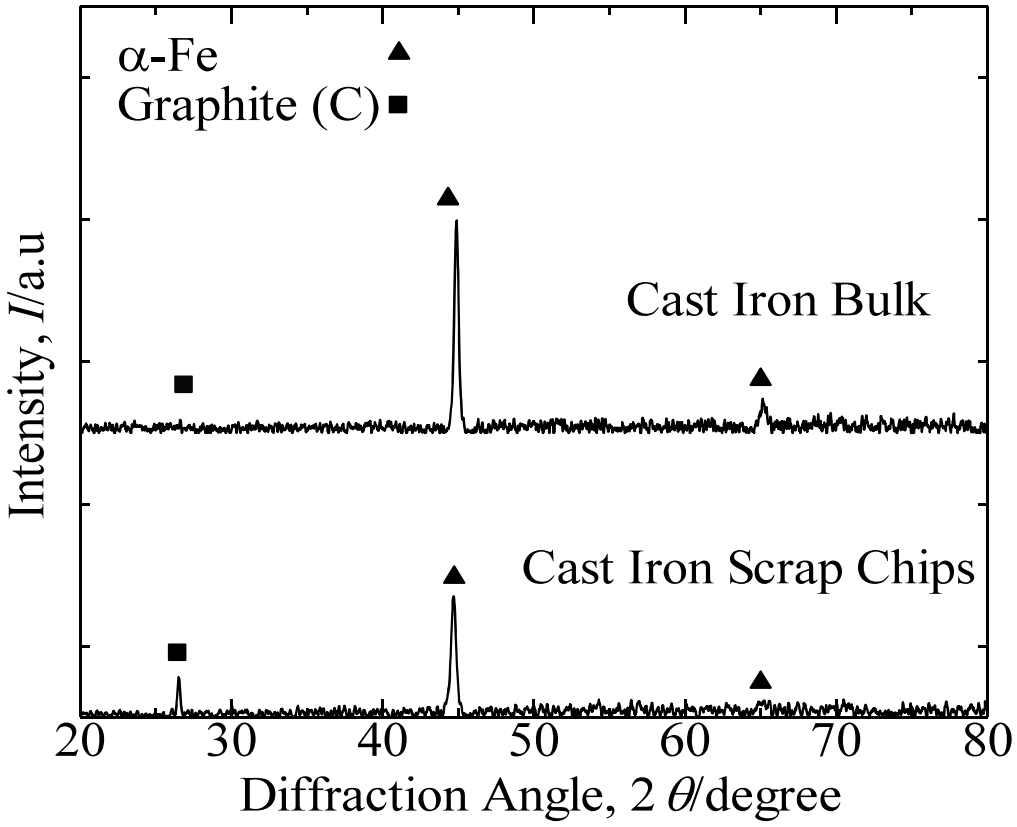

Figure 2.2 XRD patterns of cast iron scrap chips and cast iron bulk.

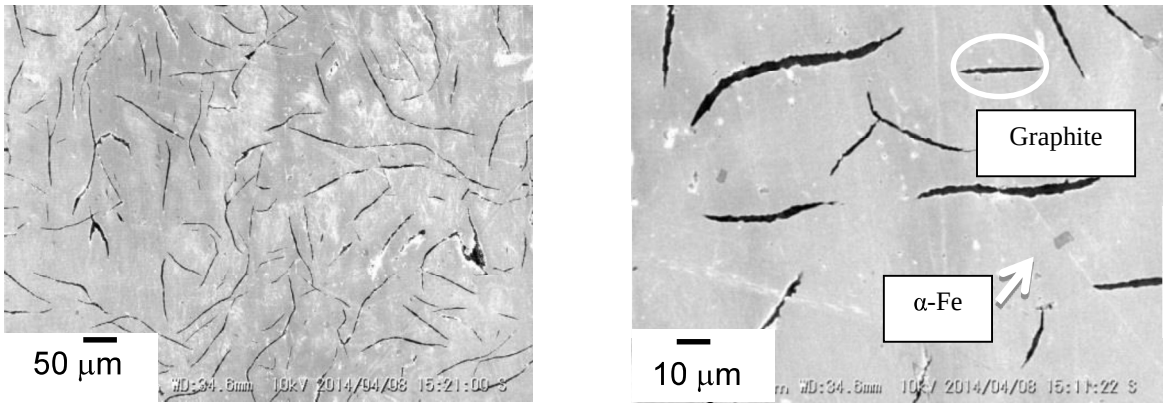

Figure 2.3 (a) Cross-sectional SEM views of cast iron bulk.

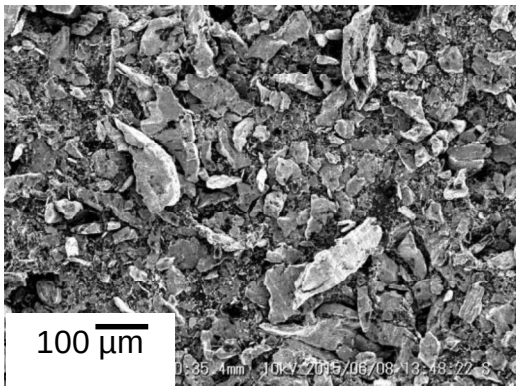

Figure 2.3 (b) SEM photo of cast iron scrap chips powder.

Table 2.1 XRF composition of elements in cast iron bulk and GDMS composition of elements in cast iron scrap chips.

Element	XRF (mass %)	GDSM (mass %)
Silicon (Si)	2.1	2.2
Carbon (C)	6.0	2.0
Oxygen (O)	1.3	0.5
Manganese (Mn)	0.3	0.3
Minor elements: Mg, S, P	<0.1	<0.1
Iron (Fe)	Balance	Balance

Figure 2.4 provides the SEM microstructures of the annealed C.I.-Si1.86 and C.I.-Si2 samples at 900 °C for 6 d. By comparing the SEM microstructure of the C.I.-1.86Si sample, the excess Si obtained is approximately 20% less compared to that of the C.I.-Si2 sample. The open porosity observed in both samples was below 1% after sintering, and thus, these were considered as dense samples.

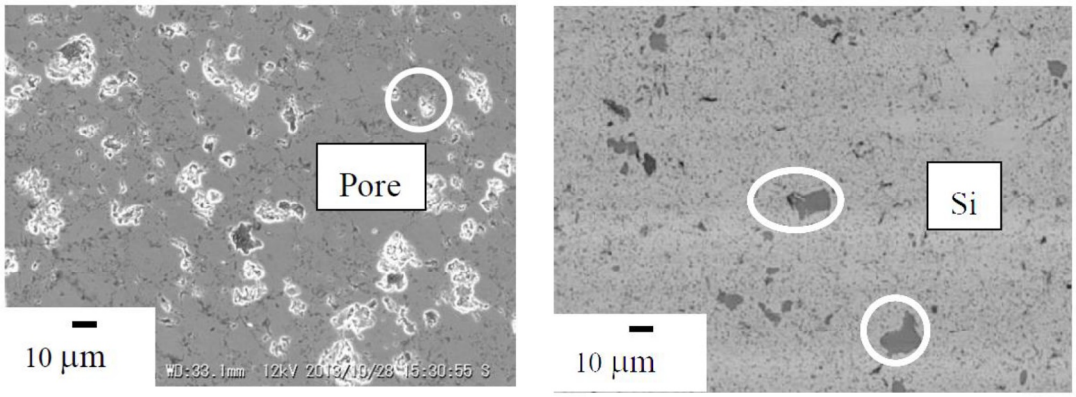

(a) C.I.-Si1.86 (C.I.-1.86Si) (b) C.I.-Si2 (C.I.-2Si)

Figure 2.4 SEM microstructures of annealed C.I.-1.86Si and C.I.-2Si samples at 900°C for 5 days.

Figure 2.5 shows the SEM image and the corresponding EDX elemental mapping of annealed C.I.-Si1.86 sample. As can be seen from the mapping images of EDX, the dominant elements were silicon and iron. Taking into account the XRD results, this sample composed of β-$FeSi_2$ and had remained minor elements such as Mn and C.

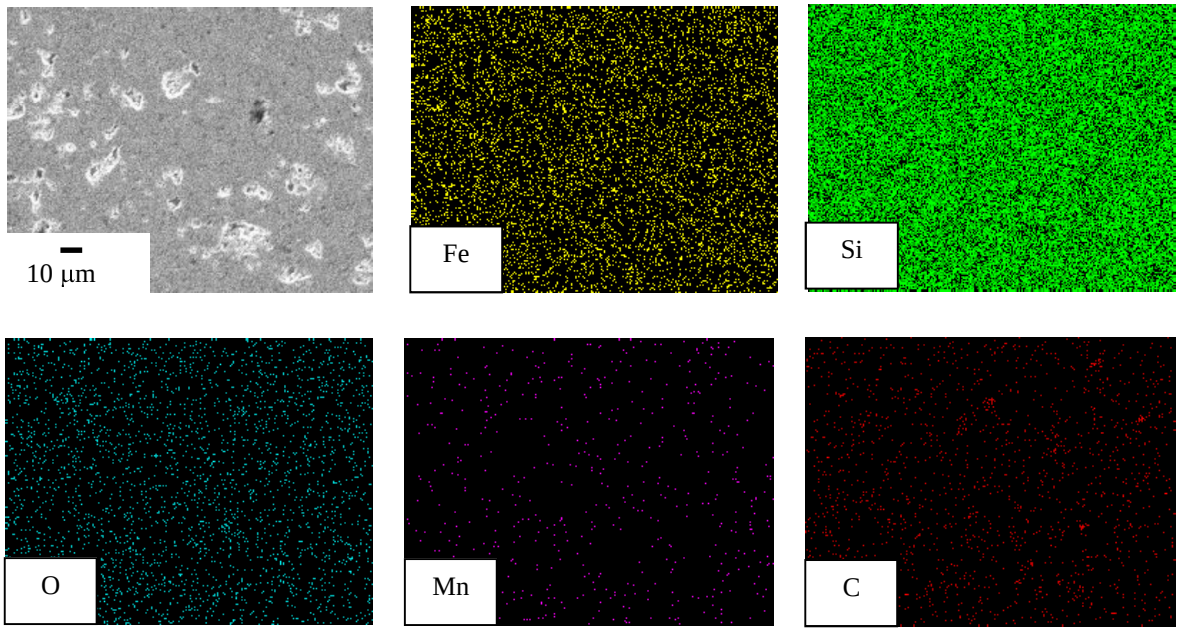

Figure 2.5 SEM image and EDX result of the C.I.-Si1.86 (C.I.-1.86Si).

2.4 Discussion

The concentration of carbon and oxygen between XRF and GDMS analysis is different due to the different samples were used. For GDMS analysis, the sintered sample of cast iron scrap chips was prepared. However, for the XRF, the scrap chips of cast iron without any treatment was used. Therefore, during the sintering process, it might be obtained, some chemical reaction between the cast iron and the graphite (diffuse as Co_2). Another possibility is the different features between XRF and GDMS, for example the XRF analyzers determine the chemistry of a sample by measuring the fluorescent x-ray emitted from a sample when it is excited by a primary x-ray source (same principle with EDXS). On the other hand, in the GDMS, the sample to be analyzed forms the cathode in a gas discharge or plasma. The ions are then extracted into a mass spectrometer where they are separated according to their mass to charge ratio, and thus identified and measured. Thus, GDMS provides trace-level quantitative surveys of bulk sample and thick films compare than XRF because it has higher detection limits and limit sensitivities with some element combinations.

By considering the XRF and GDSM analysis of the cast iron bulk, the specimen already contained 2.1-2.2 mass% of silicon. The C.I.-Si2 (C.I.-2Si) sample consists

primarily of β-$FeSi_2$ with a slight excess of remaining Si (large black dots). The black dot was determined using electron probe micro-analyzer (EPMA) analysis to be free silicon after sintering. To optimize the numerical chemical composition of Si in the cast iron scrap chips samples, the ratio of powder mixture was reduced from C.I.:Si = 1:2 to C.I.:Si = 1:1.86 for lesser free silicon after sintering. It is necessary to control the composition ratio of C.I.:Si at approximately 1:1.86 to avoid the formation of ε-FeSi in the future. It was reported that the presence of ε-FeSi could arise from a deficiency of Si due to the oxidation during the powder preparation and/or the evaporation during sintering [7]. Additionally, the influence of excess Si in the β-$FeSi_2$ specimen prepared from cast iron scrap chips may lead to high thermal conductivity, because the microstructural properties of the materials also have an influence on the materials' thermoelectric properties. By reducing the numerical chemical composition of excess Si in the powder mixture of the C.I.-Si1.86 sample made from cast iron scrap chips, the thermoelectric performance was significantly enhanced for the C.I.-Si2 sample compared to that of the sample prepared from pure Fe as discussed deeply in chapter 3.

2.5 Conclusion

The scrap chips of cast iron used in the present study was characterized. The optimum numerical chemical composition of Si in the cast iron scrap chips samples, the ratio of powder mixture was reduced from C.I.:Si = 1:2 to C.I.:Si = 1:1.86 for β-$FeSi_2$ lesser free silicon. By reducing the numerical chemical composition of excess Si in the powder mixture of the C.I.-Si1.86 sample made from cast iron scrap chips, the thermoelectric performance was significantly enhanced for the C.I.-Si2 sample compared to that of the sample prepared from pure Fe as discussed deeply in chapter 3. The cast iron scrap chips could be preferable for use as a starting material to fabricate iron-based alloys (β-$FeSi_2$ and Fe_2VAl) toward eco-friendly and cost effective production process.

2.6 References

1. Elbel, T., Senberger, J., Zadera, A., & Hampl. J. (2008). Behaviour of oxygen in cast irons. *International Scientific Journal, 33*, 111–116.
2. Elisabeth, W., & Ann, Guesanier. (2003). Metallographic preparation of cast iron. Retrieved from URL:http://www.struers.com/resources/elements/12/129414/Application_Note_Cast_Iron_English.pdf. Accessed 2015-11-30.
3. Nanko, M., Chang, S., Matsumaru, K., Ishizaki, K., & Takeda, M. (2006). Isothermal oxidation of sintered β-$FeSi_2$ in air. *Mat. Sci. Forum, 522*, 641.
4. Laila, A., & Nanko, M. (2015). Characterization of Cast-Iron Scraps toward β-$FeSi_2$ Thermoelectric Materials. *Materials Science Forum, 804,* 3-6.
5. Laila, A., Nanko, M., & Takeda, M. (2014). Upgrade recycling of cast iron scrap chips towards β-$FeSi_2$ thermoelectric materials. *Materials, 7*, 6304–6316.
6. Hesse, J., & Buckson, K. (1972). *J. Mater. Sci., 5*, 272.
7. Cho, W. S., Choi, S. W., & Park, K. W. S. (1999). Microstructure and thermoelectric properties of p-type Fe0.9Mn0.1Si2 compounds prepared by pressure less sintering. *Mater. Sci. Eng., B68*, 116.

Chapter 3: Upgrade Recycling of Cast Iron Scrap Chips towards β-$FeSi_2$ Thermoelectric Materials

3.1. Introduction

Iron-based alloys often contain more than 2 mass% carbon, 1-3 mass% silicon and other elements. During the course of solidification and crystallization, graphite precipitates from the melt, which is known as “cast iron”. Ferritic alloys are used in machinery, oil and gas equipment for water piping, packer parts, boilers, valve bodies and valve parts. During mechanical processing, cast iron scrap chips are generated. The recycling of cast iron scrap chips is an interesting subject to explore because these chips can be used as a starting material when preparing an iron based material.

Thermoelectric materials have recently attracted renewed interest for potential applications in waste heat recovery systems. To effectively utilize the low temperatures, small scale and widely scattered waste heat, thermoelectric generation provides a solution. This methodology has a conversion efficiency that is independent of the energy scale and is capable of converting thermal energy to electricity. Thermoelectric material properties are typically evaluated using a dimensionless figure of merit, *ZT*, which is expressed as:

$$ZT = \alpha^2 \sigma / k\,(T) \qquad (1\text{-}2)$$

where α is the Seebeck coefficient, σ is the electrical conductivity, and k is the thermal conductivity. It is evident that a large Seebeck coefficient, α, a high electrical conductivity, σ, and a low thermal conductivity, k, are required to obtain a high dimensionless thermoelectric figure of merit, *ZT*, and it is essential for thermoelectric materials to have high values of *ZT*.

Semiconducting β-$FeSi_2$ is considered an attractive thermoelectric material because of its high Seebeck coefficient and because it is eco-friendly (the material is

composed of two naturally abundant non toxic elements, iron and silicon) [1-4]. In addition, β-$FeSi_2$ has an excellent oxidation resistance at high temperatures such as800°C [5,6]. Sintered β-$FeSi_2$ has a high mechanical strength, heat resistance and is chemically stable at high temperatures [7]. Therefore, this material has proven to be very useful in thermoelectric generators operating in high temperature conditions without any protection. High temperature oxidation on β-$FeSi_2$ was discussed on oxidation process in semiconductor devices [8]. In order to discuss the lifetime of thermoelectric devices at high temperatures, long-term oxidation should be examined. The previous authors reported amorphous SiO_2 was developed as an oxide scale at temperature ranging from 800 to 950°C in air [9]. Growth rate of oxide layer on doped β-$FeSi_2$ followed a parabolic law and its rates were similar to oxidation of undoped samples. In addition, they concluded that sintered β-$FeSi_2$ showed excellent oxidation resistance in high temperature thermoelectric materials. They also reported that there was no significant change in thermoelectric properties after high temperature oxidation on β-$FeSi_2$ sintered bodies [10].

Because cast iron consists mainly of iron with carbon and silicon, scrap chips of cast iron are expected to be a good starting material for preparing β-$FeSi_2$. We have already proposed the upgrade recycling of cast iron scrap chips to produce β-$FeSi_2$ thermoelectric material. It is well known that extrinsic thermoelectric β-$FeSi_2$ can be prepared by doping Mn or Al to produce p-type material and Co to produce n-type material. However, there are some limitations on the dopant effects in β-$FeSi_2$ prepared utilizing cast iron scrap chips. Thus, in the present study, the thermoelectric performance and the physical characterizations of β-$FeSi_2$ synthesized from cast iron scrap chips using various doping elements (Co, Al and Mn) were evaluated. The purpose of this report is to reveal that the cast iron scrap chips are effective as a starting material for fabricating β-$FeSi_2$ and determining if the optimum thermoelectric performance is comparable to what has been previously reported. In this chapter, oxidation behavior of undoped, n-type and p-type β-$FeSi_2$ prepared from cast iron scrap chips is reported. As well, the thermoelectric properties of oxidized β-$FeSi_2$ prepared using cast iron scrap chips are also described briefly. Furthermore, the fabrication of

thermocouple n-type and p-type β-$FeSi_2$ prepared using cast iron scrap chips is obtained and the evaluation of the coefficient thermal expansion is evaluated.

3.2 Experimental Procedure

The starting materials for the p-type and n-type β-$FeSi_2$ were prepared using the solid-state reaction technique with cast iron scrap chips (the prefix "C.I." stands for "cast iron scrap chips" and the prefix "P" stands for "pure Fe", which denotes the alloys formed from pure Fe), along with silicon grains (purity: 99.99%) and Co powder (purity: 99%) for n-type material and Al powder (purity: 99%) and Mn powder (purity: 99%) for p-type material. The chemical composition of the n-type material was cast iron: Co: Si=(1-Co): (0.02<Co<0.08): 1.86 for n-type. For the p-type material, the chemical composition was cast iron: Al: Si=1: (0.09<Al<0.12): (1.86-Al) and cast iron: Mn: Si=(1-Mn): (0.06<Mn<0.1): 1.86. For the n-type β-$FeSi_2$ prepared from C.I. scrap chips and pure Fe, the Co and Mn dopants are substituted in the Fe sites. For the Al-dopant, β-$FeSi_2$ is prepared from C.I. scrap chips and Al is the p-type dopant, which is substituted for the Si sites [9]. The powder mixture was prepared using rotary dry ball milling for 1 d. The powder mixture was placed directly in a die and consolidated using the PECS technique at 950°C for 10 min in a vacuum at a uni-axial pressure of 80 MPa. The sintered specimens were annealed at 900°C for 6 d in a vacuum. The constituent phase and microstructure of the specimens was observed using a scanning electron microscope (SEM) and energy dispersion X-ray spectroscopy (EDXS) for elemental and chemical analyses. The X-ray diffraction (XRD) analysis of the specimens was performed with an X-ray diffractometer.

The thermoelectric properties were determined by measuring the Seebeck coefficient, α, electrical conductivity, σ, and thermal conductivity, k. The Seebeck coefficient and electrical conductivity were measured using a DC standard four probe method and a steady-state temperature gradient (ZEM-2, Ulvac Co.) from room temperature to 800°C in a stream of He gas. The thermal conductivity was calculated from the measured heat capacity and the thermal diffusivity using the laser flash method with a thermal constant analyzer (LFA 457 Micro Flash) over a temperature range from room temperature to 800°C in a vacuum. Isothermal oxidation tests were

carried out at 800°C in air by using an electric furnace. After oxidation tests, phase identification by using X-ray diffraction (XRD) and scanning electron microscopy (SEM) with energy dispersion X-ray spectroscopy (EDXS) were performed. In case of cross-sectional observation of oxidized β-$FeSi_2$, Ni-plating was carried out to protect sample surface from machining damages by cutting and grinding. The Seebeck coefficient and electrical conductivity of sintered β-$FeSi_2$ were measured by standard four-probe method and steady-state temperature gradient method (ZEM-2, Ulvac Co.) from room temperature to 800°C in a stream of He gas. The thermal conductivity was calculated from the measured heat capacity and the thermal diffusivity using the laser flash method with a thermal constant analyzer (LFA 457 Micro Flash) over a temperature range from room temperature to 800°C in a vacuum.

3.3. Results

3.3.1. Physical characteristics of undoped, p- and n-type β-$FeSi_2$ prepared utilizing cast iron scrap chips

Figure 3.1 shows XRD patterns of the annealed β-$FeSi_2$ undoped, Co-doped and Al-doped from pure Fe and cast iron scrap chips. Dominant peaks in these samples were identified as β-$FeSi_2$ for all samples. Small amount of ε-FeSi phase is also detected in all samples. XRD patterns proved that after annealing 900^{o}C for 5 d, the simple transition of peritectiod reaction, α+ε → β for all samples which have been almost completely transformed to the β phase. It was also confirmed that the isothermal annealing near the high temperature transformation temperature led to the distinct formation of ε-FeSi.

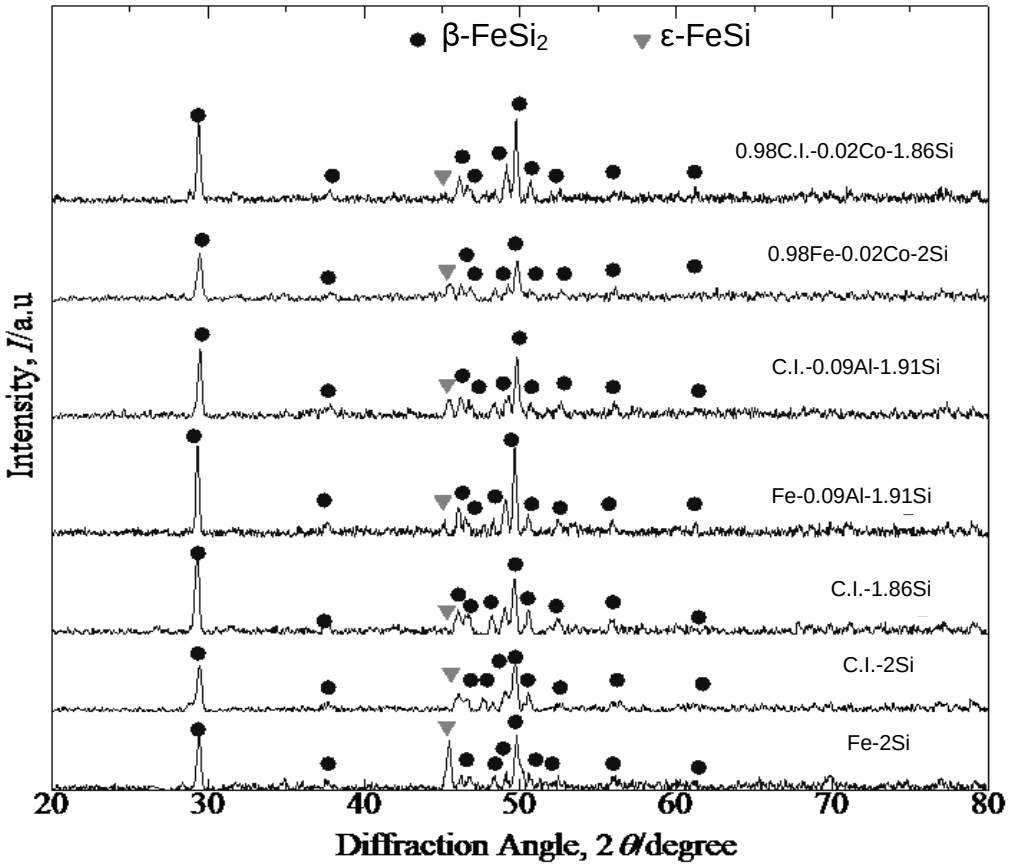

Figure 3.1 XRD patterns of the annealed β-$FeSi_2$ samples at 900^{o}C for 6 d.

Figure 3.2 shows the SEM microstructure for annealed β-$FeSi_2$ of undoped, Co-doped and Al-doped β-$FeSi_2$ from pure Fe and cast iron scrap chips. As can be seen in SEM image (e) C.I.-Co0.02 were observed Si-rich phase (black dot) with small pores (white dot). Table 2 shows the porosity data of sintered β-$FeSi_2$ from pure Fe and cast iron scrap chips. The open porosity observed for all samples were below 1% after sintered and thus considered as dense samples. For n-type β-$FeSi_2$ from C.I. scrap chips and pure Fe, the Co dopant is definitely substituted for Fe atom. In the case of the Al-dopant β-$FeSi_2$ from C.I. scrap chips and pure Fe, the Al is a p-type dopant and is substituted for Si atom.

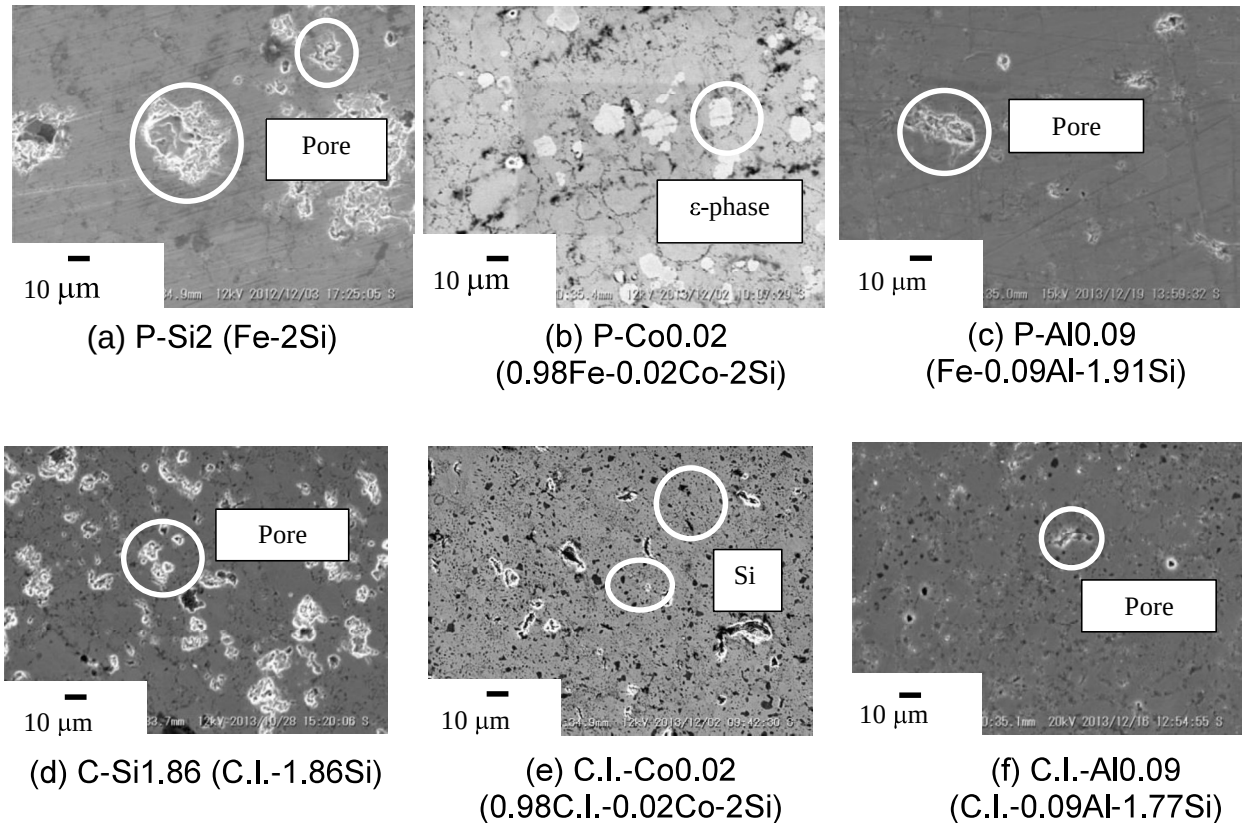

Figure 3.2 SEM microstructures of the annealed β-$FeSi_2$ samples at 900°C for 6 d.

Table 3.1 Porosity data of the sintered β-$FeSi_2$ samples.

Sample Name (Numerical Chemical Composition)	Archimedes Measurement	
	Density	Open porosity
P-Si2 (Fe-2Si)	4.7 g/cm^3	0.3%
C.I.-Si2 (C.I.-2Si)	4.4 g/cm^3	0.2%
C.I.-Si1.86 (C.I.-1.86Si)	4.7 g/cm^3	0.4%
P-Co0.02 (0.98Fe-0.02Co-2Si)	4.7 g/cm^3	0.2%
C.I.-Co0.02 (0.98C.I.-0.02Co-2Si)	4.3 g/cm^3	0.3%
P-Al0.09 (Fe-0.09Al-1.91Si)	4.4 g/cm^3	0.5%
C.I.-Al0.09 (C.I.-0.09Al-1.77Si)	4.5 g/cm^3	0.3%

3.3.2 Thermoelectric performance of undoped, p- and n-type β-$FeSi_2$ prepared utilizing cast iron scrap chips

Figure 3.3 plots the temperature dependence of Seebeck coefficient, *α*, of the annealed β-$FeSi_2$ samples evaluated at temperature ranging from room temperature to 800°C. In this present work, for the undoped sample, C.I.-Si1.86 sample shows significantly higher Seebeck coefficient than the C.I.-Si2 sample ones. For the doped specimens, it could be seen that the different value signs of Seebeck coefficient exhibited for Al doped and Co doped β-$FeSi_2$. The positive values of Al doped samples correspond to the p-type behavior indicating that the electrical conductivity is mainly due to holes, while n-type behavior is attributed to Co doped samples from their negative values of Seebeck coefficient indicating electron conduction. The absolute value of the Seebeck coefficient increases with increasing measuring temperature to a maximum and then it decreases with a further increase of the temperature [11]. The Seebeck coefficients of Co-doped and Al-doped β-$FeSi_2$ prepared from cast iron scrap chips were obtained 90% to almost 100% performance compared to the samples prepared from pure Fe and other reported studies [12,13]. Furthermore, the temperature trend transition and the maximal absolute values for C.I.-Al0.09 and C.I.-Co0.02 samples are 400^{o}C and 354 μVK^{-1} and 500^{o}C and -221 μVK^{-1}. The preceding increase of α could be attributed to a more acute scattering of carries with the increase in temperature, and the subsequent decrease of Seebeck coefficient could be due to a rapid increase in carrier concentration with the increase in temperature [13]. The Seebeck coefficient of Al-doping β-$FeSi_2$ prepared from cast iron scrap chips obtained large value than Al-doping β-$FeSi_2$ made from pure Fe. In the Co-doping ones, the difference was much smaller. This is because the Al-doping in C.I. scrap chips sample maybe sensitive in impurity compared with Co-doping and may lead to low carrier concentration.

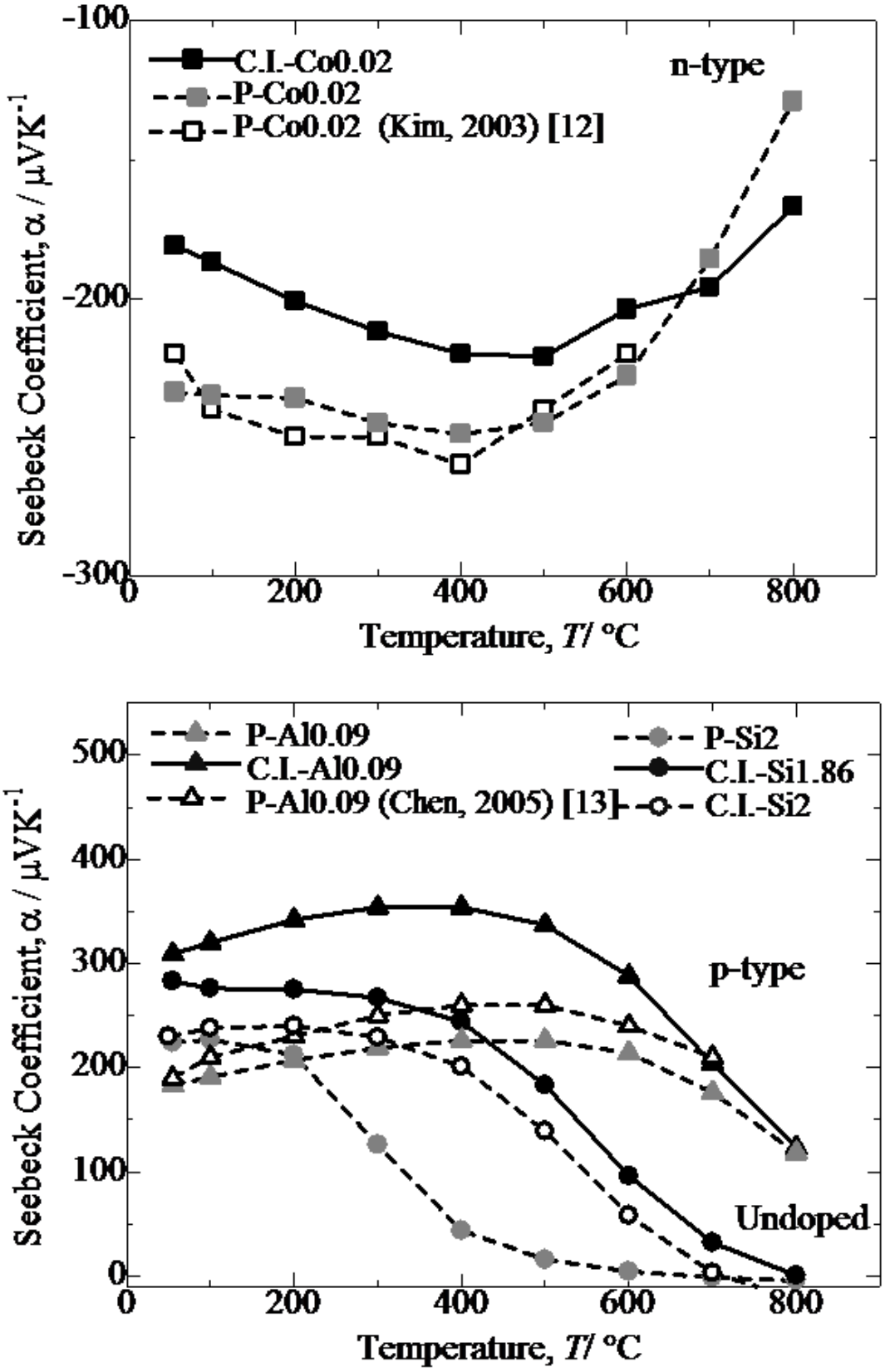

Figure 3.3 Temperature dependence of Seebeck Coefficient, *α*, of the annealed β-$FeSi_2$ samples at 900°C for 6 d.

The temperature dependence of the electrical conductivity of annealed β-$FeSi_2$ samples measured from room temperature to 800^oC is shown in Figure 3.4. The electrical conductivity for doped ones decreases with increasing measuring temperature until 500^oC and then increases with further temperature increase. In addition, a shaper increase is displayed for undoped specimen above the room temperature. The electrical conductivity of C.I.-Si1.86 sample was comparatively same as C.I.-Si2 specimen for undoped ones but significantly higher than P-Si2 sample respectively. It was found that the excess Si in cast iron scrap chips samples may lead to increase the carrier scattering effect of the free Si phase which is much stronger at lower temperature than at higher temperature [2]. As a result, it is considered that the impurity conductive region for Co-doped and Al-doped β-$FeSi_2$ from cast iron scrap chips correspond to 50-800^oC and the intrinsic conductive region for undoped β-$FeSi_2$ correspond to 500-800^oC, respectively.

Figure 3.5 shows the variation of the logarithm of electrical conductivity against the reciprocal of measuring temperature. In this study, compared to the electrical conductivity of others reported literature [12,13] and samples prepared from pure Fe, the values of β-$FeSi_2$ from cast iron scrap chips are 70% in p-type and comparatively same in n-type performance. Also, by comparing the undoped sample prepared from cast iron scrap chips, the electrical conductivity obtained significantly higher than pure Fe. The electrical conductivity of doped ones from the both of C.I. scrap chips and pure Fe is almost constant in temperature range of RT~800°C. This behavior is typical as extrinsic conductive range. On the other hand, σ of undoped ones increases with increasing temperature. This behavior is regarded as intrinsic behavior. As a result, it is confirmed undoped and Co-doping β-$FeSi_2$ from cast iron scrap chips showed positive impact in the electrical conductivity performance as compared with others reported literature [12,13] and samples prepared from pure Fe. However, in the case of Al-doped β-$FeSi_2$ from cast iron scrap, the value of electrical conductivity obtained large than one from pure Fe. This finding indicated that the Al doping in C.I. sample is more sensitive and cause the low carrier concentration effect on the synthesis and the thermoelectric performance. Taking into account the Seebeck coefficient result, the Al-doping in C.I. scrap chips also obtained large difference value compared to the Al-doping from pure Fe. The reduction in σ is considered to be caused by the easiest ability of Al-doped in

C.I. scrap chips sample to be oxidized during sintering since the C.I. consist many impurities. This is most likely oxidation of the Al-doping by impurity oxygen in cast iron scrap. Thus, the Al-doped β-$FeSi_2$ from cast iron scrap obtained low performance compare to that Al-doped β-$FeSi_2$ made from pure Fe.

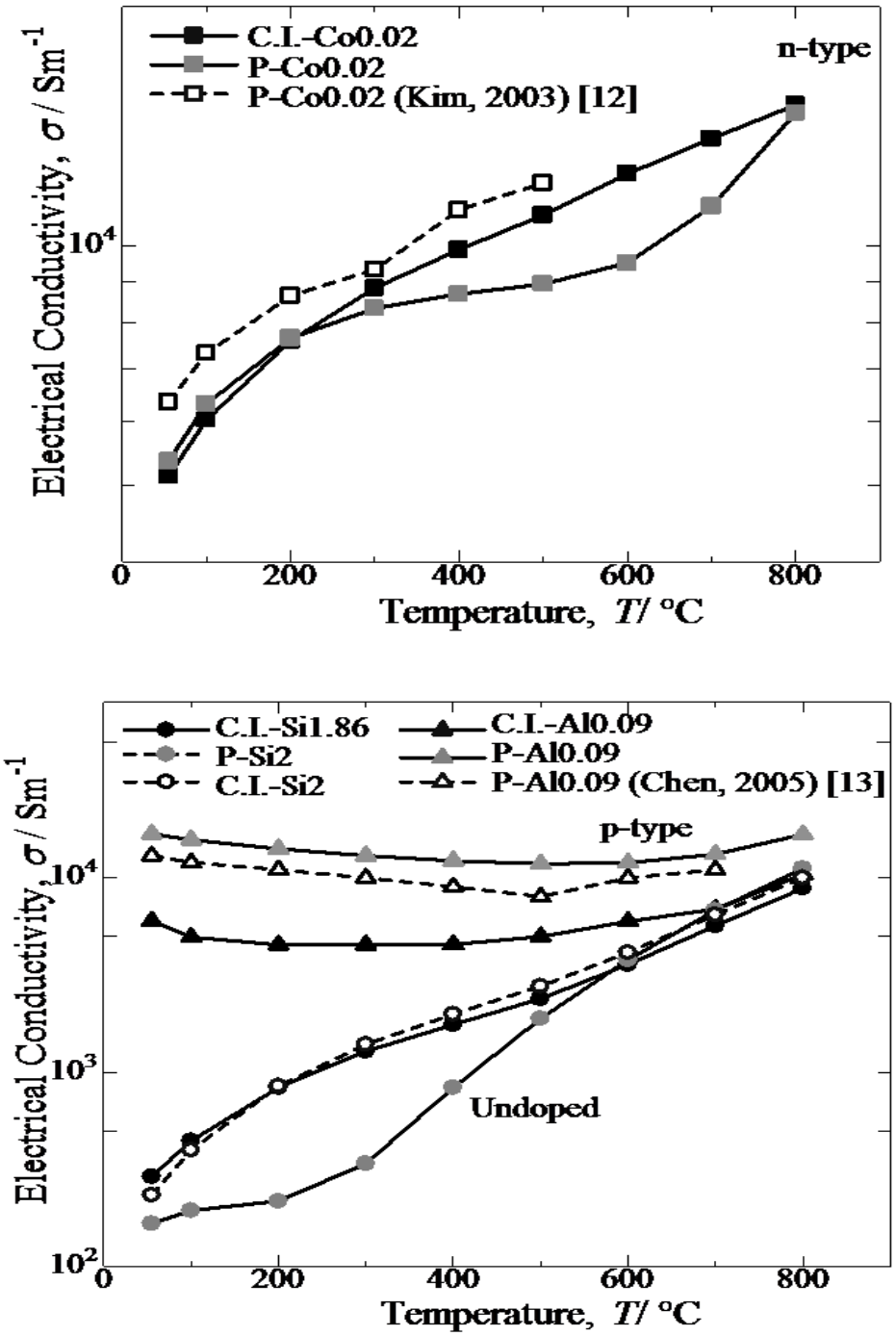

Figure 3.4 Temperature dependence of electrical conductivity, σ, of the annealed β-$FeSi_2$ samples at 900°C for 6 d.

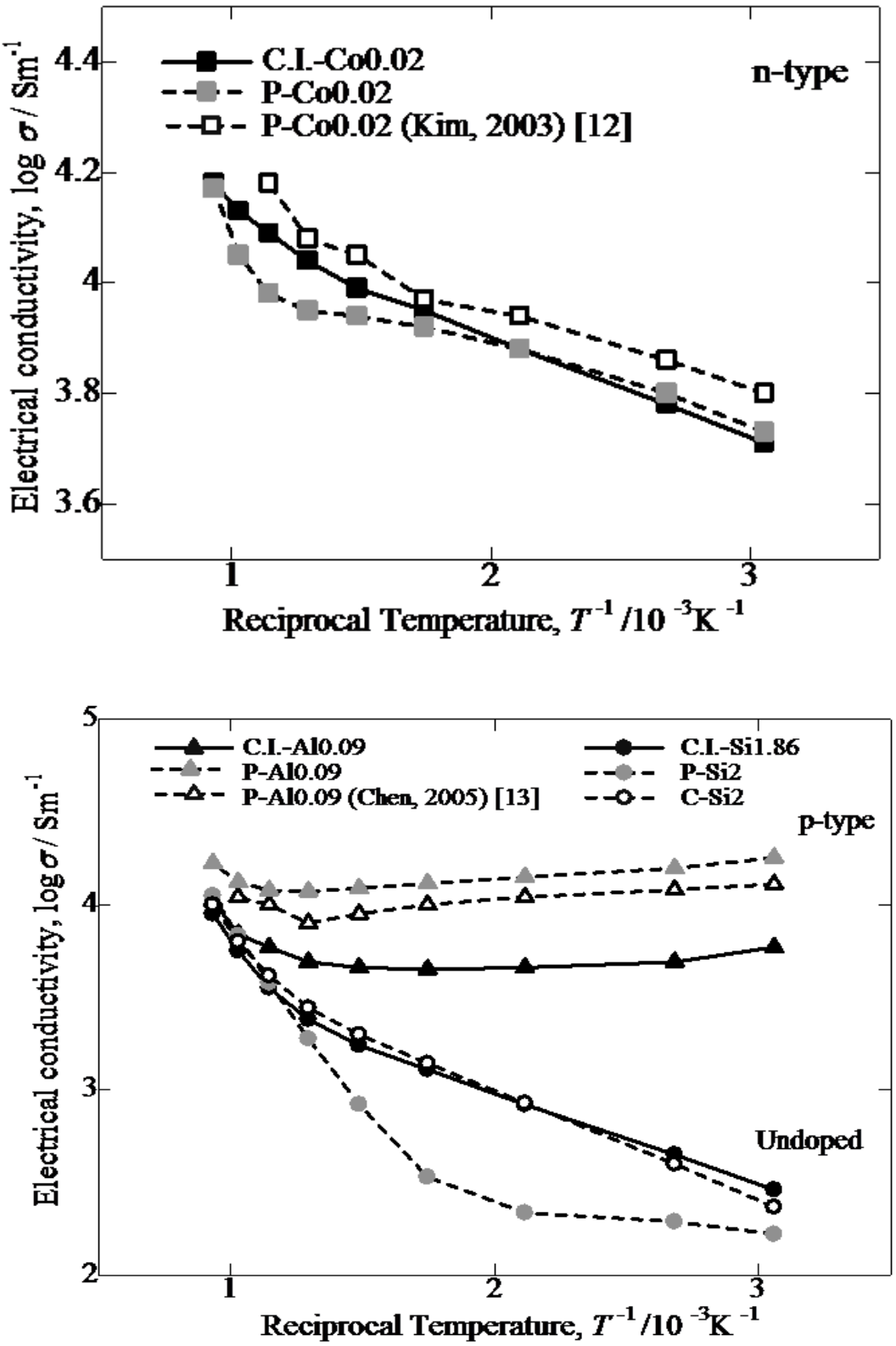

Figure 3.5 Temperature dependence of electrical conductivity plotted as log σ vs T^{-1} of the annealed β-$FeSi_2$ samples at 900°C for 6 d.

Figure 3.6 shows the thermal conductivity as a function of temperature on annealed β-$FeSi_2$ samples. For all samples, the thermal conductivity decreases with increasing the temperature. The preceding decrease of thermal conductivity could be attributed to the enhancement of phonon scattering with the temperature increase [15,16]. The comparison of the thermal conductivity achieved by Al-doped and Co-doped β-$FeSi_2$ prepared from C.I scrap chips with those reported in the literature [13,14] and from pure Fe were 70% (p-type) to almost 90% (n-type) performance. Furthermore, the Si-rich in the n-type Co dopant β-$FeSi_2$ is reported could improve the transport properties of the materials [17]. A second phase dispersion in β phase matrix is expected to increase the scattering factors in carriers and phonons, which leads to a higher Seebeck coefficient and lower thermal conductivity.

Figure 3.7 shows the variations of the dimensionless figure of merit with the measuring temperature of annealed β-$FeSi_2$ samples. For all samples, the *ZT* first increases with increasing temperature until it reaches the maximum and then decreases with the further increase in temperature. The temperatures for obtaining the maximum *ZT* are 600 and 700^{o}C, respectively, for Al-doped and Co-doped β-$FeSi_2$. The variation of *ZT* with measuring temperature resulted from combinations of effects i.e. the changes of Seebeck coefficient, electrical conductivity and thermal conductivity with measuring temperature [13]. The comparison of the *ZT* achieved from Co-doped and Al-doped β-$FeSi_2$ prepared from cast iron scarp chips than those reported in the literature [13,14] and pure Fe showed good performance in thermoelectric properties around 70% (p-type) and almost 90% (n-type). The Si rich in n-type Co dopant β-$FeSi_2$ from cast iron scrap chips was expected contributed to the higher electrical conductivity and lower thermal conductivity and thus increase the *ZT*. Based on the comparison and discussion, the undoped and the Co-doped β-$FeSi_2$ prepared from cast iron scarp chips achieved in the present work is believed to be reasonable and comparatively same performance for β-$FeSi_2$ made from pure Fe. However, the Al-doping β-$FeSi_2$ prepared from cast iron scarp chips exhibited low performance in the Seebeck coefficient and electrical conductivity compared with Al-doping made from pure Fe. This effect is due to the high sensitivity of Al-doping from C.I. scrap in impurity compared with the Co-doping.

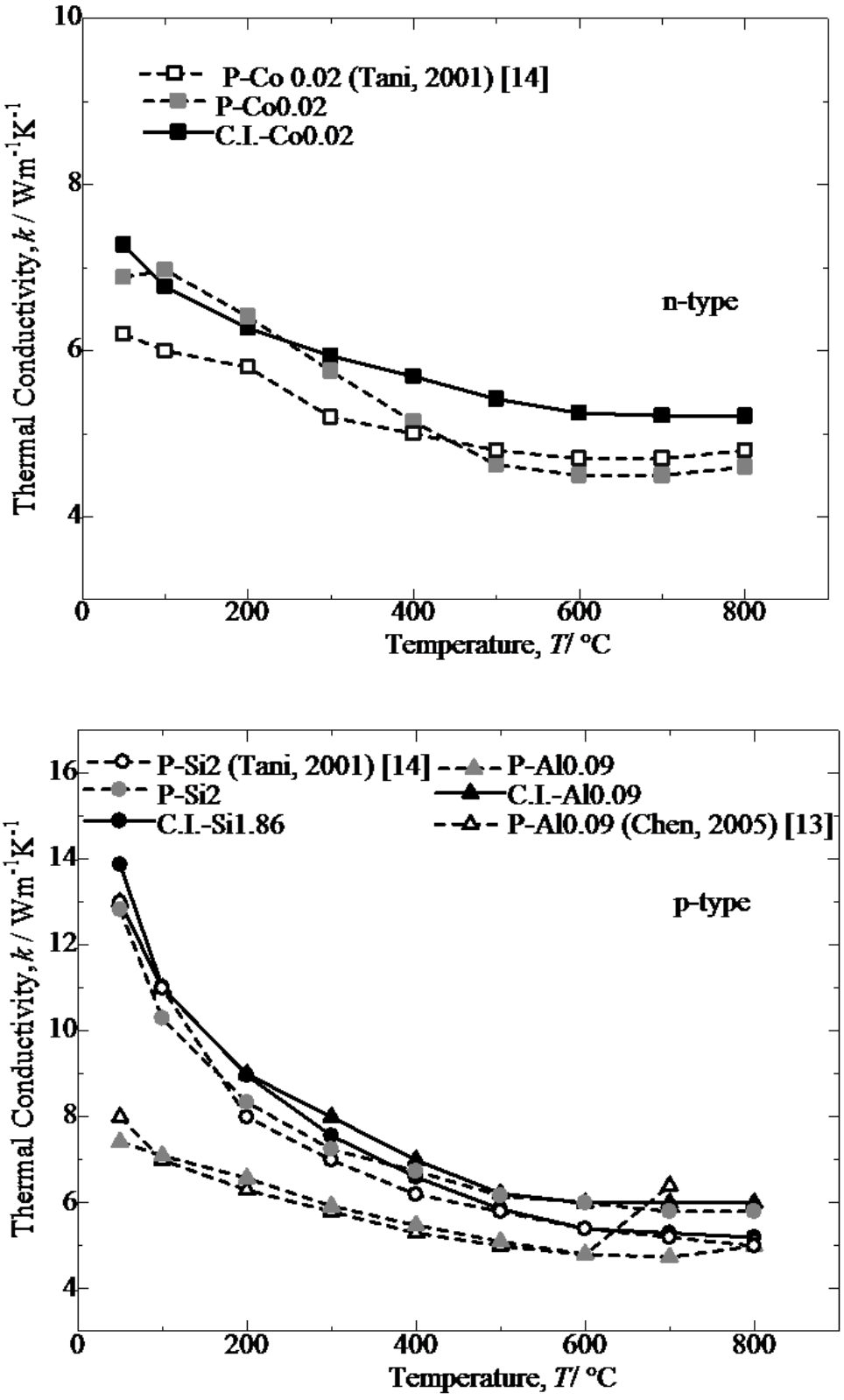

Figure 3.6 Temperature dependence of thermal conductivity, *k*, of the annealed β-$FeSi_2$ samples at 900°C for 5 d.

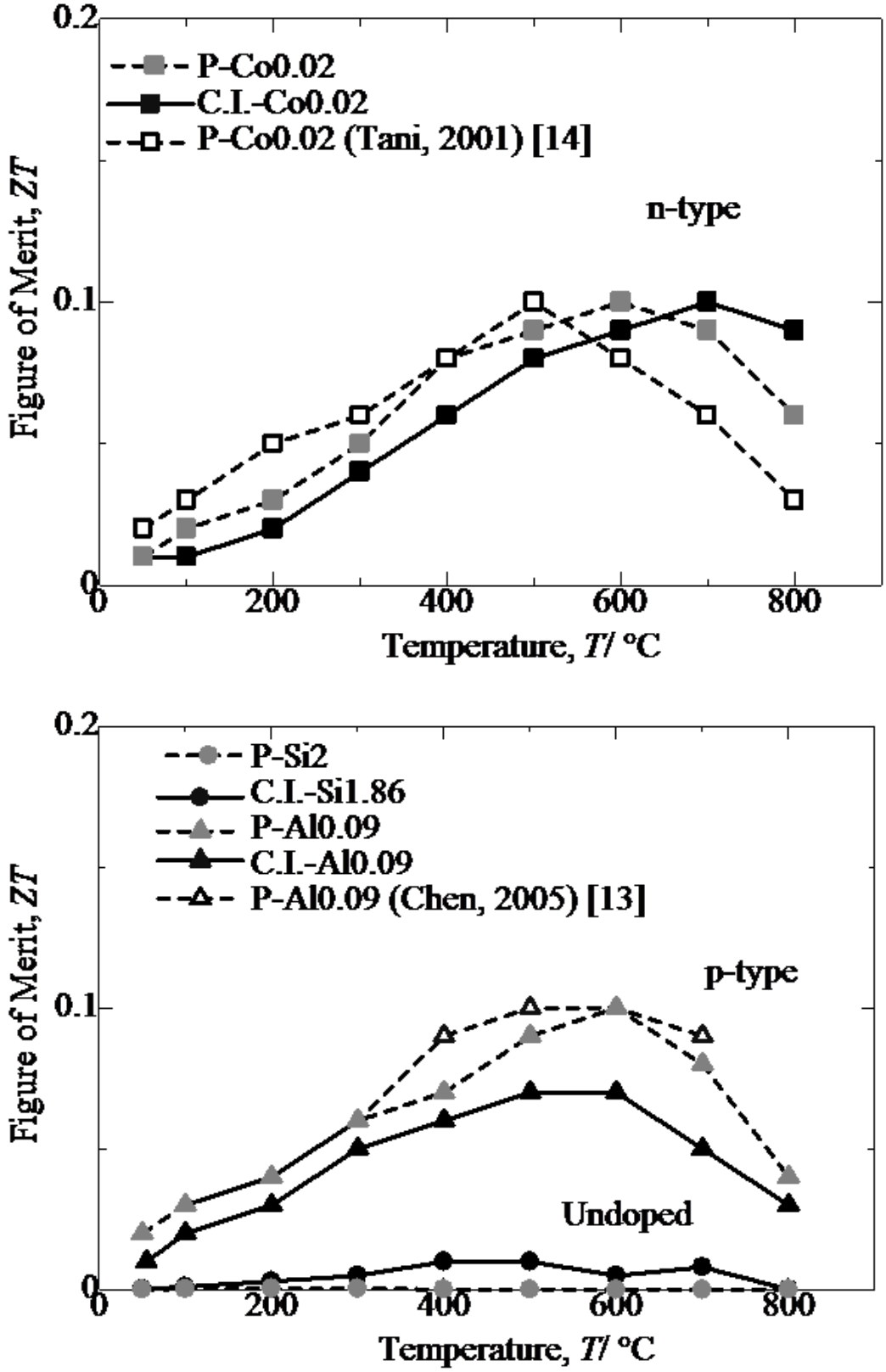

Figure 3.7 Variation of dimensional figure of merit, *ZT*, with the measuring temperature of the annealed β-$FeSi_2$ samples at 900°C for 6 d.

3.3.3. Effect of doping elements in β-$FeSi_2$ prepared utilizing cast iron scrap chips

Table 3.2 shows the density and porosity data of the sintered specimens containing various dopant element (Co, Mn and Al) concentrations for p- and n-type β-$FeSi_2$ prepared utilizing cast iron scrap chips. This result indicates that the porosity for all the samples was less than 1% after sintering. Figure 3.8 shows the XRD patterns of the annealed β-$FeSi_2$ containing undoped, Co-doped, Mn-doped and Al-doped samples prepared from cast iron scrap chips. The prefix "C.I." stands for "cast iron scrap chips", which denotes those alloys as being formed from cast iron scrap chips. The dominant peak in all of these samples was β-$FeSi_2$. All the samples are composed mainly of the β-$FeSi_2$ phase, which means the phase transformation from α-Fe_2Si_5 and ε-FeSi to β-$FeSi_2$ is nearly completed after annealing at 900°C for 6 d. The samples consisted of small amounts of the ε-FeSi phase. It was also confirmed that the isothermal annealing near the high temperature transformation temperature led to the distinct formation of ε-FeSi [19].

Table 3.2 Porosity data for the sintered β-$FeSi_2$ samples of Co, Al and Mn doped.

Sample Name (Numerical Chemical Composition)	Archimedes Measurement	
	Density	Open porosity
C.I.-Co0.02 (0.98C.I.-0.02Co-1.86Si)	4.3 g/cm^3	0.3%
C.I.-Co0.0.6 (0.94C.I.-0.06Co-1.86Si)	4.3 g/cm^3	0.3%
C.I.-Co0.08 (0.92C.I.-0.08Co-1.86Si)	4.3 g/cm^3	0.3%
C.I.-Al0.09 (C.I.-0.09Al-1.77Si)	4.5 g/cm^3	0.5%
C.I.-Al0.12 (C.I.-0.12Al-1.74Si)	4.5 g/cm^3	0.5%
C.I.-Mn0.06 (0.94C.I.-0.06Mn-1.86Si)	4.4 g/cm^3	0.5%
C.I.-Mn0.08 (0.92C.I.-0.08Mn-1.86Si)	4.4 g/cm^3	0.5%
C.I.-Mn0.1 (0.90C.I.-0.1Mn-1.86Si)	4.4 g/cm^3	0.5%

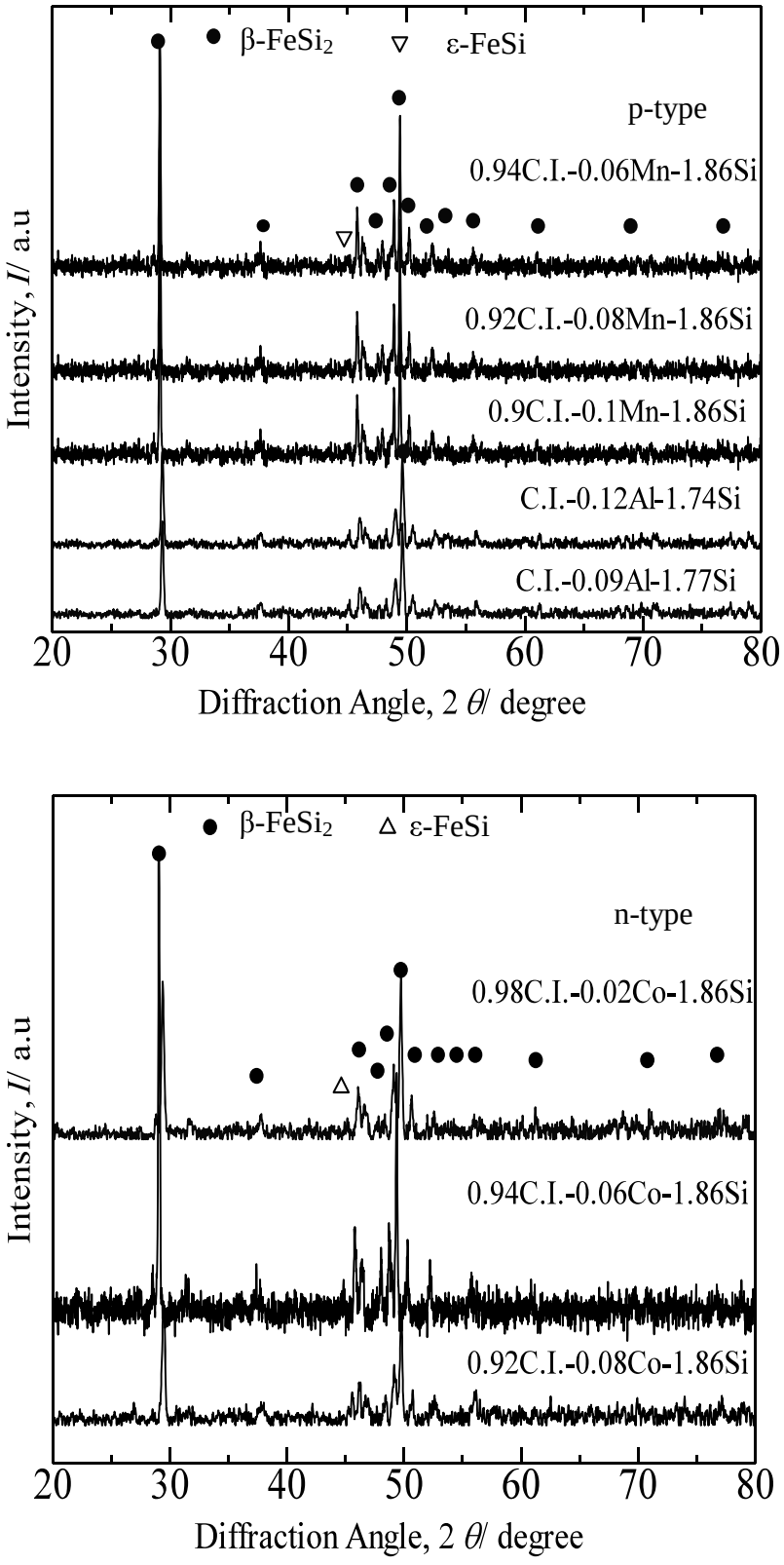

Figure 3.8 XRD patterns of the annealed β-$FeSi_2$ samples at 900°C for 6 d.

Figure 3.9 (a) shows SEM images of the microstructures for annealed un-doped, Co-doped, Mn-doped and Al-doped β-$FeSi_2$ prepared from cast iron scrap chips. The SEM image of the annealed β-$FeSi_2$ prepared from cast iron scrap chips showed excess Si particles (shown as black dots) with small pores (shown as white dots). Several black Si particles were detected in the β-phase matrix. Very few pores were detected in the undoped, Co-doped, Mn-doped and Al- doped samples. The pore size that could be observed from the SEM images was estimated to be less than approximately 10 μm. The open porosity, as provided in Table 3.2 observed in all samples was less than 1% after sintering, and we consider these to be dense samples. Figure 3.9(b) shows the SEM images and the corresponding EDX elemental mapping results for (i) 0.94C.I.-0.06Co-1.86Si (C.I.-Co0.0.6), (ii) 0.92C.I.-0.08Mn-1.86Si (C.I.-Mn0.08) and (iii) C.I.-0.09Al-1.77Si (C.I.-Al0.09) in the annealed β-$FeSi_2$ prepared from cast iron scrap chips. It is clear that the distribution of the Co, Mn and Al dopant concentrations in these specimens, as well as for the remaining annealed β-$FeSi_2$ prepared from cast iron scrap chips were uniformly dispersed throughout the β phase.

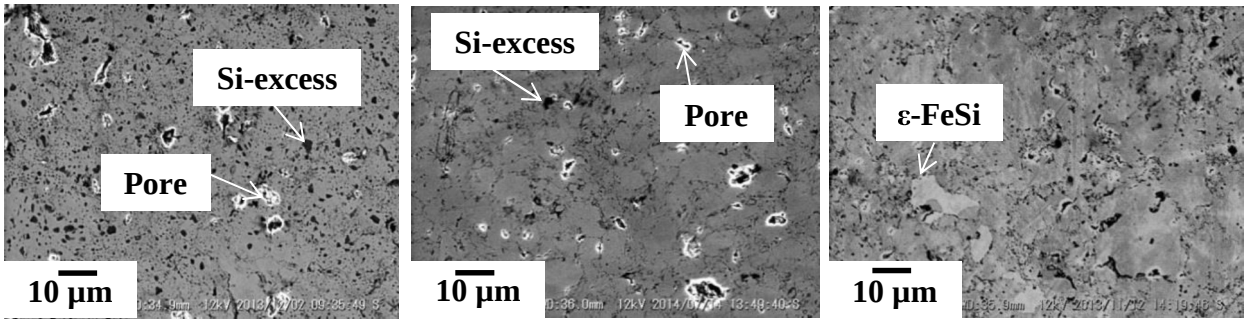

(i) C.I.-0.02Co (0.98C.I.-0.02Co-1.86Si) (ii) C.I.-0.06Co (0.94C.I.-0.06Co-1.86Si) (iii) C.I.-0.08Co (0.94C.I.-0.08Co-1.86Si)

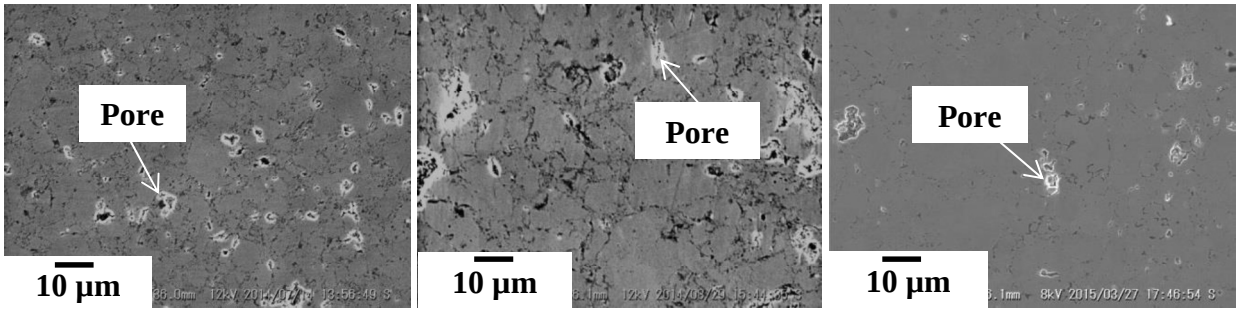

(iv) C.I.-0.06Mn (0.94C.I.-0.06Mn-1.86Si) (v) C.I.-0.08Mn (0.94C.I.-0.08Mn-1.86Si) (vi) C.I.-0.1Mn (0.94C.I.-0.1Mn-1.86Si)

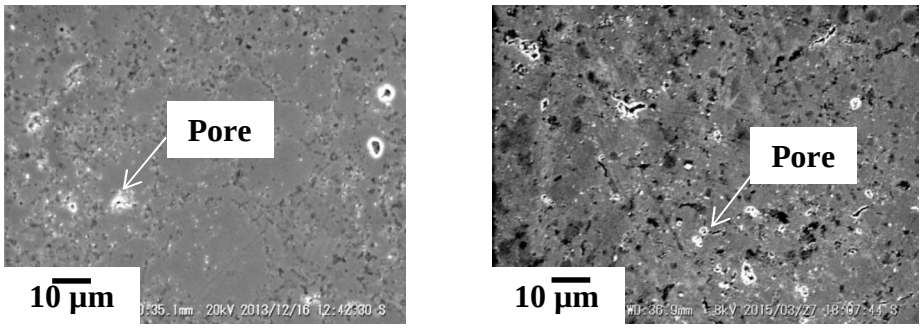

(vii) C.I.-0.09Al (C.I.-0.09Al-1.77Si)

(viii) C.I.-0.12Al (C.I.-0.12Al-1.74Si)

Figure 3.9 (a). SEM photos on microstructures of the annealed β-$FeSi_2$ samples at 900°C for 6 d.

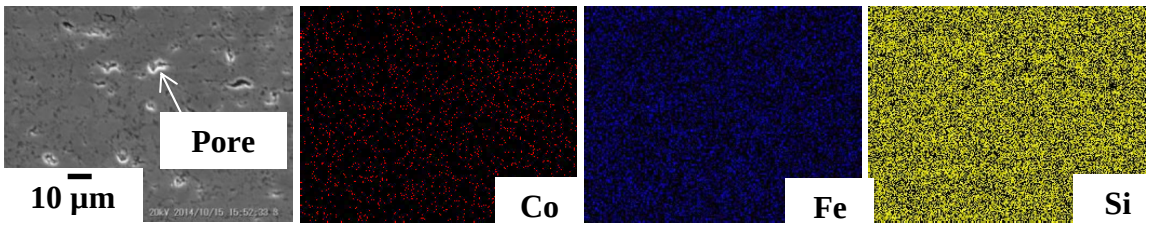

(i) C.I.-0.06Co (0.94C.I.-0.06Co-1.86Si)

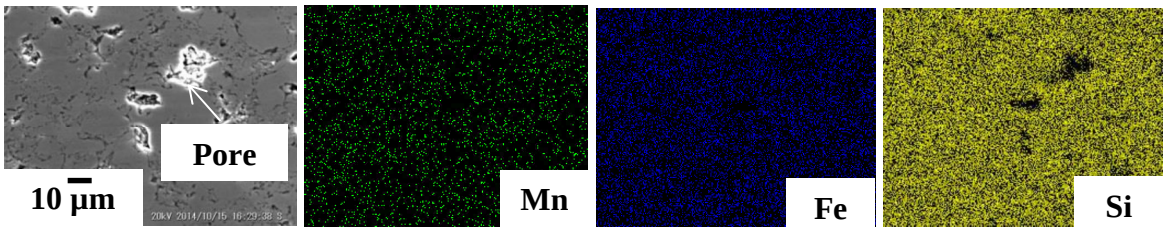

(ii) C.I.-0.08Mn (0.94C.I.-0.08Mn-1.86Si)

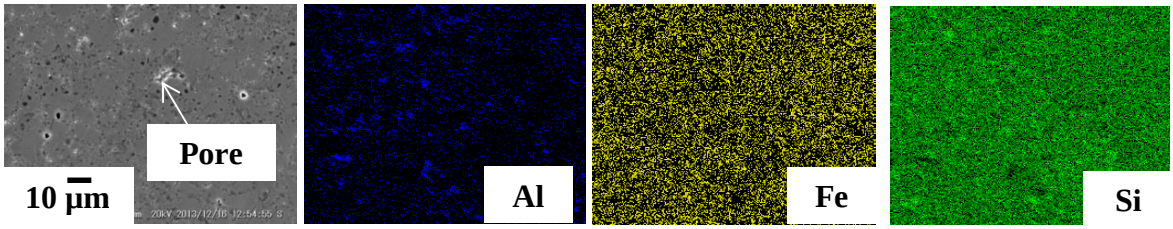

(iii) C.I.-0.09Al(C.I.-0.09Al-1.77Si)

Figure 3.9 (b). SEM image and EDX result of (i) C.I.-0.06Co (0.94C.I.-0.06Co-1.86Si), (ii) C.I.-0.08Mn (0.94C.I.-0.08Mn-1.86Si) and (iii) C.I.-0.09Al (C.I.-0.09Al-1.77Si) of the annealed β-$FeSi_2$ samples prepared utilizing cast iron scrap chips.

The temperature dependence of the Seebeck coefficient, α, for the annealed p- and n-type β-$FeSi_2$ specimens evaluated from room temperature to 800°C is shown in Figure 3.10. In the present work [20,21], we see different signs for the Seebeck coefficients exhibited for the Al-, Mn- and Co-doped β-$FeSi_2$ prepared from cast iron scrap chips. The positive values associated with the Mn-doped (0.06<Mn<0.1) and Al-doped (0.09<Al<0.12) samples correspond to p-type behavior, indicating that the electrical conductivity is dominated by hole conduction. However, n-type behavior is attributed to the Co-doped (0.02<Co<0.08) samples as a result of their negative Seebeck coefficient values, which is indicative of electron conduction. The absolute value of the Seebeck coefficient increases with the measurement temperature to a peak before beginning to decrease with further increases to the temperature. The Seebeck coefficients for the 0.92C.I.-0.08Mn-1.86Si (C.I.-Mn0.08) and 0.94C.I.-0.06Co-1.86Si (C.I.-Co0.0.6) specimens prepared from cast iron scrap chips were obtained to be between 90% and almost 100%, respectively, of the performance observed for the other specimens and from other reported studies [14][23]. As the Al dopant (0.09<Al<0.12) was replaced by the Mn dopant (0.06<Mn<0.1), the Seebeck coefficients was found to decrease. The decrease in the Seebeck coefficient could be caused by an increase in the carrier concentration. In the present study, it was revealed that the Al dopant (0.09<Al<0.12) is more sensitive to the cast iron scrap chips due to the Al dopant (0.09<Al<0.12) being easily oxidized during processing because the cast iron contains many impurities. This is most likely a result of oxygen impurities in the cast iron scrap. The Al-doped sample is partially oxidized during machining and exhibited a low performance compared to the Mn-doped (0.06<Mn<0.1) β-$FeSi_2$. Thus, the results of this study indicated that β-$FeSi_2$ prepared utilizing cast iron scrap was successfully optimized and is comparable to what has been previously reported [12-14,23].

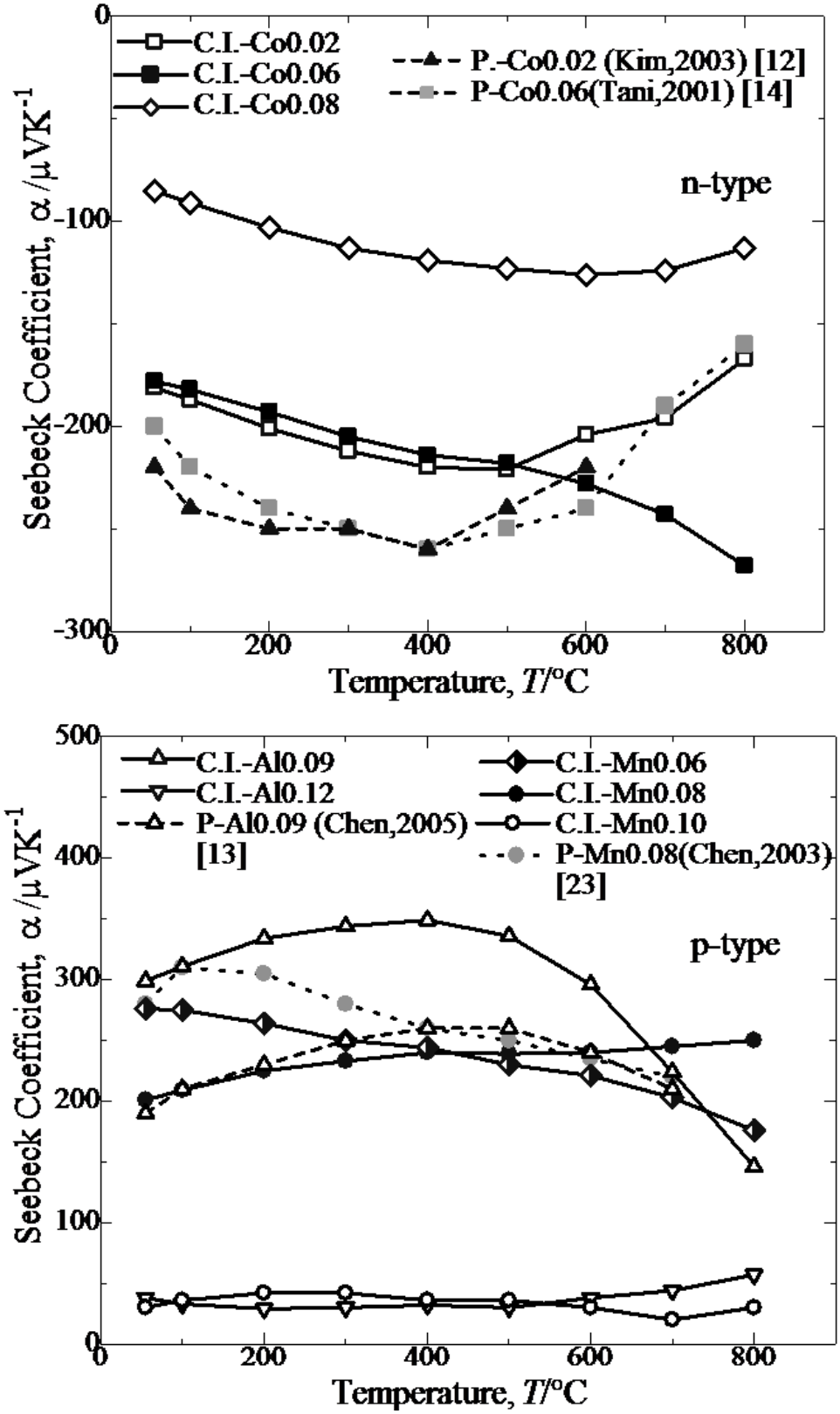

Figure 3.10 Temperature dependence of Seebeck coefficient, *α*, for the annealed β-$FeSi_2$ samples at 900°C for 6.

Figure 3.11 shows the temperature dependence of the electrical conductivity for the annealed β-$FeSi_2$ specimens between room temperature to 800°C. The electrical conductivity of the C.I.-0.09Al-1.77Si (C.I.-Al0.09) specimen decreased with increasing temperatures until reaching 400°C. As this point, further temperature increases resulted in increases to the electrical conductivity. The temperature dependence of the electrical conductivity below 400°C could be attributed to the carrier mobility, which decreased with increasing temperature. This is a result of the acceptor being exhausted and carrier scattering occurring via lattice vibration [12]. The intrinsic conduction dominated when the temperature is above 400°C, which leads to the increase in the electrical conductivity as the temperature increased. The electrical conductivities for the Co-doped (0.02<Co<0.08) and Mn-doped (0.06<Mn<0.1) β-$FeSi_2$ prepared using cast iron scrap chips, along with other examples reported in the literature [14,21-23], are nearly constant over the temperature range from room temperature to 800°C. This behavior is typical for the extrinsic conductivity range. Thus, we confirm that Mn-doped (0.06<Mn<0.1) and Co-doped (0.02<Co<0.08) β-$FeSi_2$ prepared using cast iron scrap chips exhibit positive impacts on the electrical conductivity compared to other results reported on in the literature [14,23]. Conversely, for p-type β-$FeSi_2$ prepared using cast iron scrap chips, the C.I.-0.09Al-1.77Si (C.I.-Al0.09) exhibited a lower electrical conductivity compared to 0.94C.I.-0.06Mn-1.86Si (C.I.-Mn0.06) and 0.92C.I.-0.08Mn-1.86Si (C.I.-Mn0.08) at temperatures greater than 200°C. This finding indicated that the C.I.-0.09Al-1.77Si (C.I.-Al0.09) is more sensitive to the presence of the cast iron scrap chips, and results in a low concentration upon synthesis. As the Al dopant was replaced by the Mn dopant, the electrical conductivity was enhanced and improved. Therefore, by doping with different substitution concentrations of Co (0.02<Co<0.08), Mn (0.06<Mn<0.1) and Al (0.09<Co<0.12), the conduction type and properties of the β-$FeSi_2$ can be modified and improved, even when using cast iron scrap chips as a starting material.

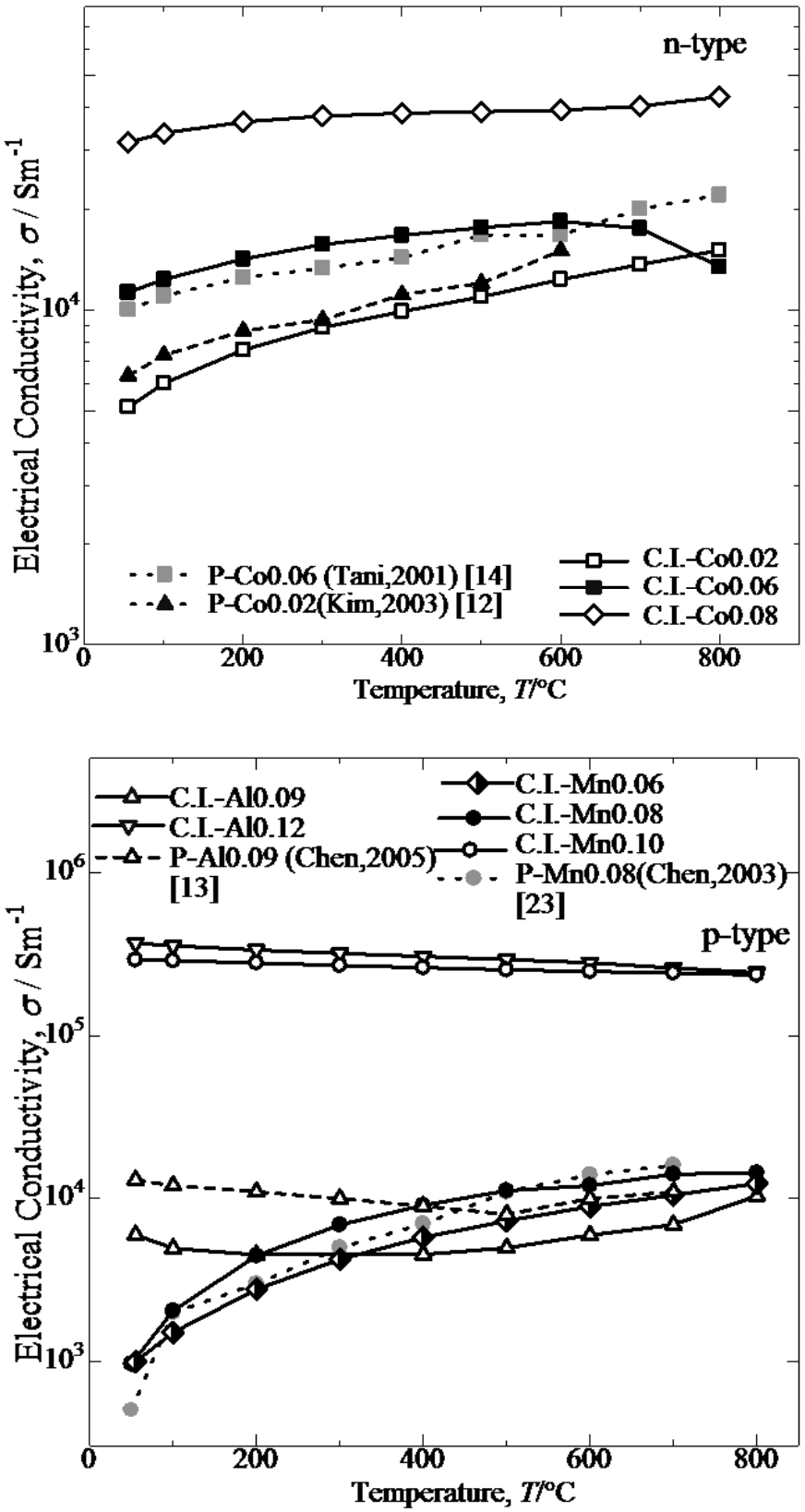

Figure 3.11 Temperature dependence of electrical conductivity, σ, for the annealed β-$FeSi_2$ samples at 900°C for 6 d.

The thermal conductivity, *k* of the annealed p- and n-type β-$FeSi_2$ specimens evaluated from room temperature to 800°C is shown in Figure 3.12 For all the specimens, the thermal conductivity, *k* decreased rapidly as the temperature increased. Similar trends for the thermal conductivity as a function of measurement temperature was reported by Ito et al. [24]. The preceding decrease in the thermal conductivity may be attributed to the enhancement of phonon scattering as the temperature increases [13,14]. As shown in Figure 3.12, the thermal conductivity of the 0.92C.I.-0.08 Mn-1.86Si (C.I.-Mn0.08) specimen could be decreased by ≈ 30% compared with the C.I.-0.09Al-1.77Si (C.I.-Al0.09) specimens. However, the Co-doped (0.02<Co<0.08) specimens' thermal conductivity was much lower than the p-type doped 0.92C.I.-0.08Mn-1.86Si (C.I.-Mn0.08) and C.I.-0.09Al-1.77Si (C.I-Al0.09) specimens, respectively. This result could be due to the effect of the Si-rich concentration in the n-type Co-doped (0.02<Co<0.08) β-$FeSi_2$ prepared using cast iron scrap chips. It was reported that this may improve the transport properties of the materials, which is effective at decreasing the thermal conductivity [17,18]. Furthermore, in general, increases in the dopant content tend to enhance the phonon scattering due to lattice short range distortions, resulting in a decrease in the thermal conductivity [25]. Thus, it was found that by doping with different substitution concentrations of Co (0.02<Co<0.08), Mn (0.06<Mn<0.1) and Al (0.09<Co<0.12), the conduction type and properties of the β-$FeSi_2$ can be modified and improved, even when using cast iron scrap chips as a starting material.

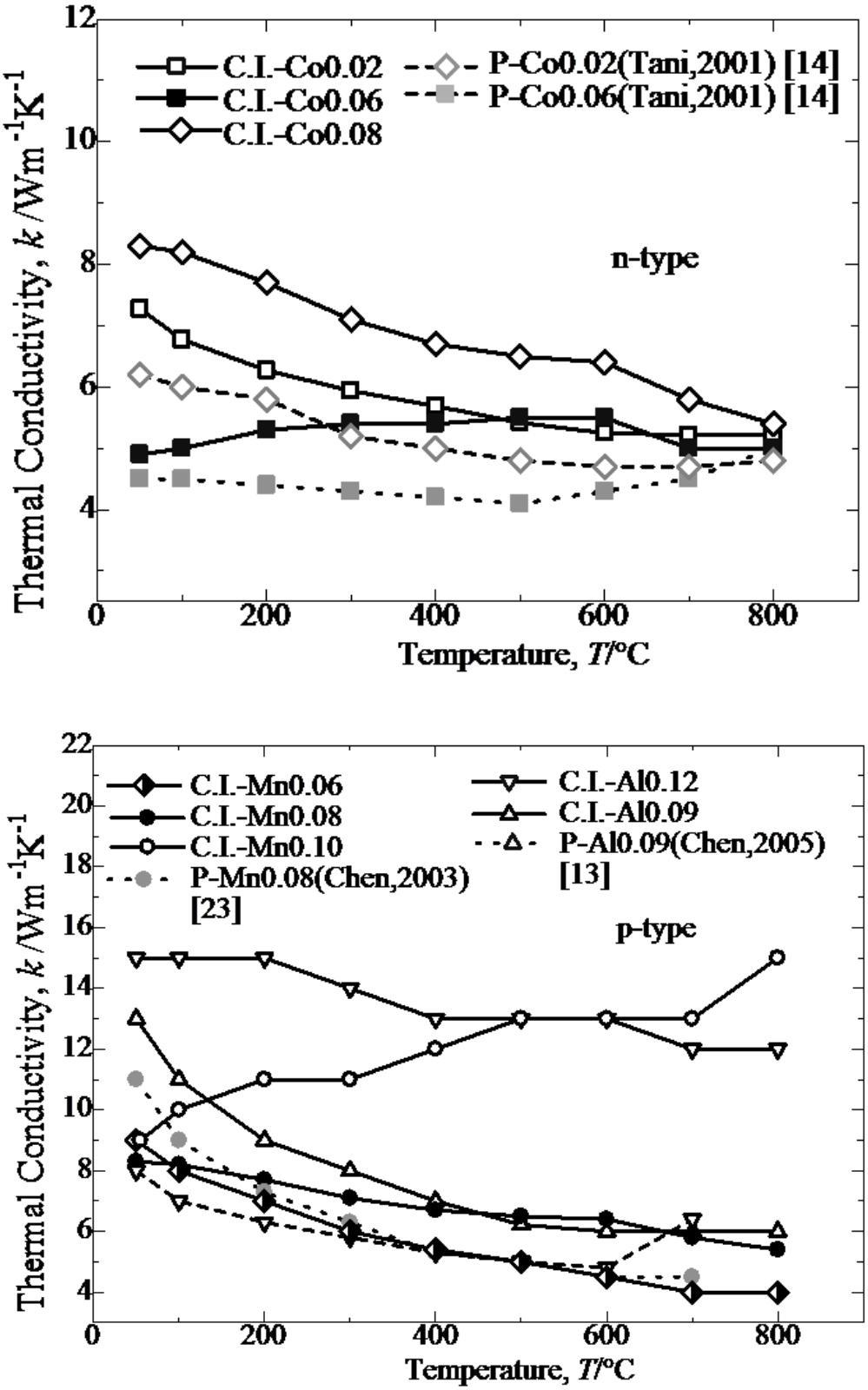

Figure 3.12 Temperature dependence of thermal conductivity, *k*, for the annealed β-$FeSi_2$ samples at 900°C for 6 d.

Figure 3.13 summarizes the function of temperature on the dimensionless figure of merit, *ZT,* for the various doping elements in the p- and n-type β-$FeSi_2$ specimens prepared utilizing cast iron scrap chips. Significant efforts have been undertaken to obtain a high value figure of merit, which represents the efficiency of thermoelectric materials [26,27]. The comparison of the *ZT* values achieved for the n-type 0.94C.I.-0.06Co-1.86Si (C.I-Co0.06) specimen and the p-type 0.92C.I.-0.08 Mn-1.86Si (C.I.-Mn0.08) specimen with the other various doping elements indicated the highest *ZT* values were 0.22 at 700°C and 0.17 at 800°C, respectively. Due to the higher substitutions necessary to achieve the concentration effect, the highest *ZT* value was obtained from the n-type 0.94C.I.-0.06Co-1.86Si (C.I-Co0.06) specimen. Additionally, the p-type specimen prepared from p-type 0.92C.I.-0.08Mn-1.86Si (C.I.-Mn0.08) has a better *ZT* value due to the compatibility of the cast iron scrap chips, compared to the results in previously published reports [20,21]. By doping with the various elements, the conduction type and properties of the β-$FeSi_2$ prepared utilizing cast-iron scrap chips could be modified and improved. The value of *ZT* increases with the temperature before reaching a maximum and decreasing. Additionally, the *ZT* value increases with the substitution concentration of the doping elements. Therefore, we have demonstrated that the cast iron scrap chips are effective as a starting material for fabricating β-$FeSi_2$ and are capable of producing a material comparable to conventional β-$FeSi_2$ fabricated from pure Fe.

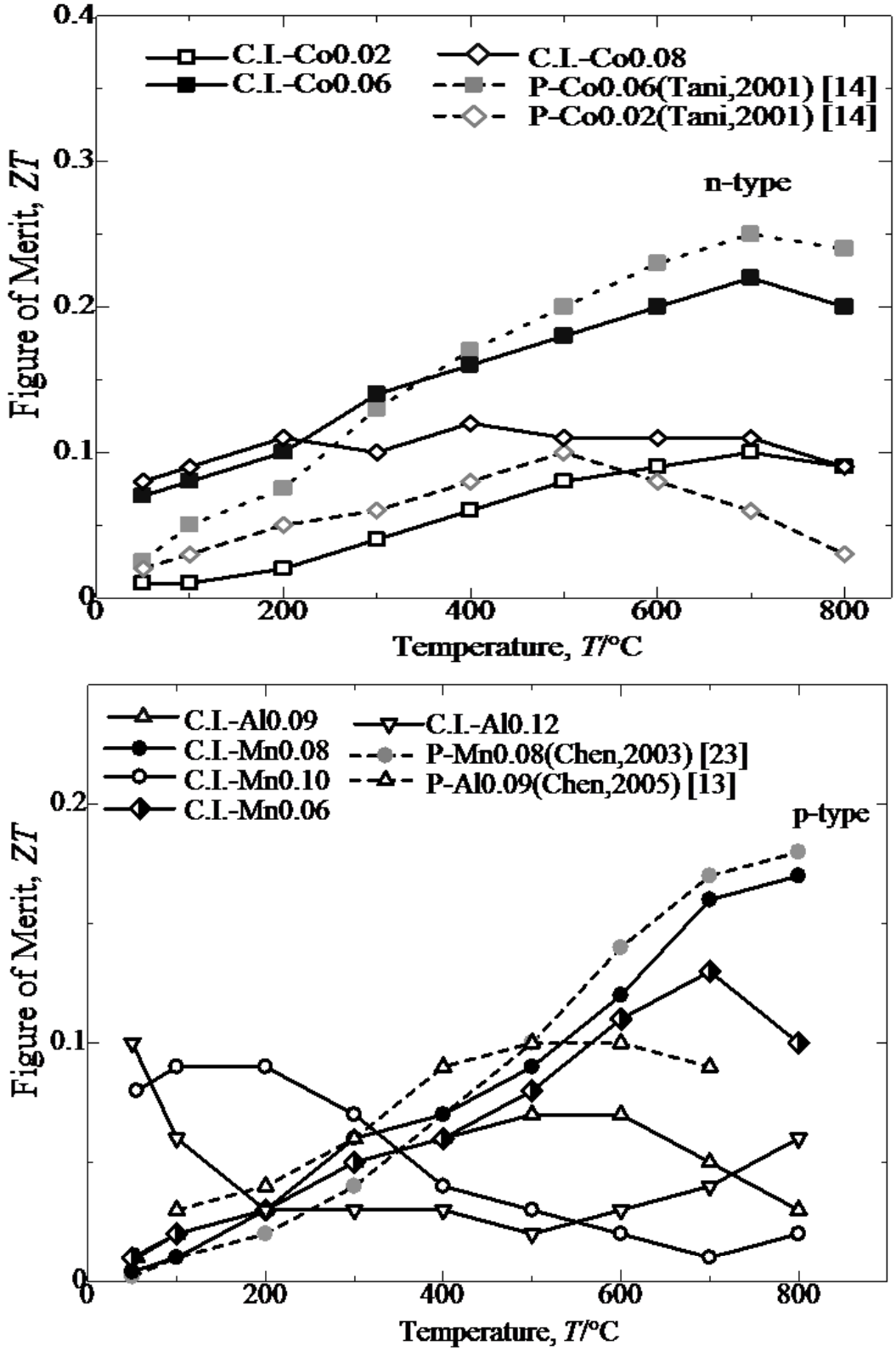

Figure 3.13 Variation in dimensional figure of merit, *ZT*, with the measuring temperature of the annealed β-$FeSi_2$ samples at 900°C for 6 d.

3.3.4. Isothermal oxidation of sintered in β-$FeSi_2$ prepared utilizing cast iron scrap chips

Figure 3.14 (a) shows XRD patterns of annealed β-$FeSi_2$ undoped, Co-doped and Al-doped from pure Fe and cast iron scrap chips. Dominant peaks in these samples could be identified as β-$FeSi_2$ for all samples. Almost fully β-$FeSi_2$ with a small amount of ε-FeSi was obtained after annealing treatment at temperature 900°C for 5 d in order to stabilize the desired volume fraction of β phase. Figure 3.14 (b) shows XRD patterns of β-$FeSi_2$ specimens oxidized at 800°C for 14 d. An oxidation product such as FeO, cristobalite and ferrosilite were not identified in oxidized β-$FeSi_2$. A peak of ε-FeSi phase increases slightly after oxidation experiment. Formation of ε-FeSi is caused by consumption of Si in β-$FeSi_2$ by high-temperature oxidation.

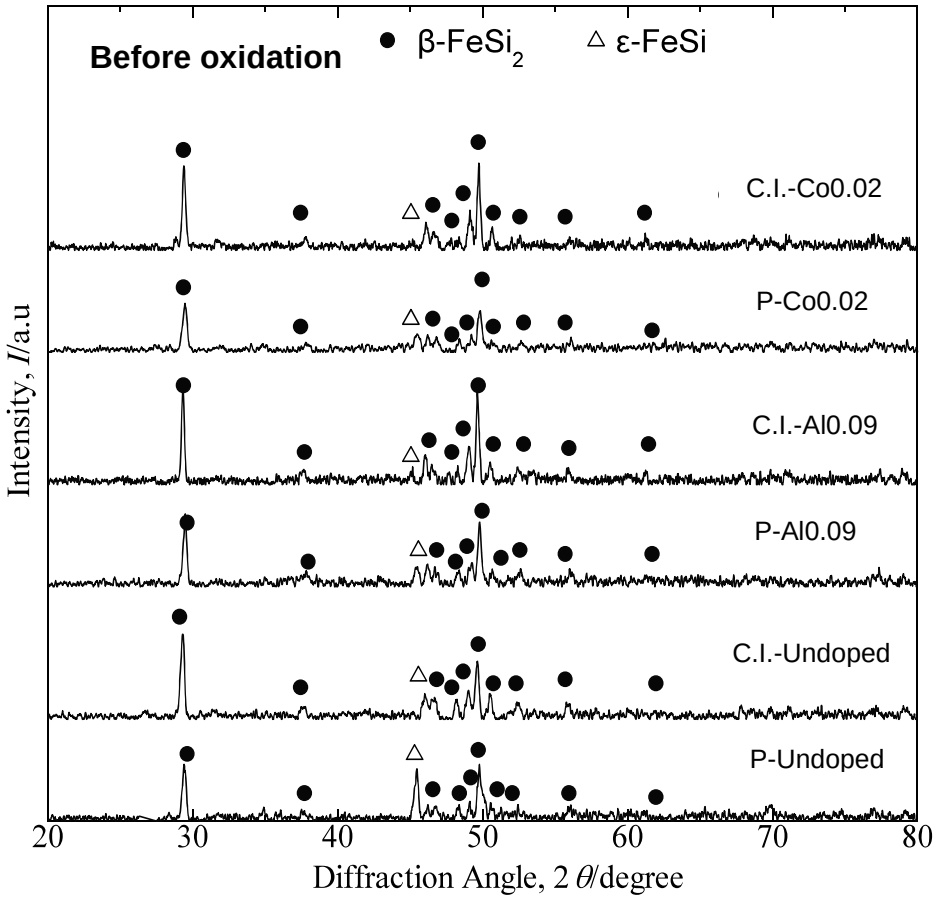

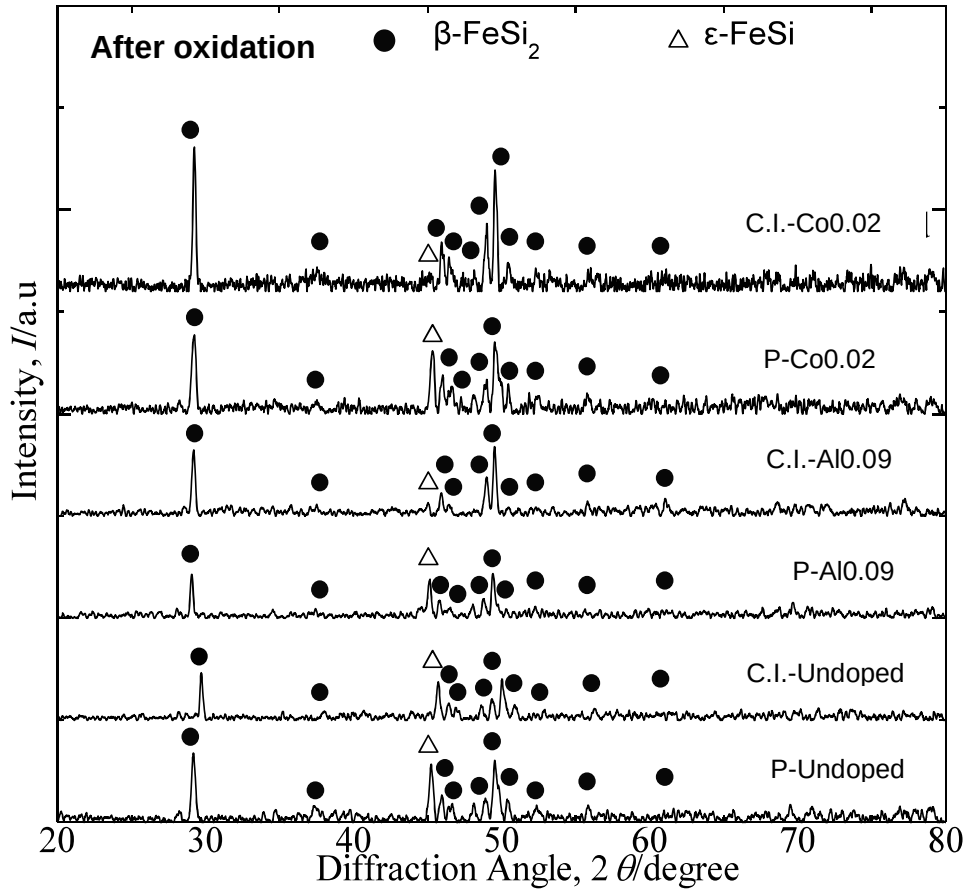

Figure 3.14 (a) XRD patterns of the annealed β-$FeSi_2$ samples before and **(b)** oxidized at 800°C for 14 d in air.

Figure 3.15 shows SEM images of the microstructures for annealed undoped, Co-doped and Al-doped β-$FeSi_2$ prepared from cast iron scrap chips. The SEM image of the annealed β-$FeSi_2$ prepared from cast iron scrap chips showed excess Si particles (shown as black dots) with small pores (shown as white dots). Several black Si particles were detected in the β-phase matrix. Very few pores were detected in the undoped, Co-doped and Al-doped samples. The pore size that could be observed from the SEM images was estimated to be less than approximately 10 μm.

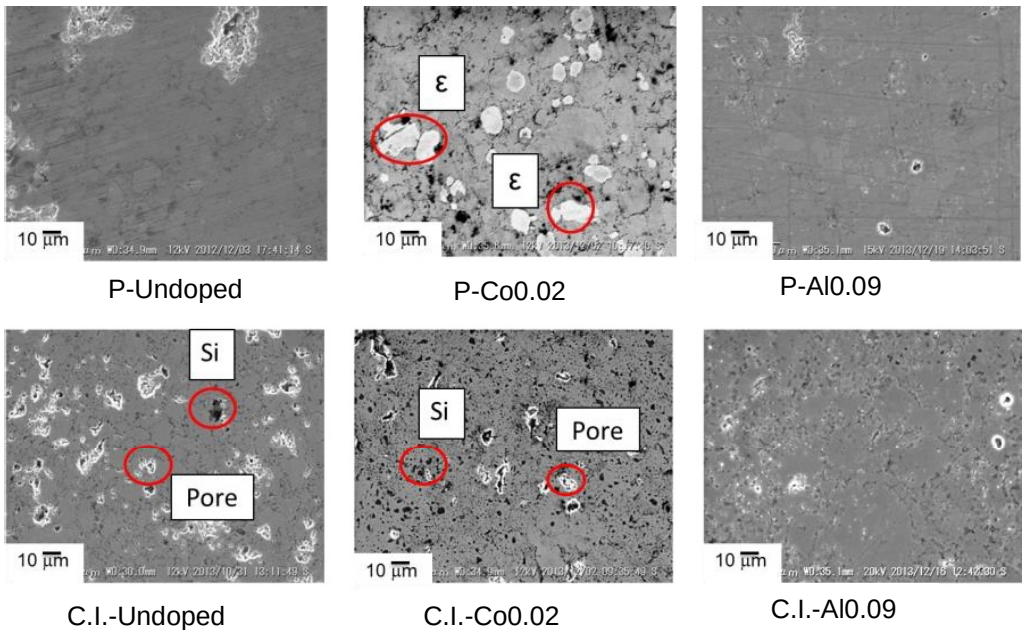

Figure 3.15 SEM microstructures of the annealed β-$FeSi_2$ samples at 900°C for 6 d.

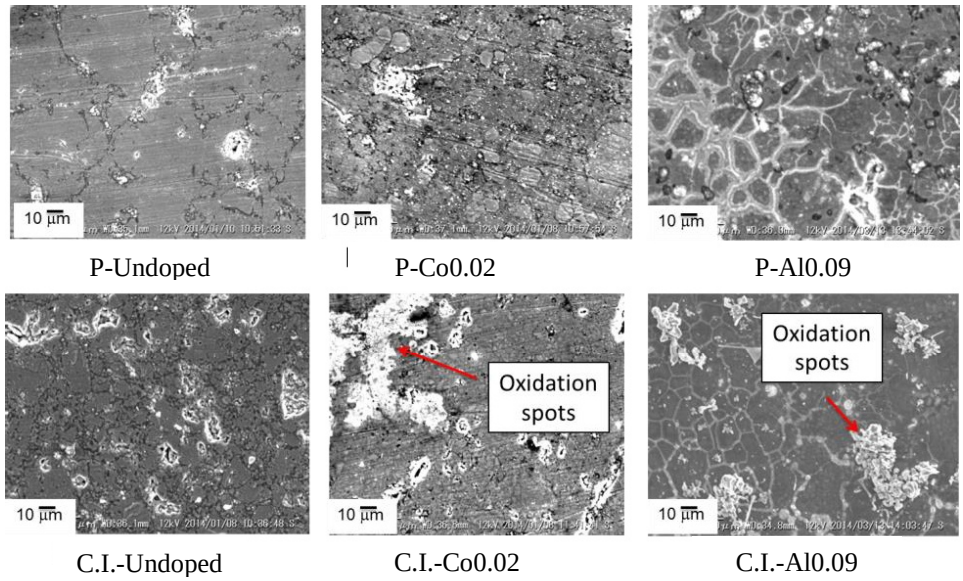

Figure 3.16 SEM microstructures of the annealed β-$FeSi_2$ samples oxidized at 800°C for 14 d in air.

Fig. 3.16 shows the SEM images on surface morphology of oxidized β-$FeSi_2$ prepared from pure Fe and cast iron scrap chips. Any cracks of oxidized β-$FeSi_2$ samples were not observed after high temperature oxidation. Furthermore, anomaly

oxidation such as formation of large nodules was not observed on the surface morphology. However, some white spots (oxidation spots) were observed on the surface morphology of oxidized β-$FeSi_2$.

Figure 3.17 shows the SEM images and the corresponding EDX elemental mapping results for oxidized C.I.-Co0.0.2 specimen prepared from cast iron scrap chips. It is clear that the distribution of the Si and O elements observed on the white spots (oxidation spots) in this specimen, as well as for the remaining oxidized β-$FeSi_2$ prepared from cast iron scrap chips were uniformly dispersed throughout the β phase.

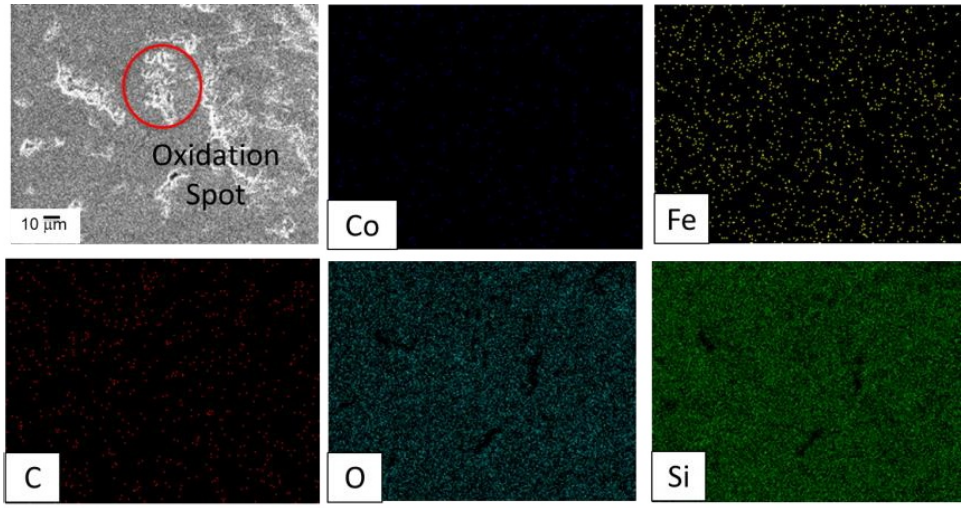

Figure 3.17 SEM image and EDXresults of oxidized C.I.-Co0.0.2 specimen at 800°C for 14 d.

Fig. 3.18 shows the cross sectional views of sintered β-$FeSi_2$ samples after oxidation at 800°C for 14 d in air. An oxide scale is observed approximately 0.5-1 µm in thickness. Taking account of the XRD results, the oxide scale is most likely amorphous SiO_2 as similar with Si and other silicide materials such as $NiSi_2$ [28] and $CoSi_2$ [29]. Anomaly oxidation such as formation of nodules was not observed. Cracks of β-$FeSi_2$ samples and oxide scale were not observed. An oxide scale is observed in all β-$FeSi_2$ samples made of pure Fe and cast iron scrap chips. Bright grains are also observed below the oxide scale after oxidation. The bright grain consists of less Si and more Fe than β-$FeSi_2$ phase as shown in Figure 3.18.

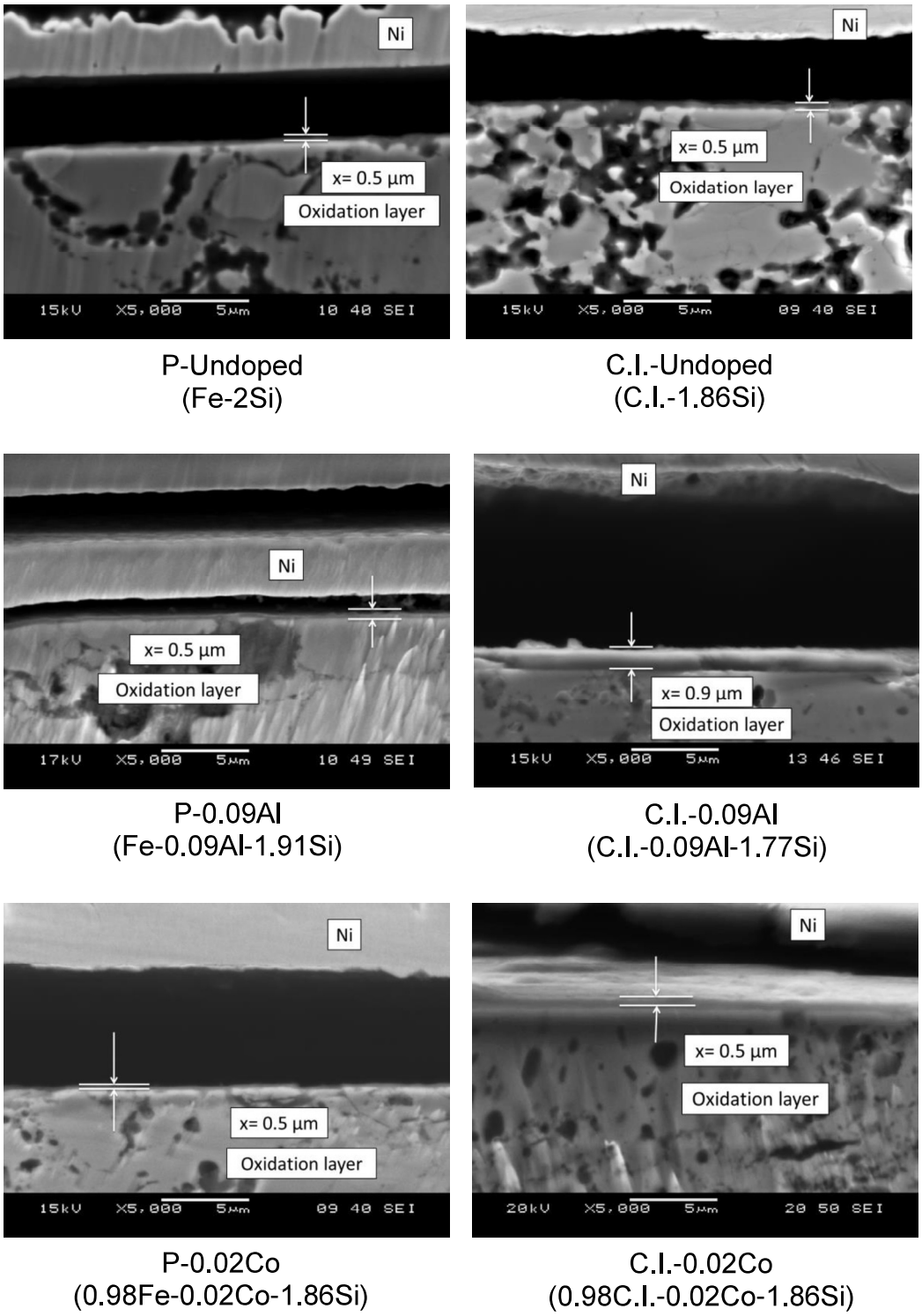

Figure 3.18 Cross-sectional SEM views of the annealed β-$FeSi_2$ samples oxidized at 800°C for 14 d in air.

Figure 3.19 (a), (b) and (c) show thermoelectric properties of annealed β-$FeSi_2$ thermoelectric materials before and after high temperature oxidation at 800°C for 14 d in air. Seebeck coefficient, α, electrical conductivity, σ, and thermal conductivity, k, of the annealed samples agree with the reported data of sintered β-$FeSi_2$ [13,30]. Their thermoelectric properties of β-$FeSi_2$ specimens prepared using cast iron scrap chips at high temperature oxidation test are similar to those as annealed samples. Isothermal oxidation at high temperature is air does not degrade thermoelectric properties of annealed β-$FeSi_2$ specimens even when using cast iron scrap chips as a starting material. Since anomaly oxidation such as grain boundary oxidation or crack formation was not observed in oxidation of β-$FeSi_2$ specimens prepared using cast iron scrap chips at 800°C, thermoelectric properties of annealed of β-$FeSi_2$ bodies would not change significantly by formation of granular ε-FeSi.

Based on the present experimental results, thickness of SiO_2 scale oxidized at 800°C for 1 y can be estimated to be few microns. The formation of granular ε-FeSi for consumption of Si in β-$FeSi_2$ by oxidation did not degrade oxidation resistance. According to Asanabe et. al., electrical conductivity of ε-FeSi is almost constant at higher temperature [31]. Since thickness of a continuous of ε-FeSi layer would be as same as the oxide scale, the shortcut of the ε-FeSi layer with a few microns in thickness is negligible. Therefore thermoelectric β-$FeSi_2$ prepared using cast iron scrap chips has probably a long lifetime at high temperature around 800°C in air. β-$FeSi_2$ has excellent potential in high temperature stability for high temperature thermoelectric devices even when using cast iron scrap chips as a starting material.

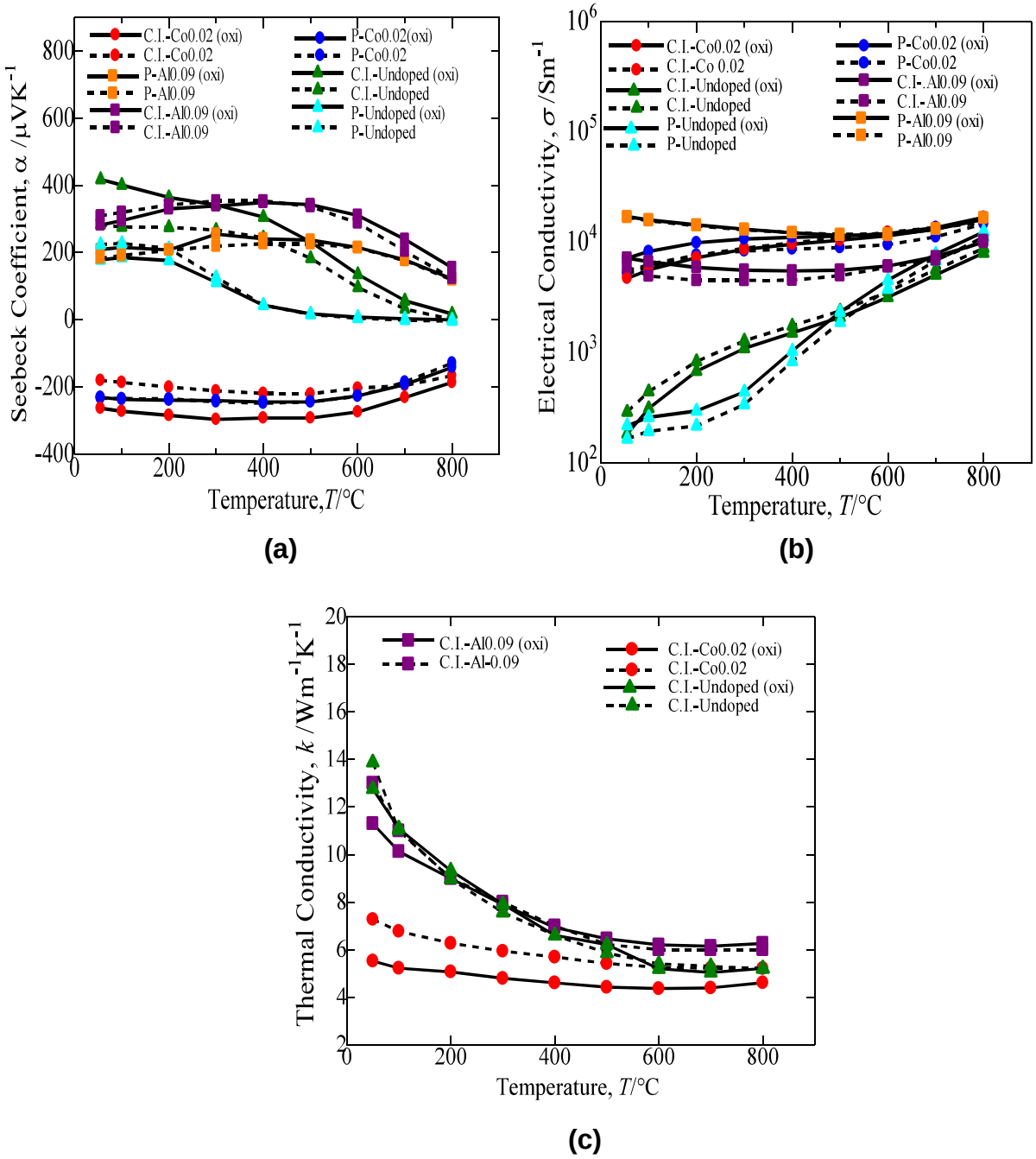

Figure 3.19 (a) Seebeck coefficient, **(b)** electrical conductivity and **(c)** thermal conductivity with the measuring temperature of annealed β-$FeSi_2$ specimens before and after high temperature oxidation at 800°C for 14 d in air.

3.3.5 Fabrication of thermocouple p-type and n-type β-$FeSi_2$ prepared utilizing cast iron scrap chips

Based on the results, the optimized Co substitution concentration for the n-type specimen is 0.94C.I.-0.06Co-1.86Si (C.I-Co0.06), which produces *ZT*= 0.22 at 700°C. For the p-type specimen, *ZT*= 0.17 at 800°C for 0.92C.I.-0.08Mn-1.86Si (C.I.-Mn0.08). Figure 3.20 (a) shows the image of thermocouple n-type C.I-Co0.06 and p-type C.I.-Mn0.08 β-$FeSi_2$ prepared utilizing cast iron scrap chips. As indicated in Figure 3.20 (b) is the illustration of thermocouple n-type and p-type β-$FeSi_2$ with dimensions 20 mm x 5mm for each module.

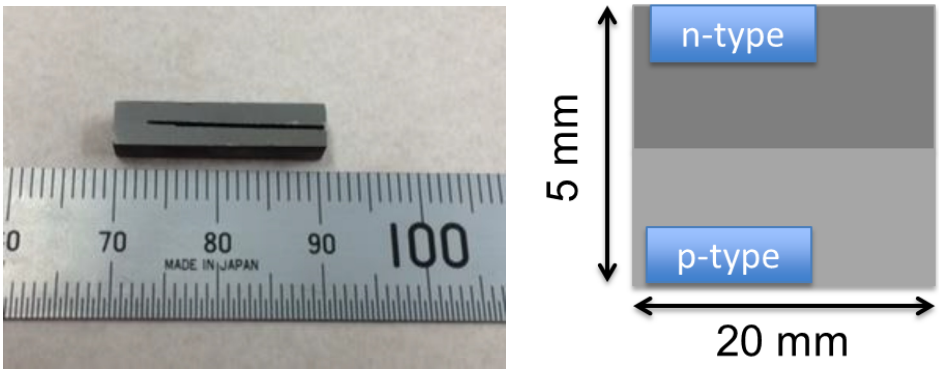

Figure 3.20 (a) Image of the thermocouple n-type and p-type β-$FeSi_2$ specimens prepared using cast iron srcap chips and **(b)** illustration of the thermocouple n-type and p-type β-$FeSi_2$ thermoelectric materials.

Figure 3.21 shows the SEM images of the microstructures for physical connected of n-type and p-type β-$FeSi_2$ specimens prepared using cast iron scrap chips. The SEM image of the thermocouple n-type and p-type β-$FeSi_2$ prepared from cast iron scrap chips showed excess Si particles (shown as black dots) with small pores (shown as white dots). Several black Si particles were detected in the β-phase matrix. Very few pores were detected in this sample. The pore size that could be observed from the SEM images was estimated to be less than approximately 10 µm. The open porosity observed in this thermocouple n-type and p-type was less than 1% after sintering, and we consider this to be dense samples. Thus, the thermocouple n-type

and p-type β-$FeSi_2$ specimens prepared using cast iron scrap chips with optimum Co and Mn substitution concentration was successfully fabricated, yet when using cast iron scrap chips as a starting material. Figure 3.22 shows the SEM images and the corresponding EDX elemental mapping results for thermocouple n-type and p-type β-FeSi2 specimens prepared using cast iron scrap chips (i) 0.94C.I.-0.06Co-1.86Si (C.I.-Co0.0.6) and (ii) 0.92C.I.-0.08Mn-1.86Si (C.I.-Mn0.08). It is clear that the distribution of the Co and Mn dopant concentrations in these specimens, as well as for the remaining annealed β-$FeSi_2$ prepared from cast iron scrap chips were uniformly dispersed throughout the β phase.

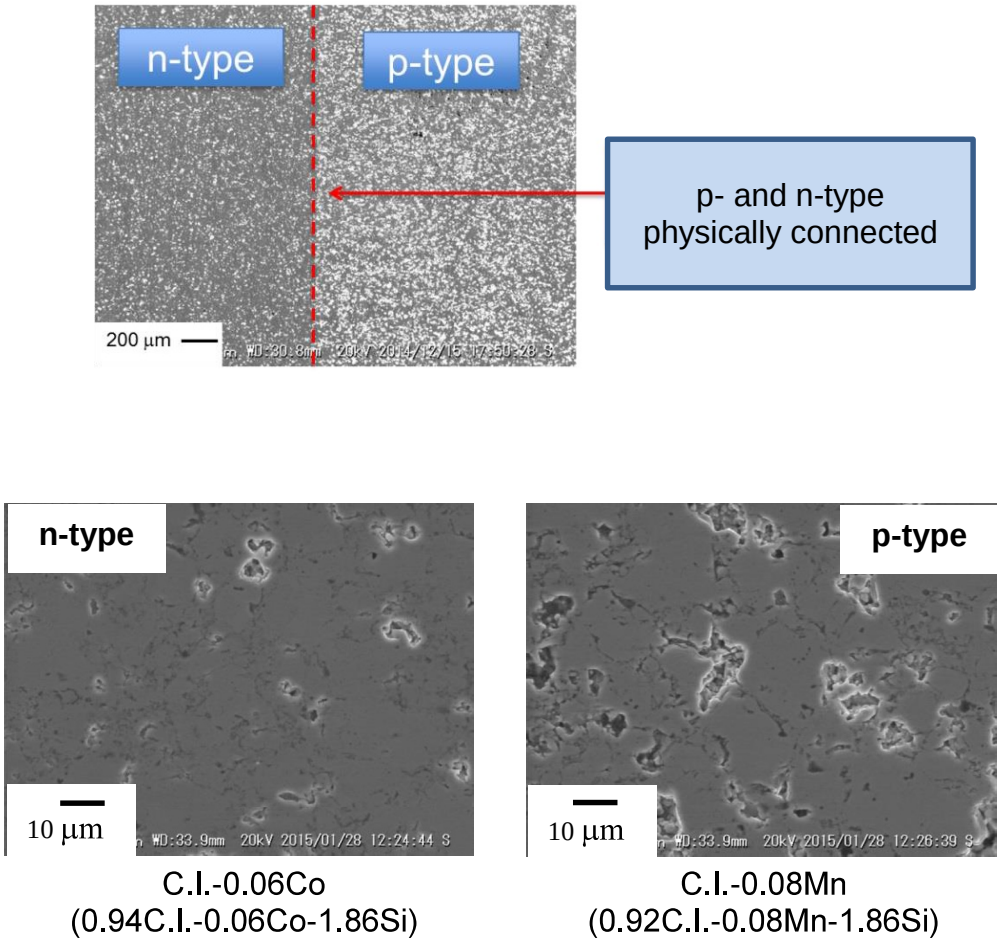

Figure 3.21 SEM images of the microstructure for thermocouple n-type and p-type β-$FeSi_2$ specimens prepared using cast iron scrap chips.

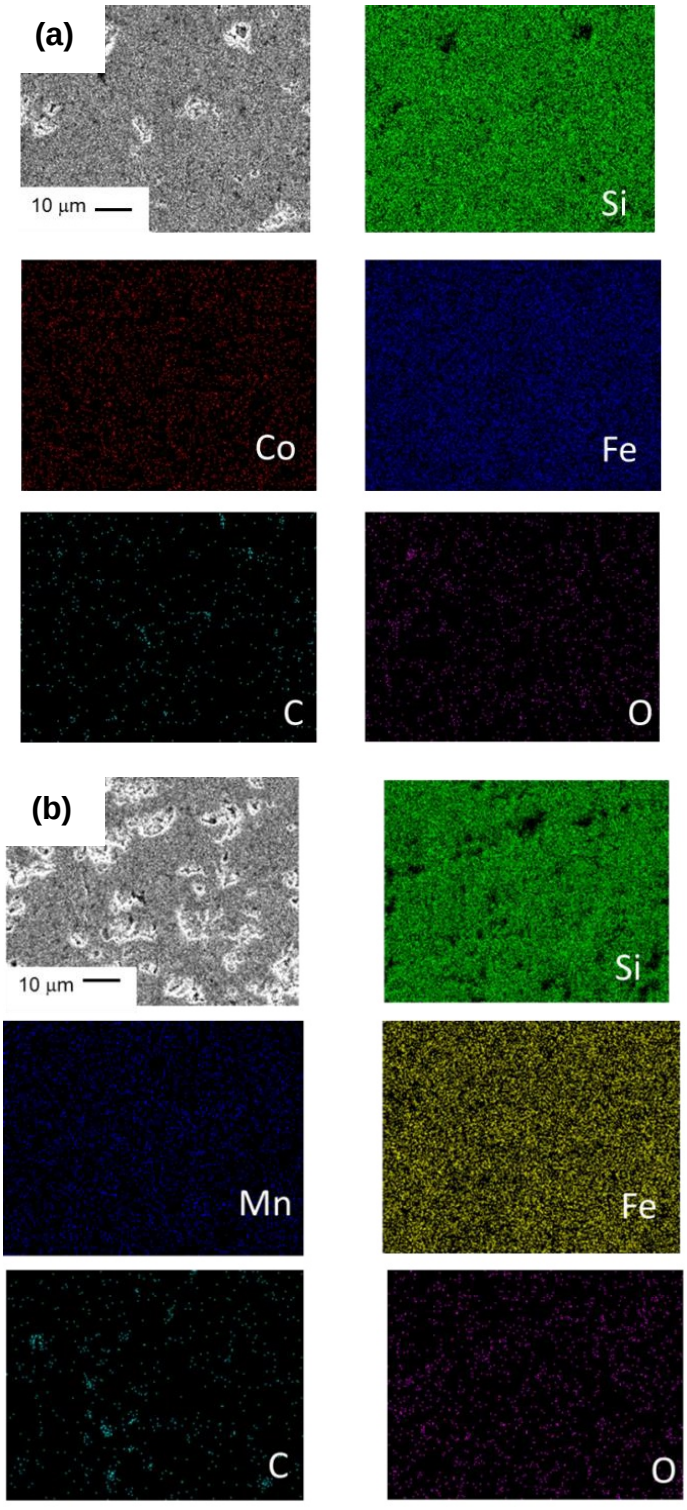

Figure 3.22 SEM image and EDX result of thermocouple n-type (a) C.I.-0.06Co (0.94C.I.-0.06Co-1.86Si) and p-type (b) C.I.-0.08Mn (0.94C.I.-0.08Mn-1.86Si) β-$FeSi_2$ samples prepared utilizing cast iron scrap chips.

3.3.6 Evaluation of coefficient thermal expansion of p-type and n-type β-$FeSi_2$ prepared utilizing cast iron scrap chips.

The coefficient of thermal expansion (CTE) is a key design parameter for thermoelectric, especially in energy harvesting applications since stresses generated by CTE mismatch, thermal gradient and the transients scale with the CTE of thermoelectric materials. CTE of materials is the tendency of materials to change in volume or linear or area in response to a change in temperature, through heat transfer. Thus, in the present study, the evaluation of CTE is obtained for β-$FeSi_2$ samples prepared utilizing cast iron scrap chips. Figure 3.23 presents the results of CTE value for β-$FeSi_2$ samples prepared utilizing cast iron scrap chips and pure Fe. It can be seen clearly, both n-type and p-type for β-$FeSi_2$ samples prepared utilizing cast iron scrap chips obtained approximately same value in CTE. The CTE of recycled ones has lower CTE value than the ones used the pure Fe. It may be caused by low CTE of SiO_2 since the specimens made from cast iron scrap chips are more easily to oxidized compared to the specimens made from pure Fe.

In addition, based on the results of CTE for n-type and p-type β-$FeSi_2$ samples prepared utilizing cast iron scrap chips showed the approximately CTE value highlights the less need for care in selecting interconnecting materials in the TE module to reduce the large stresses that can be induced by the thermal expansion mismatch. Thus, it is confirmed that both n-type and p-type β-$FeSi_2$ samples prepared utilizing cast iron scrap chips have sufficient mechanical integrity to survive the in-service conditions, even using cast iron scrap chips as a starting material.

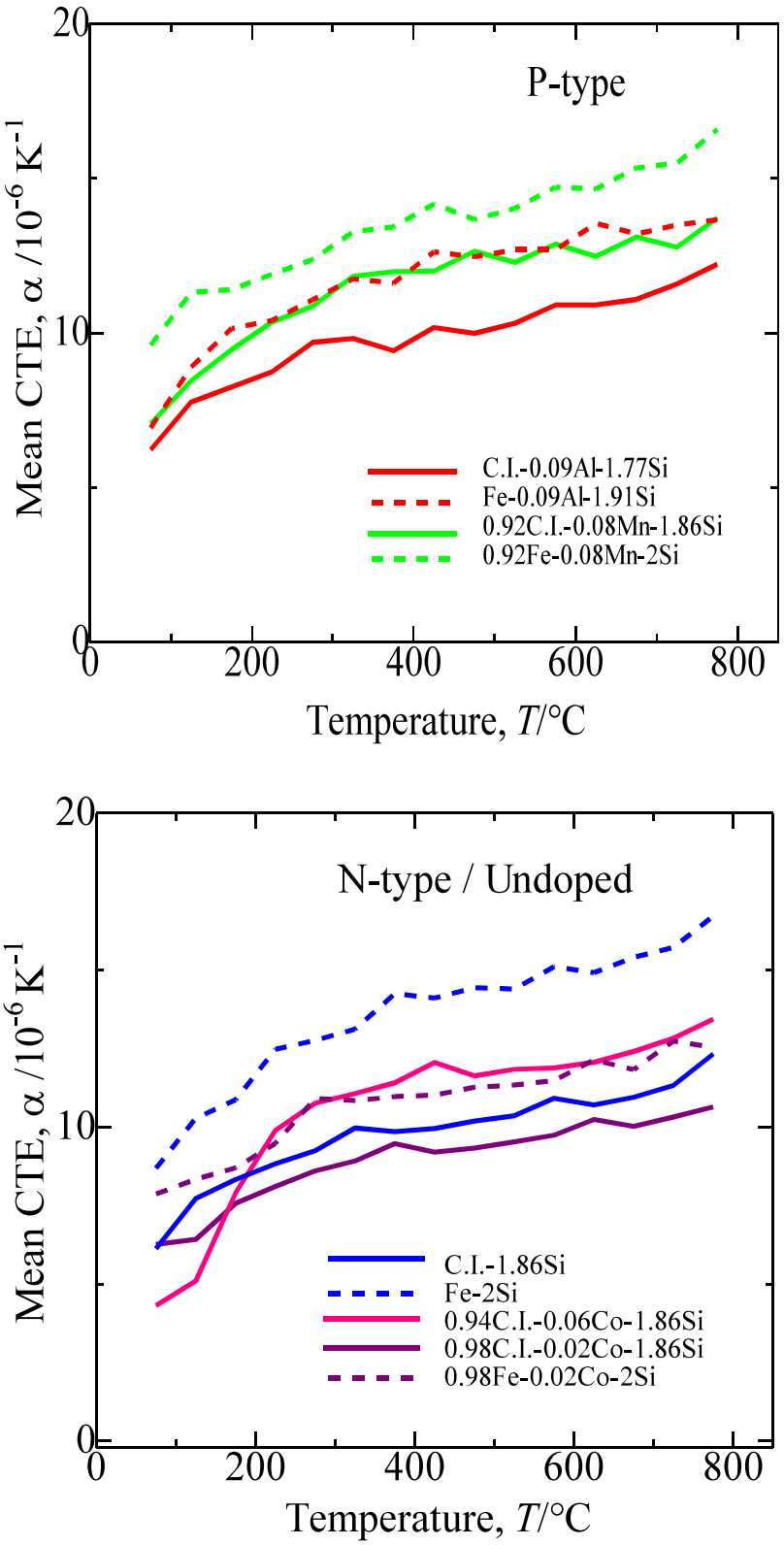

Figure 3.23 Coefficient of linear thermal expansion as a function of temperature for annealed β-$FeSi_2$ sample.

3.4 Discussion

Figure 3.4 reveals the results for the dimensionless figure of merit, *ZT,* for the n-type (0.02<Co<0.08) and (0.06<Mn<0.1) specimens, as well as for the p-type (0.09<Al<0.12) specimen. Based on the results, the optimized Co substitution concentration for the n-type specimen is 0.94C.I.-0.06Co-1.86Si (C.I-Co0.06), which produces *ZT*= 0.22 at 700°C. For the p-type specimen, *ZT*= 0.17 at 800°C for 0.92C.I.-0.08Mn-1.86Si (C.I.-Mn0.08). Therefore, there are some restrictions for the alloying elements in the β-$FeSi_2$ fabricated from cast iron scrap chips. For example, the metallic behavior (corresponding to an excessively high electrical conductivity) and a high sensitivity to dopant oxidation in the cast iron scrap chips could lead to decreases in the *ZT* value. To improve the thermoelectric performance of the p-type β-$FeSi_2$ prepared utilizing cast iron scarp chips, Mn (0.06<Mn<0.1) was chosen to replace Al (0.09<Al<0.12) as the dopant element for the p-type β-$FeSi_2$ specimen. In the case of the p-type specimen with Al doping (0.09<Al<0.12), it is important to avoid any oxidation during sintering. For Mn doping (0.06<Mn<0.1), the oxidation is not as severe [32]. It is difficult to control Al doping (0.09<Al<0.12) as a result of oxidation, especially when using cast iron scrap chips, as shown in Table 1. An optimum composition for the p-type 0.92C.I.-0.08Mn-1.86Si (C.I.-Mn0.08) and 0.94C.I.-0.06Co-1.86Si (C.I-Co0.06) specimens to provide the largest *ZT* value for the present system were determined. This effect is caused by the high affinity of Al to oxygen compared to the Mn and Co. The replacement of Al (0.09<Al<0.12) with Mn (0.06<Mn<0.1) as a concentration substitution in p-type β-$FeSi_2$ is quite effective for improving the thermoelectric performance in the β-$FeSi_2$ prepared from cast iron scrap chips. Hence, the conduction type and properties of β-$FeSi_2$ can be modified and improved, even when cast iron scrap chips are used as a starting material.

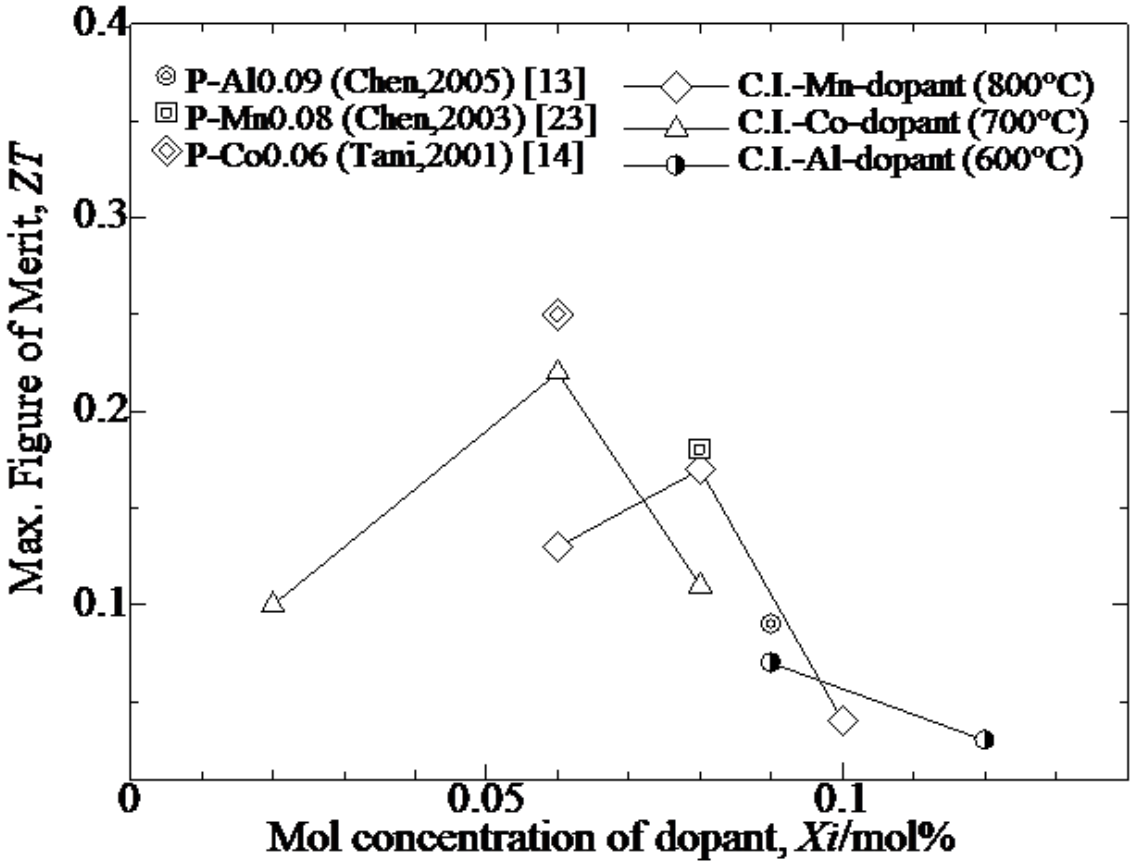

Figure 3.24 Effects of mol substitution concentration on dimensionless figure of merit of the annealed β-$FeSi_2$ samples with cast iron scrap chips at 900°C for 6 d.

The greatest insight into the nature of the chemical bonds in the β-$FeSi_2$ is obtained from spectroscopy measurements of the valence bands and comparing them with those of the pure constituents. Figure 3.25 (a) shows the X-ray photo spectroscopy (XPS) of C.I.-Al0.09 specimen after annealing at 900°C for 6 d and the excitation X-ray energies ranging from 63 to 723 eV. One peak at 74.5 eV is assigned to Al_2O_3 (oxide peak) respectively as an evidence for the previous argument. As described in the previous report [20], the Al doping element is not compatible with cast iron scrap chips because the ability to be more easier to oxidize during the preparation processes. Table 3.3 shows the comparisons of the valence bands for Al constituents in different samples. It is clearly seen that the peak of C.I-Al0.09 specimen is matched with the peak of Al_2O_3 in Al constituent. Thus, it is confirmed that the C.I-Al0.09 specimen contained oxide and tend to

decrease the thermoelectric properties. As compared with the XPS result of C.I.-Co0.02 specimen as shown in Figure 3.26 and Table 3.4, there is no oxide peak revealed in this sample and the thermoelectric performances also showed no significant change compared to that n-type β-$FeSi_2$ prepared using pure Fe. Thus, it is confirmed only Al-doped is not compatible with the cast iron scrap chips compared to that Co-doped, respectively.

Table 3.3 XPS spectrums of Al elements with different binding energy.

Element	Binding energy (eV)
Al (standard)	72.92 / 72.7
Al_2O_3	74.10
AlO(OH)	76
Al in C.I.-Al0.09 sample	74.10

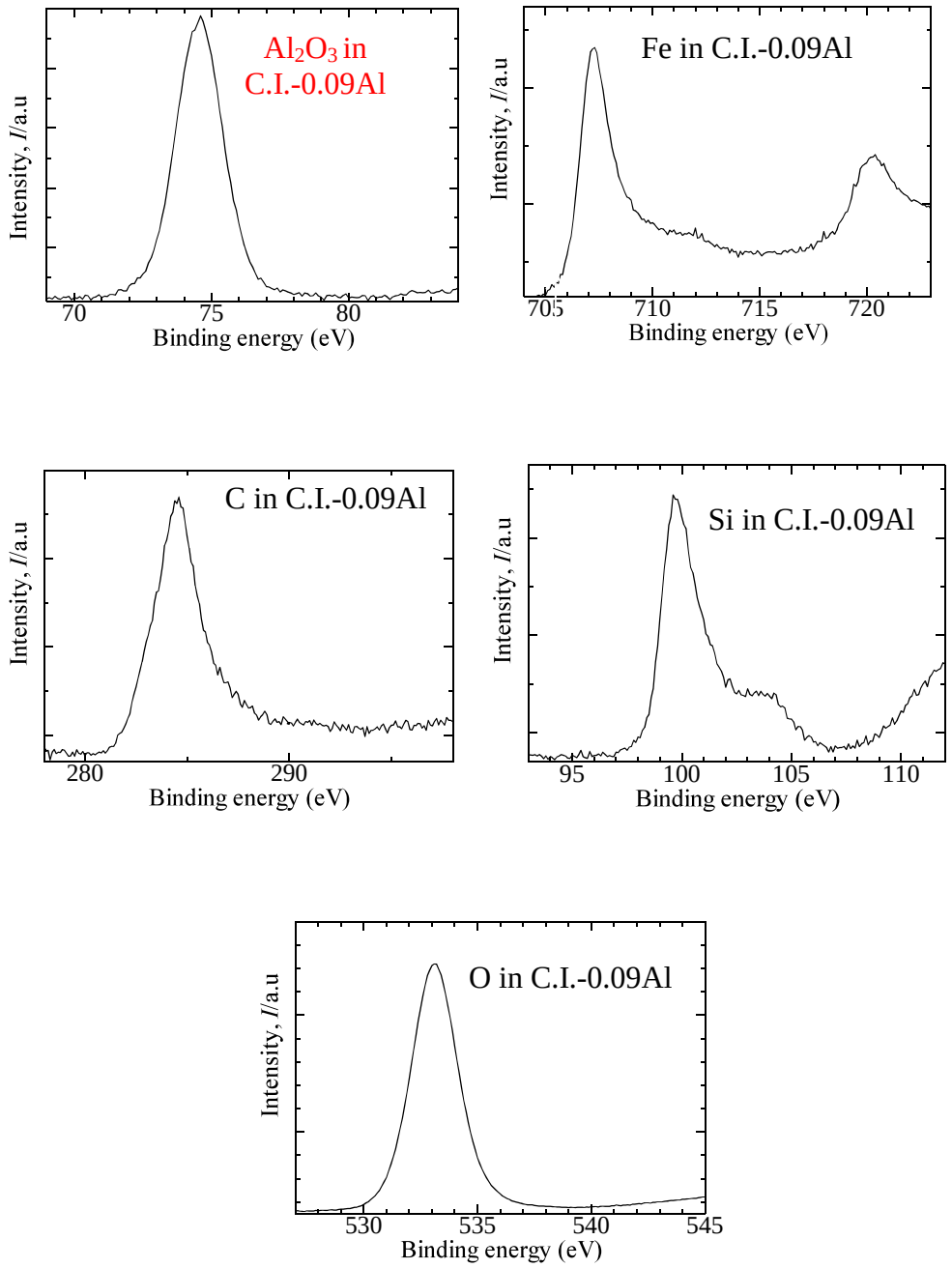

Figure 3.25 XPS spectrums of the annealed C.I.-0.09Al specimen at 900°C for 6 d.

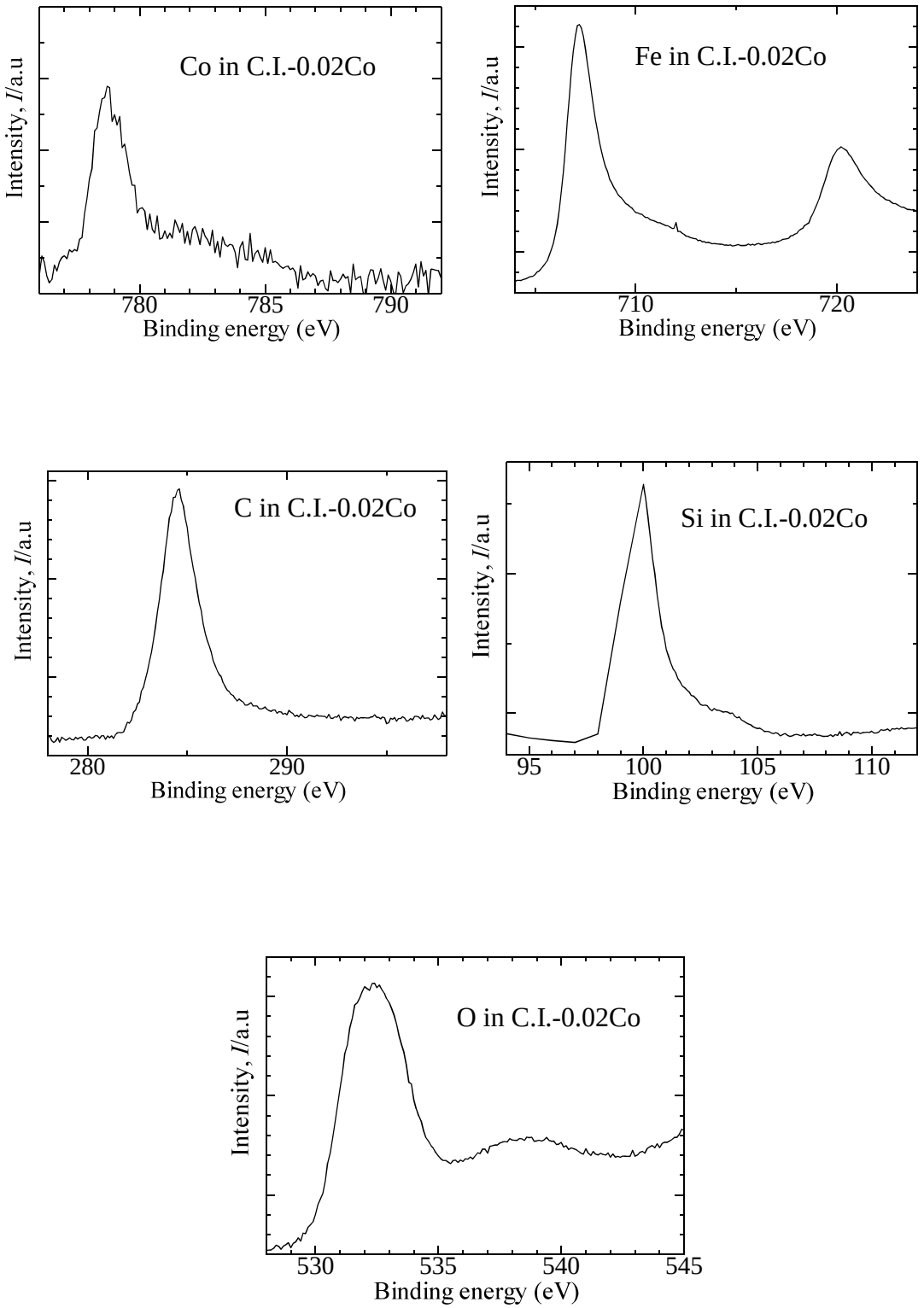

Figure 3.26 XPS spectrums of the annealed C.I.-0.02Co specimen at 900°C for 6 d

Table 3.4 XPS spectrums of C elements with different binding energy.

Element	Binding energy (eV)
C graphite (standard)	284.5/284.2
SiC alpha	282.5
CO_2	291.9
C in C.I.-Co0.02 sample	284.7

3.5 Conclusion

The thermoelectric properties of undoped, p-type and n-type β-$FeSi_2$ have been determined by measuring the Seebeck coeefficient, α, electrical conductivity, σ, and thermal conductivity, k, from room temperature to 800°C. The thermoelectric properties are strongly affected by the Co-doped (0.02<Co<0.08) substitution concentration (for n-type specimens) and Mn-doped (0.06<Mn<0.1) substitution concentration (for p-type specimens). The dimensionless figure of merit for the n-type 0.94C.I.-0.06Co-1.86Si (C.I-Co0.06) and the p-type 0.92C.I.-0.08 Mn-1.86Si (C.I.-Mn0.08) β-$FeSi_2$ achieved approximately 90% performance compared with β-$FeSi_2$ synthesized from pure Fe and was improved by approximately a factor of two compared with the p-type C.I.-0.09Al-1.77Si (C.I.-Al0.09) and n-type 0.948C.I.-0.02Co-1.86Si (C.I.-Co0.02) specimens that have been published previously [20]. Thus, the objective of this study to evaluate the effect of doping elements in β-$FeSi_2$ prepared utilizing cast iron scrap chips was successfully achieved, and an optimum thermoelectric performance was determined. Compared with the p-type 0.92C.I.-0.08 Mn-1.86Si (C.I.-Mn0.08) specimens prepared from cast iron scrap chips, the n-type 0.94C.I.-0.06Co-1.86Si (C.I-Co0.06) specimen possessed a high electrical conductivity, low thermal conductivity and a high dimensionless figure of merit, ZT = 0.22, at a measurement temperature of 700°C due to the high carrier concentration and optimum substitution concentration. The achieved ZT is assumed to be comparatively the same for β-$FeSi_2$ thermoelectric materials made

from pure Fe. The optimum value of *ZT* obtained in the present study is preferable for use as a starting material to produce β-$FeSi_2$ thermoelectric materials and showed promise as an eco-friendly and cost-effective production process for thermoelectric materials. We conclude that the cast iron scrap chips were successful at fabricating p-type 0.92C.I.-0.08 Mn-1.86Si (C.I.-Mn0.08) and n-type 0.94C.I.-0.06Co-1.86Si (C.I-Co0.06) β-$FeSi_2$ thermoelectric materials and that optimum thermoelectric performances were determined that were comparable with the previously reported results. Thus, the physical connected of n-type and p-type β-$FeSi_2$ specimens prepared using cast iron scrap chips with optimum Co (C.I-Co0.06) and Mn (C.I.-Mn0.08) substitution concentration was successfully fabricated, yet when using cast iron scrap chips as a starting material. As well, the thermoelectric β-$FeSi_2$ prepared using cast iron scrap chips has probably a long lifetime at high temperature around 800°C in air and has excellent potential in high temperature stability for high temperature thermoelectric devices even when using cast iron scrap chips as a starting material. In addition, based on the results of CTE for n-type and p-type β-$FeSi_2$ samples prepared utilizing cast iron scrap chips showed the approximately CTE value highlights the less need for care in selecting interconnecting materials in the TE module to reduce the large stresses that can be induced by the thermal expansion mismatch. However, Al doping (0.09<Al<0.12) is not suitable for use with cast iron scrap chips as a starting material for β-$FeSi_2$ thermoelectric materials due to the tendency of the Al dopant (0.09<Al<0.12) to be oxidized during machining.

3.6 References

1. Nishida, I. A. (Eds.). (2001). *Thermoelectric –principles and applications (pp. 199)*. Tokyo, Jp: Realiza Inc.
2. Cho, W. S., Choi, S. W., & Park, K. (1999). Microstructure and thermoelectric properties of p-type $Fe_{0.9}Mn_{0.1}Si_2$ compounds prepared by pressureless sintering, *Mater.Sci. Eng., B68*, 116–122.
3. Ito, M., & Takiguchi, Y. (2005). Thermoelectric properties of p-type $Fe_{0.9}Mn_{0.1}Si_2$ with rare-earth oxide addition, *Materials Transactions, 46*, 1497–1501.
4. Ivanenko, L., Shaposhnikov, V., Filonov, A., Krivosheeva, A., Borisenko, V., Migas, D., Miglio, L., Behr, G., & Schumann, J. (2004). Electronic properties of semiconducting silicides: fundamentals and recent predictions, *Thin Solid Films, 461,*141–147.
5. Kanda, T., Mukojima, M., Aoyama, I., & Ishimabushi, H. (2004). Kinzoku, 74, 793.
6. Deal, B. E., & Grove, A. S. (1965). *J. Appl. Phys., 36,* 3770.
7. Ware, R. M., & McNeil, D. J. (1964). Iron silicide as a thermoelectric generator material, *Proc Inst Elect Eng,111*, 178–182.
8. Stolt, T. et al., (1990). Oxidation of titanium, manganese, iron, and niobium silicides: Marker experiments, *J. Appl. Phys., 68*, 5133.
9. Chang, S. H., Nanko, M., Matsumaru, K., Ishizaki, K., & Takeda, M. (2006). High temperature oxidation of sintered β-$FeSi_2$ bodies at elevated temperatures, *J. Jpn. Inst. Metals, 70,* 20–24.
10. Nanko, M., Chang, S. H., Matsumaru, K., Ishizaki, K., & Takeda, M. (2006). Isothermal Oxidation of Sintered β-$FeSi_2$ in Air, *Materials Science Forum, 522,* 641–648.
11. Ito, M., Nagai, H., Oda, E., Katsuyama, S., & Majima, K. (2002). Effects of p doping on the thermoelectric properties of β-$FeSi_2$. *J. Appl. Phys., 91*,2138–2142.
12. Kim, S. W., Cho, M. K., Mishima, Y., & Choi, D. C. (2003). High temperature thermoelectric properties of p- and n-type β-$FeSi_2$ with some dopants. *Intermetallics, 11*, 399–405.
13. Chen, H. Y., Zao, X. B., Zhu, T. J., Lu, Y. F., Ni, H. L., Muller, E., & Mrotzek, A. (2005). Influence of nitrogenizing and Al-doping on microstructures and thermoelectric properties of iron disilicide materials. *Intermettallics, 13*, 704–709.

14. Tani, J., & Kido, H. (2001). Thermoelectric Properties of β-$Fe_{(1-x)}Co_xSi_2$ Semiconductors. *J. Appl. Physics., 40*, 3236–3239.
15. Ito, M., Nagai, H., Tahata, T., Katsuyama, S., & Majima, K. (2002). Effects of Zr substitution on phase transformation and thermoelectric properties of β-$FeSi_2$. *J. Appl. Phys., 92,* 3217–3222.
16. Ware, R. M., & McNeill, D. J. (1964). *Proc. IEE,111*, 178.
17. Jiang, J. X., Sasakawa, T., Matsugi, K., Sasaki, G., & Yanagisawa, O. (2005). Thermoelectric properties of β-FeSi2 with Si dispersoids formed by decomposition of α-Fe_2Si_5 based alloys. *J. Alloy. Compd., 391*, 115–122.
18. Nogi, K., & Kita, T. (2000). Influence of copper addition to Fe_2Si_5 on thermoelectric properties of iron-silicides produced by spark-plasma sintering. *J. Mat. Sci., 35*, 862–869.
19. Ur, S. C. (2003). Mechanical Alloying and Thermoelectric Properties of Co doped $FeSi_2$, *Twenty Second International Conference on Thermoelectric-ICT*, 149-152.
20. Laila, A., Nanko, M., & Takeda, M. (2014). Upgrade recycling of cast iron scrap chips towards β-$FeSi_2$ thermoelectric materials, *Materials, 7*, 6304–6316.
21. Laila, A., & Nanko, M. (2014). Characterization of cast iron scrap chops toward towards β-$FeSi_2$ thermoelectric materials*. Materials Science Forum, 804*, (2015), 3–6.
22. He, Z., Platzek, D., Stiewe, C., Chen, H., Karpinski, G., & Muller, E. (2007). Thermoelectric properties of hot-pressed Al and Co doped iron disilicide materials. *J. Alloy. Compd., 438*, 303–309.
23. Chen, H. Y., Zhao, X. B., Lu, Y. F., Mueller, E., & Mrotzek, A. (2003). Microstructures and thermoelectric properties of $Fe_{0.92}Mn_{0.08}Si_x$ alloys prepared by rapid solidification and hot pressing. *J. Appl. Physics., 94*, 15.
24. Ito, M., Nagai, H., Tahata, T., Katsuyama, S., & Majima, K. (2002). Effect of Zr substitution on phase transformation and thermoelectric properties β-$FeSi_2$. *J. Appl. Physics. Stat., 92,* 3217.
25. Yamashita, O., Tomiyoshi, S., & Sadatomi, N. (2003). Thermoelectric properties of p- and n-type $FeSi_2$ prepared by spray drying, compaction and sintering technique. *J. Mater. Sci., 38*, 1623–1629.

26. Goldsmid, H. J. (Eds.). (1995). *CRC Handbook of thermoelectricity.* Boca Raton: CRC Press.
27. Nagai, H., Katsura, T., Katsuyama, S., Majima, K., & Ito, M. (1998). Thermoelectric properties of β-$FeSi_2$ mechanically alloyed with Si and C. *J. Mat. Trans., 39,* 1140–1145.
28. Bartur, M., & Nicolet, M. A.(1982). *Appl. Phys. Lett*., *40*, 175
29. Strydom, W. J., & Lombaard, J. C. (1985). *Thin Solid Films, 131*, 125.
30. Isoda, Y., Imai, Y., & Shinohara, Y. (2003). *J. Jpn. Inst. Met., 67*, 410.
31. Asanabe, S., Shinoda, D., & Sasaki, Y. (1964). *Phys. Rev., 134*, 774.
32. Nishida, I. (1972). Study of semiconductors to metal transition in Mn-doped $FeSi_2$, *Phys. Rev., B7,* 2710.

Chapter 4: Development of eco-friendly Fe_2VAl thermoelectric materials prepared utilizing cast iron scrap chips

4.1. Introduction

Effective use of waste heat where more than 60% of the original energy is released into the atmosphere is being sought against the recent social background. For examples the concerns over the future supply of energy and the emergence of environmental issues. In order to effectively utilize the low temperature, small scale and widely scattered of waste heat, the thermoelectric generation which has a conversion of efficiency independent to energy scale and capable to convert the thermal energy to the electricity will provide the solution [1]. Thermoelectric materials have recently attracted renewed interest for their potential applications in a waste heat recovery system without any harmful emission. Thermoelectric material consists of abundant and cheap elements are required for the widespread use of devices.

The Heusler-type intermetallic compound Fe_2VAl has received intense attention because of the occurrence of a semiconductor-like temperature dependence of electrical resistivity over a wide temperature range up to 1200 K and above. Fe_2VAl is also one of a promising candidate for thermoelectric semiconductors due to its rich resources, good mechanical strength and high electrical response [2]. In addition, Fe_2VAl has thermoelectric power generation near room temperature because of its high power factor compared to the conventional thermoelectric materials, such as Bi-Te and Pb-Te [3]. Fe_2VAl is a semimetal with a narrow pseudogap at the Fermi level [4-5]. Thus, small stoichiometries deviations could cause large changes in transport properties [6]. The methods for controlling the pseudogap in Fe_2VAl have been reported by several researchers, such as change its stoichiometry in chemical composition [7-8] and substitute the fourth element [9-16]. These proposed methods increase the absolute values of Seebeck coefficient and reduce the electrical resistivity of Fe_2VAl, however thermal conductivity is comparatively large. As a result, the small *ZT* will be obtained and it is essential to decrease the thermal conductivity for obtaining high performance of Fe_2VAl. The arc-melting method based on ingot metallurgy [6-9], mechanical alloying [14-16] and the combination of them [10] are the conventional

fabrication processes of Fe_2VAl. In these conventional methods, the metal powders with high impurity such as pure Fe is required as a raw material to synthesize Fe_2VAl which is resulting in high costs of the final products.

Cast iron is essentially an iron-carbon alloy containing more than 2 mass% carbon, 1-3 mass% silicon, manganese, sulphur and phosphorus, which modify the structure and properties of the resulting alloy markedly [17]. It used in the oil and gas industry for making water conduit pipes, packer parts, boilers, valve bodies and valve parts. During the mechanical processing, the cast iron scrap chips were generated due to the machining operations. Recycling of cast iron scrap chips is an interesting subject because it can be utilized as starting materials for preparing an iron based material, β-$FeSi_2$ and Fe_2VAl. We have already proposed upgrade recycling of cast iron scrap chips towards β-$FeSi_2$ thermoelectric materials [18-20]. Thus, in the present study, the upgrade recycling of cast iron scrap chips towards eco-friendly Fe_2VAl thermoelectric materials is promoted. The thermoelectric performance and the physical characterizations of Fe_2VAl synthesized from cast iron scrap chips for undoped and p-type were evaluated. The purpose of this report is to reveal that the cast iron scrap chips can be utilize as a starting material for fabricating other iron based materials such as Fe_2VAl and prevailed comparable thermoelectric performance to that previously reported.

4.2 Experimental Procedure

The numerical chemical compositions were cast iron (C.I.) or Fe: V: Al= 2: 1: 1 for undoped, cast iron (C.I.) or Fe: V: Ti: Al= 2: 0.9: 0.1: 1 for p-type and (C.I.) or Fe: V: Al: Si= 2: 1: 0.9: 0.1 for n-type. The starting materials for undoped and p-type Fe_2VAl were prepared by the solid-state reaction technique of cast iron scrap chips (The prefix "C.I." presumably stands for "cast iron scrap chips"), silicon grains (purity:99.99%), vanadium grains (purity:99.99%), powders of dopant element Ti (purity:99%) for p-type and powders of dopant element Si (purity:99.99%) for n-type. The powder mixture underwent a solid-state reaction at 1200°C for 12 h in vacuum.

The reacted powder was prepared by using a rotary dry ball milling for 1 d. Then, the reacted powder was directly put in a die and consolidated by using a pulsed electric current sintering technique at 950°C for 10 min in vacuum under an uni-axial pressure of 80 MPa. Sintered specimens were annealed at 900°C for 2 d and 450°C for 6 h in a vacuum to obtain the homogenized and the Heusler phase. The phase composition and morphology of specimens was observed by a scanning electron microscope (SEM) and electron probe micro analyzer (EPMA). The X-ray diffraction (XRD) analysis of specimens was conducted for phase identification by X-ray diffractometer.

The thermoelectric properties of sintered Fe_2VAl were evaluated by measuring Seebeck coefficient, α, electrical conductivity, σ, and thermal conductivity, k. The Seebeck coefficient and electrical conductivity were measured by a DC standard four probe method and the steady-state temperature gradient (ZEM-2, Ulvac Co.) from room temperature to 500°C in a stream of He gas. The thermal conductivity was calculated from measured heat capacity and thermal diffusivity by the laser flash method using the thermal constant analyzer (LFA 457 Micro Flash) in a temperature range from room temperature to 500°C under the vacuum.

4.3. Results

4.3.1. Physical characterization

Table 1 shows the density and porosity data of sintered specimens for undoped and p-type Fe_2VAl prepared by utilizing pure Fe and cast iron scrap chips. This result indicates that the open porosity for all samples was below 1% after sintering.

Table 4.1 Porosity data for the sintered Fe_2VAl samples.

Numerical Chemical Composition	Archimedes Measurement	
	Density	Open porosity
2Fe-V-Al (Undoped)	6.34 g/cm^3	0.1%
2C.I.-V-Al (Undoped)	6.14 g/cm^3	0.1%
2Fe-0.9V-0.1Ti-Al (p-type)	6.23 g/cm^3	0.4%
2C.I.-0.9V-0.1Ti-Al (p-type)	6.10 g/cm^3	0.3%
2Fe-V-0.9Al-0.1Si (n-type)	6.20 g/cm^3	0.3%
2C.I.-V-0.9Al-0.1Si (n-type)	6.09 g/cm^3	0.2%

Figure 4.1 shows the XRD pattern of solid-state reacted powder and annealed samples of Fe_2VAl prepared by utilizing pure Fe and cast iron scrap chips. The prefix "C.I." presumably stands for "cast iron scrap chips", which denotes those alloys formed from cast iron scrap chips. The XRD pattern of solid-state reacted powder showed the $D0_3$-type Fe_3Al crystal structure. After annealing treatment, it is seen that the diffraction spectra in these alloys were identified in the expected $L2_1$ structure, the Heusler-type appear in a lower 2θ angle such as 111 and 200. This result indicates that the Heusler structural Fe_2VAl alloy is obtained. However, traces of an impurity phase or secondary phase was observed such as the oxides of Al_2O_3, V_2O_5 and V_2O_3.

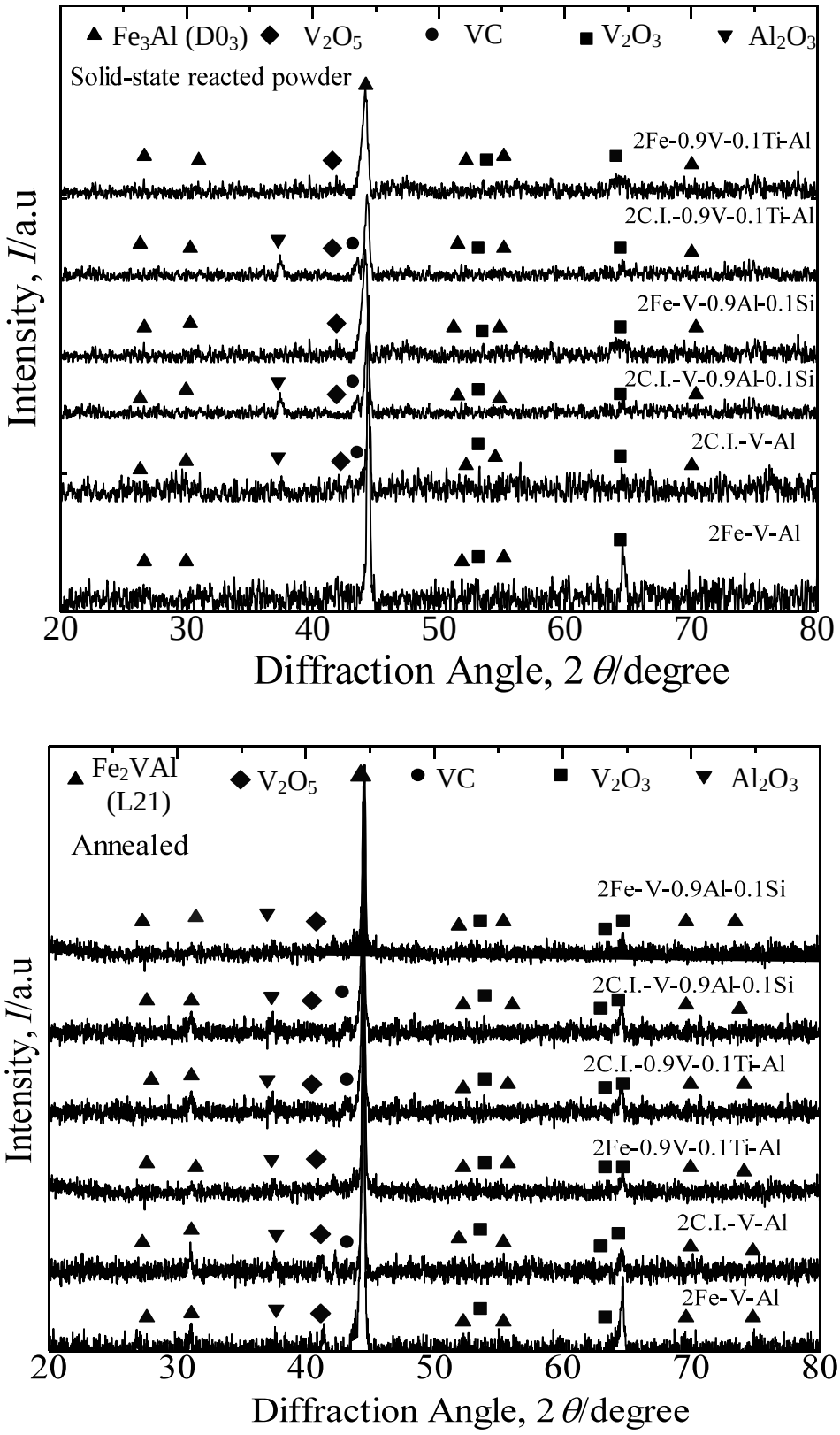

Figure 4.1 XRD patterns of the heat-treated powder and annealed Fe_2VAl samples at 900°C for 2 d and 450°C for 6 h.

Figure 4.2 provides the SEM microstructures for annealed Fe_2VAl alloys prepared using pure Fe and cast iron scrap chips, respectively. The SEM images of annealed Fe_2VAl prepared from cast iron scrap chips shows larger segregation of oxide, which might be V_2O_3 or V_2O_5 phase. On the other hand, several black particles of Al_2O_3 were scarcely detectable in Fe_2VAl samples prepared using pure Fe and cast iron scrap chips. The pore size that could be observed from the SEM images was smaller than 10 µm. The open porosity as provided in Table 4.1 observed in all samples were below 1% after sintering and thus regarded as dense samples.

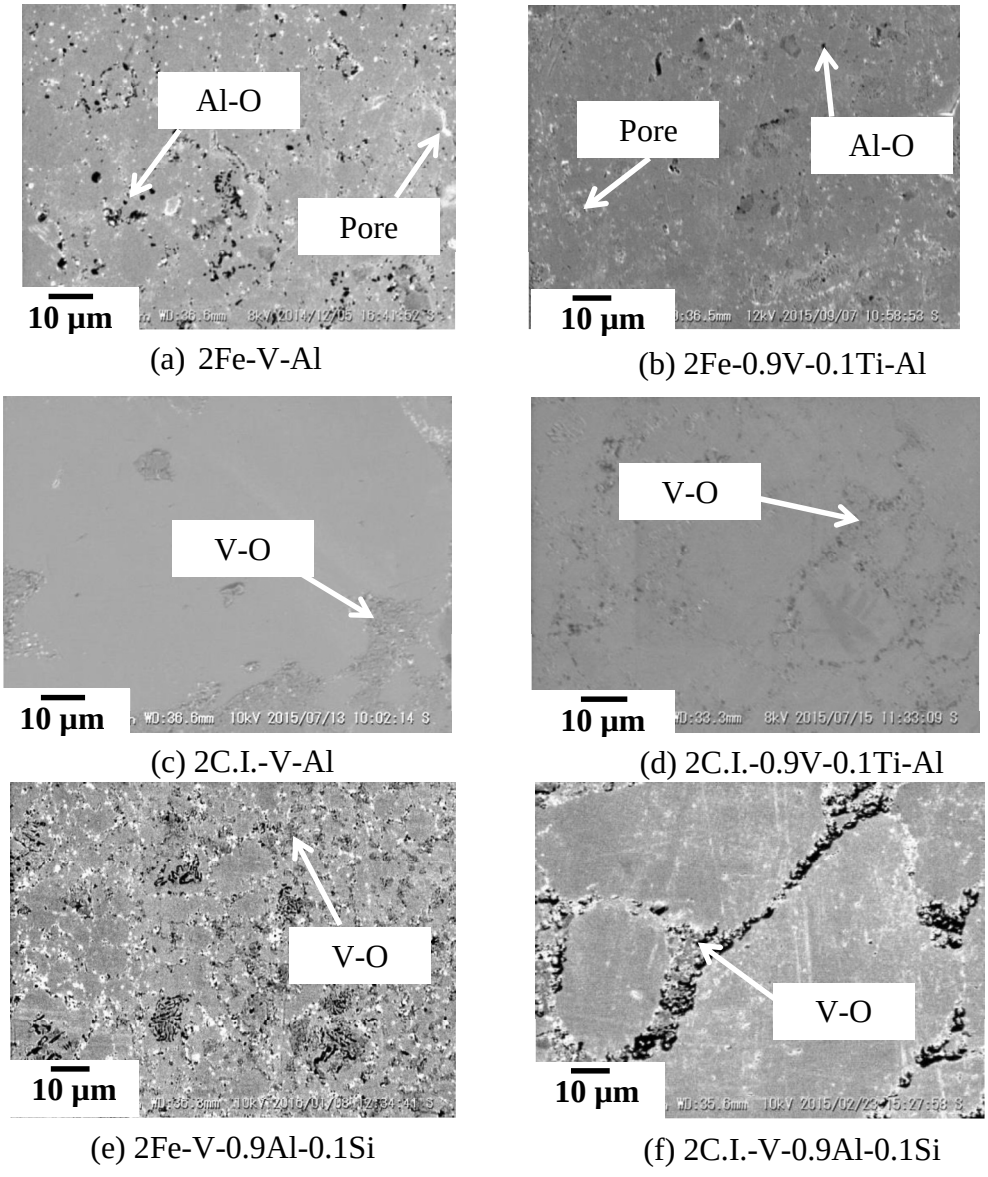

Figure 4.2 SEM microstructures of the annealed Fe_2VAl samples at 900°C for 2 d and 450°C for 6 h.

Figure 4.3 shows SEM images and elemental mapping images of the undoped and p-type Fe_2VAl prepared using cast iron scrap chips. The presence of oxides in the matrix is considered to be caused by the easiest ability of Al or V element to be oxidized during sintering since the cast iron scrap chips are strongly oxidized by machining. This is the most likely oxidation of the undoped and p-type Fe_2VAl samples made from cast iron scrap chips were caused by impurity oxygen in cast iron scrap. Another possibility about the presence of oxide in the specimens is the size of V was 75 µm which was larger than that cast iron scrap chips (<100 µm but easy to break during ball milling process), Fe (3-5 µm), Al (3 µm) and Ti (3 µm). This shows that the inside of the product cannot be diffused completed. To obtain perfectly homogenized Fe_2VAl smaller size V and longer heat treatment will be needed [2].

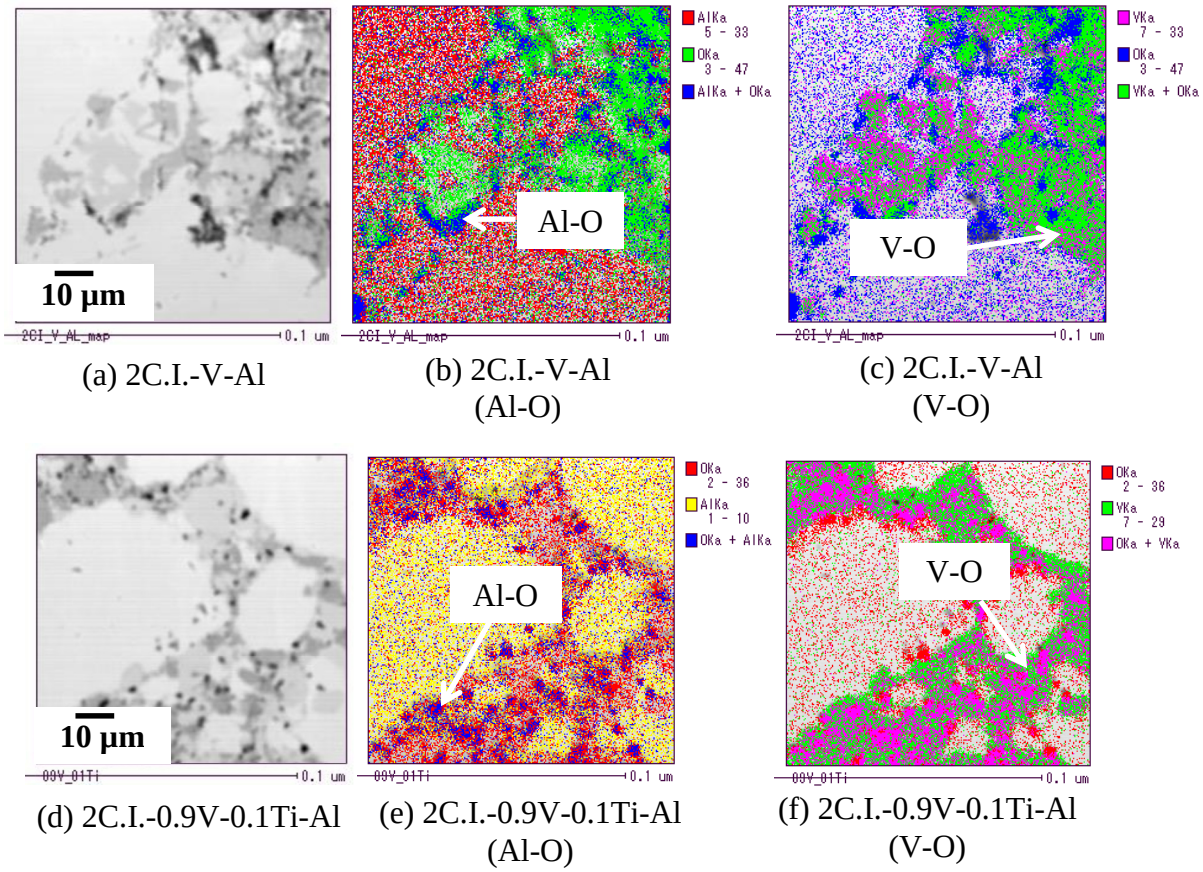

(a) 2C.I.-V-Al (b) 2C.I.-V-Al (Al-O) (c) 2C.I.-V-Al (V-O)

(d) 2C.I.-0.9V-0.1Ti-Al (e) 2C.I.-0.9V-0.1Ti-Al (Al-O) (f) 2C.I.-0.9V-0.1Ti-Al (V-O)

Figure 4.3 EPMA analyzed, elemental mapping images for O, V and Al of the annealed Fe_2VAl samples prepared by utilizing cast iron scrap chips.

4.3.2. Thermoelectric performance

Figure 4.4 shows the temperature dependence of the Seebeck coefficient of the annealed Fe_2VAl specimens between room temperature to 500°C. The Seebeck coefficient, α value of undoped, p-type and n-type Fe_2VAl prepared utilizing cast iron scrap chips are found to be positive in the entire temperature range in the present study. Such a finding suggests that the dominant carriers are hole-type in Fe_2VAl, being consistent with the previous results [6,8]. This is also in good agreement with the band-structure calculations, which revealed the existence of large hole pockets near the Fermi level density of states (DOS) in Fe_2VAl [4,5]. Upon heating, intrinsic electrons and holes are excited. If the holes have slightly higher mobility than the electrons in these materials, the p-type carriers will eventually govern the thermal transport, leading the positive α values at high temperature [5]. In addition, the upward shift of E_F will cause a higher activated energy for the hole carriers thermally excited across the pseudogap. The Seebeck coefficient values of undoped Fe_2VAl prepared using cast iron scrap chips is positive and centered around 20 μV/K since the majority carriers are holes [26], but the number of carriers and hole pockets are nearly compensated [26]. Furthermore, the Seebeck coefficient values of p-type Fe_2VAl prepared using cast iron scrap chips was about 10% smaller than those previously reported [21,22]. This reduction was attributed to the small difference in the off-stoichiometric of the specimen since the compositions of cast iron scrap chips contain some impurities. However, in this report, the n-type Fe_2VAl specimen made from cast iron scrap chips could not possible to fabricate due to the influence of some impurities in cast iron scrap chips since the compositions of cast iron scrap chips contain some impurities such as Si, Mn and C. The influence of these impurities could change the conduction type of 2Fe-V-0.9Al-0.1Si specimen prepared using cast iron scrap chips from n-type to p-type. For examples, Mn or C might be considered to be an acceptor dopant, however, Si is considered to be donor dopant by substituting Al site.

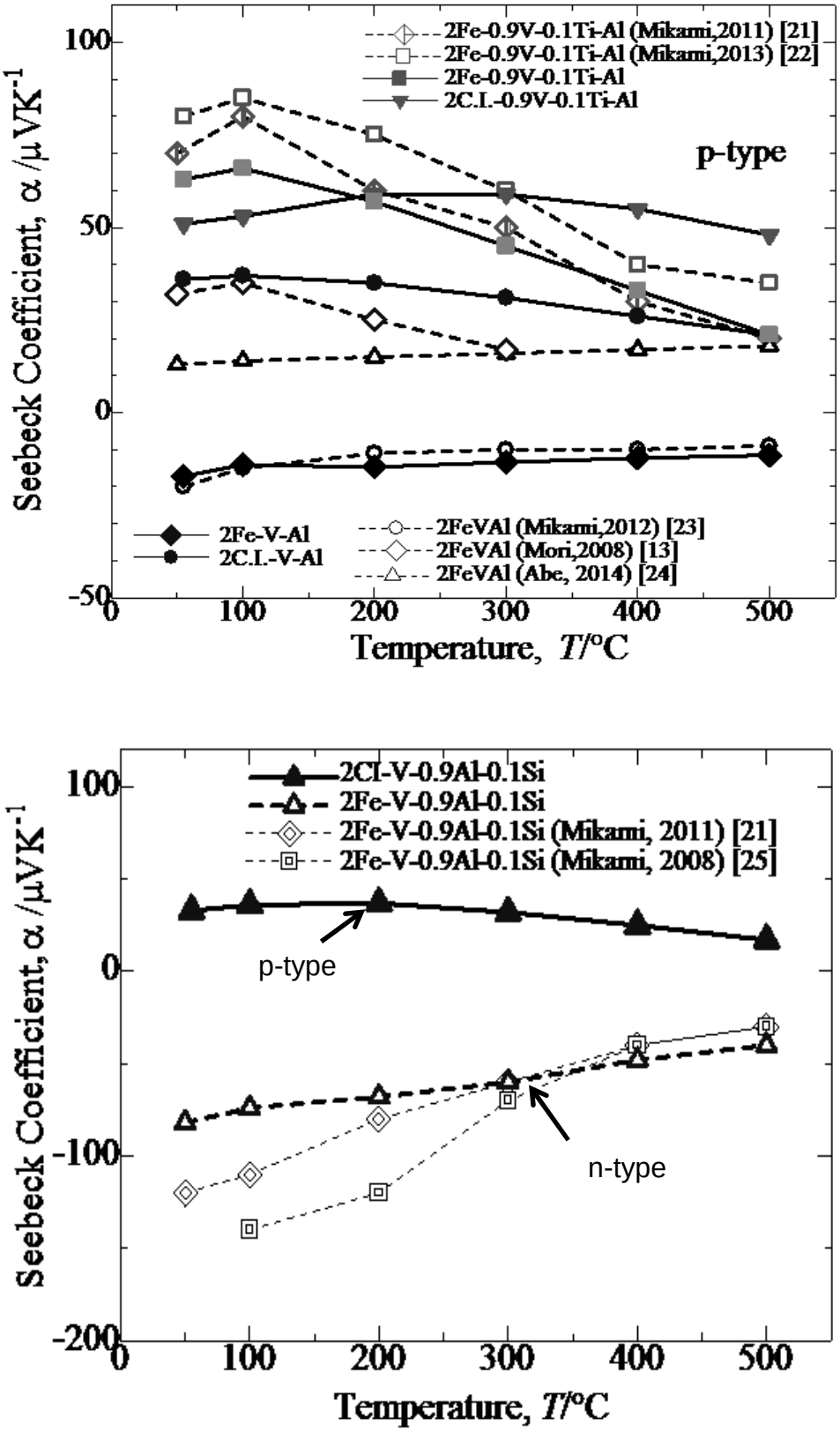

Figure 4.4 Temperature dependence of Seebeck coefficient, α, for the annealed Fe_2VAl samples at 900°C for 2 d and 450°C for 6 h.

Figure 4.5 provides the temperature dependence of electrical conductivity of the annealed Fe_2VAl specimens between room temperature to 500°C. The electrical conductivity, σ value of the Fe_2VAl specimens prepared using cast iron scrap chips exhibits a rather semiconductor-like dependence on temperature. Furthermore, the electrical conductivity values of p-type Fe_2VAl prepared using cast iron scrap chips was about 30% higher than those previously reported [21,22]. The temperature dependence of the electrical conductivity could be attributed to the carrier mobility, which decreased with the temperature increase, since the acceptor were exhausted and the scattering of the carrier by lattice vibration. Thus, it is confirmed that the Fe_2VAl specimens made from cast iron scrap chips obtained a positive impact on the electrical conductivity as compared with others reported in the literature [13,21-24] even cast iron scrap chips were used as a starting material. Nevertheless, in this report, the n-type Fe_2VAl specimen made from cast iron scrap chips could not possible to manufacture due to the influence of some impurities in cast iron scrap chips since the compositions of cast iron scrap chips contain some impurities such as Si, Mn and C. For instances, Mn or C might be considered to be an acceptor dopant, however, Si is considered to be donor dopant by substituting Al site.

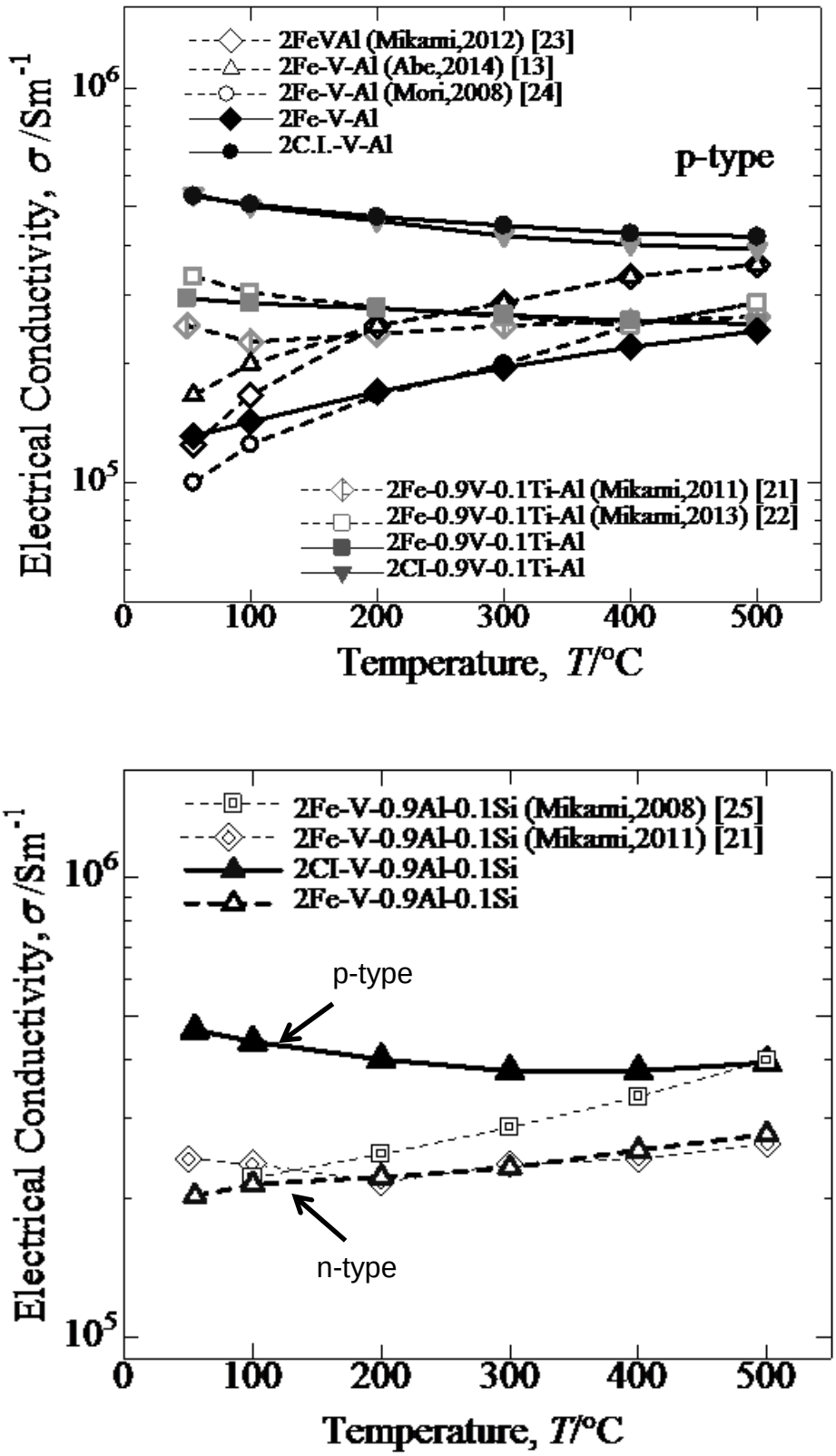

Figure 4.5 Temperature dependence of electrical conductivity, σ, for the annealed Fe_2VAl samples at 900°C for 2 d and 450°C for 6 h.

The thermal conductivity, *k* of annealed Fe_2VAl specimens evaluated from room temperature until 500°C is shown in Figure 4.6 The value of *k* for Fe_2VAl is rather large, typically 28 W/mK [13], which is almost an order of magnitude higher than that conventional thermoelectric like Bi_2Te_3. However, the thermal conductivity for Fe_2VAl specimens prepared using cast iron scrap chips could attributed decreased respectively might be due to the off-stoichiometry effect. The reduction of the thermal conductivity of Fe_2VAl specimens prepared using cast iron scrap chips is believed to be related to increase of phonon scattering by the increase of grain boundary regions due to the dispersed of impurity phases and the small difference of the composition from stoichiometry [24]. Thus, it was found that the thermal conductivity values of undoped Fe_2VAl and p-type Fe_2VAl prepared using cast iron scrap chips were about 10% smaller than those previously reported [21-24] even cast iron scrap chips were used as a starting material.

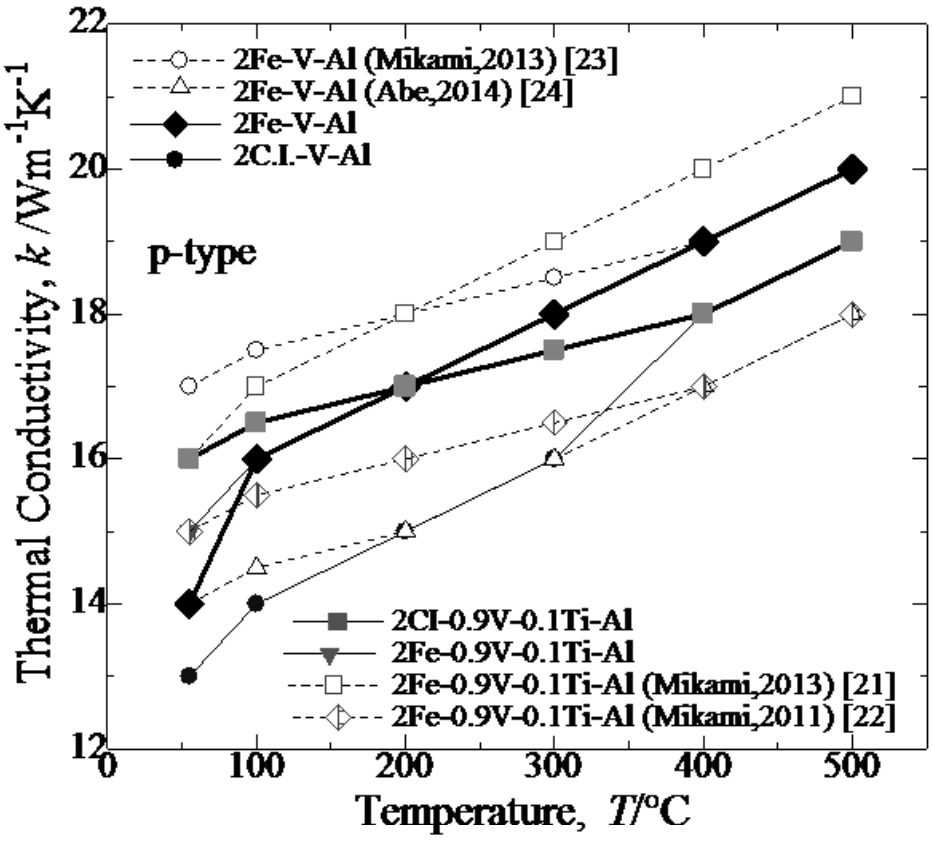

Figure 4.6 Temperature dependence of thermal conductivity, *k*, for the annealed Fe_2VAl samples at 900°C for 2 d and 450°C for 6 h.

The efficiency of thermoelectric materials can be measured by its power factor, *PF* which is proportional to $\alpha^2.\sigma$. Figure 4.7 draws a comparison of *PF* between Fe_2VAl specimens prepared using cast iron scrap chips and pure Fe as a function of temperature. The *PF* value of p-type Fe_2VAl made from cast iron scrap chips was comparable than those previously reported [21,22] and possess 1604 $\mu Wm^{-1}K^{-2}$ at 200°C, which is the highest *PF* value at a certain temperature even cast iron scrap chips were used as a starting material. In addition, it was prevailed that the *PF* values of undoped Fe_2VAl prepared using cast iron scrap chips was approximately twice improved (967 $\mu Wm^{-1}K^{-2}$ at 200°C, which is the highest *PF* value at a certain temperature) as compared than those previously reported [23,24]. It is interesting to note that the performance of undoped and p-type Fe_2VAl prepared using cast iron scrap chips are comparable to that Fe_2VAl prepared using pure Fe and reported literature especially at higher temperatures than 200°C.

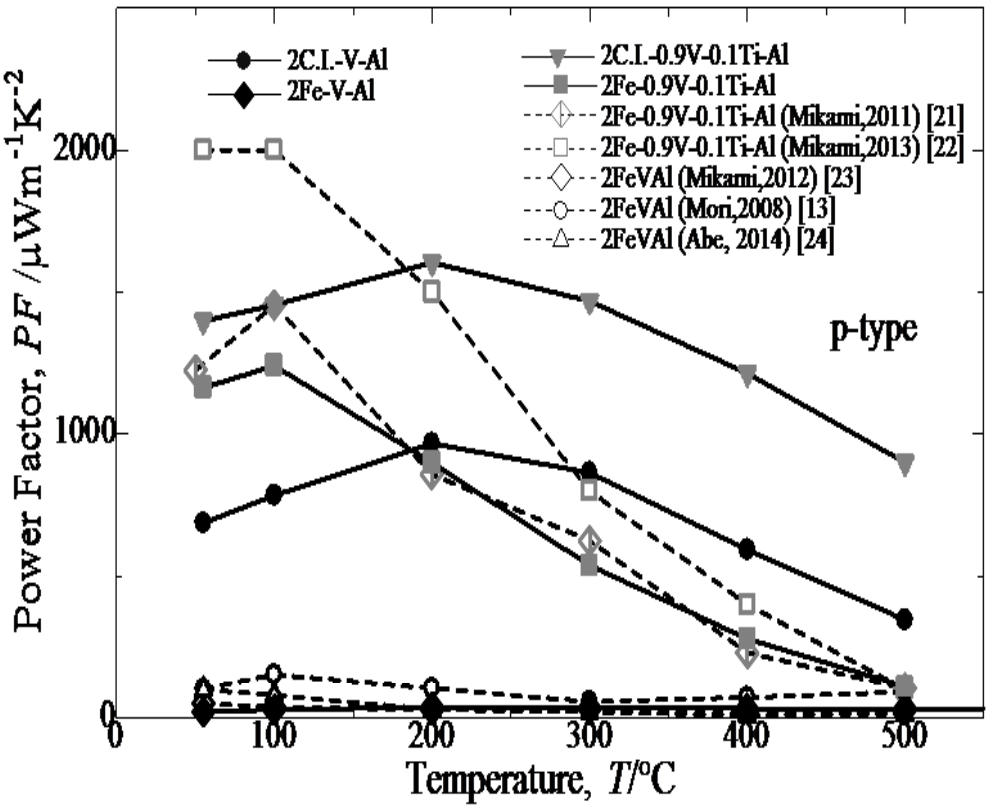

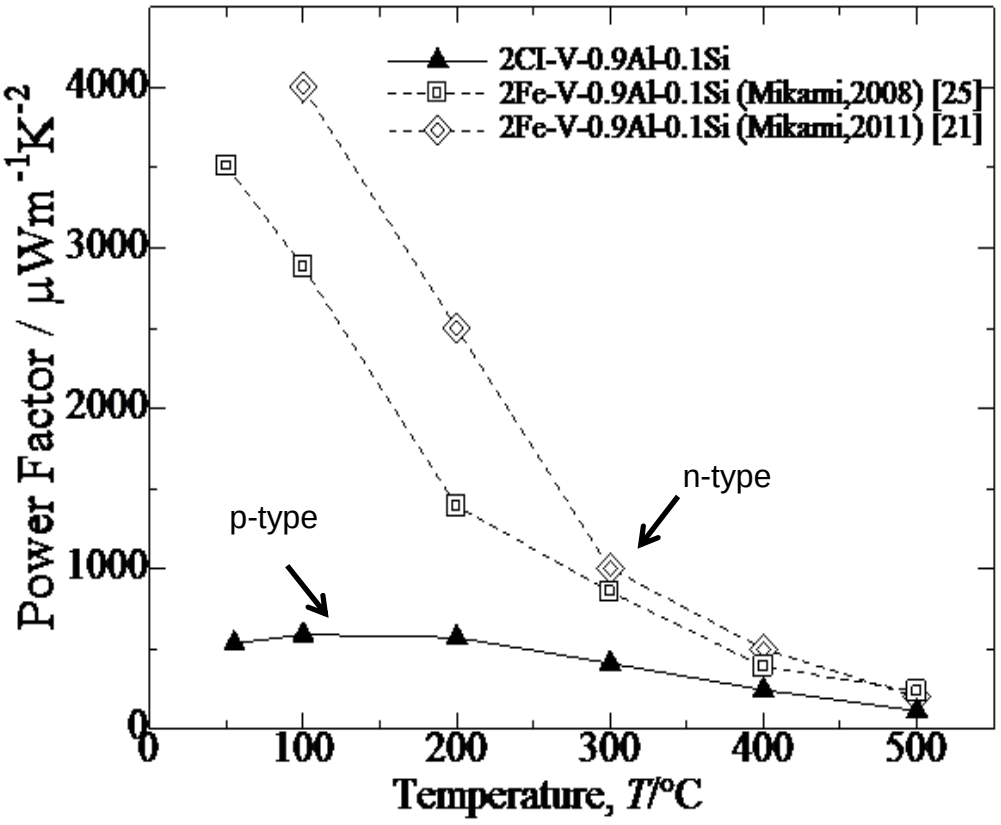

Figure 4.7 Temperature dependence of power factor, *PF*, of the annealed Fe_2VAl samples at 900°C for 2 d and 450°C for 6 h.

The thermoelectric performance is often discussed with the figure of merit, $Z= \alpha^2.\sigma/ k$, so that not only increase in the power factor *PF* but also a decrease in the thermal conductivity *k* is required. Figure 4.8 shows the variations in the dimensionless figure of merit, *ZT* with the measuring temperature of annealed Fe_2VAl specimens prepared using cast iron scrap chips and pure Fe. As a result, it was prevailed that the dimensionless figure of merit, *ZT* values of undoped Fe_2VAl prepared using cast iron scrap chips was approximately twice improved and for p-type Fe_2VAl prepared using cast iron scrap chips was about 10% smaller and than those previously reported [21-24]. Thus, undoped and p-type Fe_2VAl prepared using cast iron scrap chips obtained positive impact in thermoelectric performance even utilized the cast iron scrap chips as a starting material.

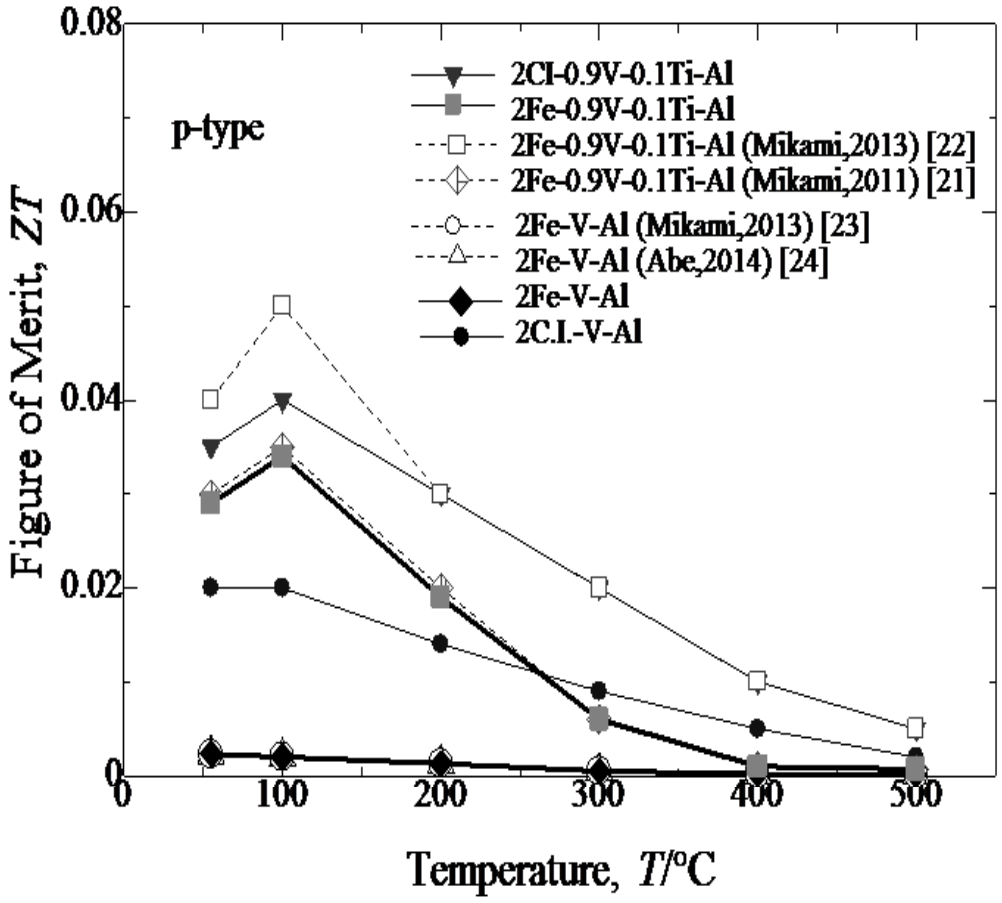

Figure 4.8 Variation in dimensional figure of merit, *ZT*, with the measuring temperature of the annealed Fe_2VAl samples at 900°C for 2 d and 450°C for 6 h.

4.4 Discussion

4.4.1 Carbon contains in cast iron scrap chips

The Seebeck coefficient values of undoped Fe_2VAl prepared using cast iron scrap chips is positive and centered around 20 μV/K since the majority carriers are holes, but the number of carriers and hole pockets are nearly compensated [26]. **T**he Seebeck coefficient values of p-type Fe_2VAl prepared using cast iron scrap chips was approximately 10% smaller than those of previously reported [21,22]. This decrease was attributed to the small difference in the off-stoichiometries of the specimen since the compositions of cast iron scrap chips contain some impurities.

Nevertheless, in the present study, the n-type Fe_2VAl specimen made from cast iron scrap chips could not possible to manufacture due to the influence of some impurities in cast iron scrap chips since the compositions of cast iron scrap chips contain some impurities such as Si, Mn and C. Meanwhile the density of states (DOS) of Fe_2VAl sharply changes on both valence band and conduction band sides of the pseudogap, the Seebeck coefficient enhances significantly when the Fermi level shifts slightly due to the doping. Thus, since the cast iron scrap chips contain some impurities such as Si, Mn, C and O, it may contribute as a dopant in Fe_2VAl alloys and slightly change the shape of the DOS structure. The rigid-band-like behavior with doping is one issue with the Fe_2VAl based thermo-electric materials for further improvement in the Seebeck coefficient, especially for n-type Fe_2VAl specimen made from cast iron scrap chips.

Figure 4.9 shows the XRD patterns of experimentally prepared of the annealed Fe_2VAl samples with or without C-doping at 900°C for 2 d and 450°C for 6 h. The mass% C are varied with 2, 4 and 6 mass% C in order to investigate the influence of C added in the n-type Fe_2VAl specimen even made from pure Fe. The VC peak was observed in the n-type Fe_2VAl specimen with 2, 4 and 6 mass% C as similar to the 2C.I.-V-0.9Al-0.1Si specimen.

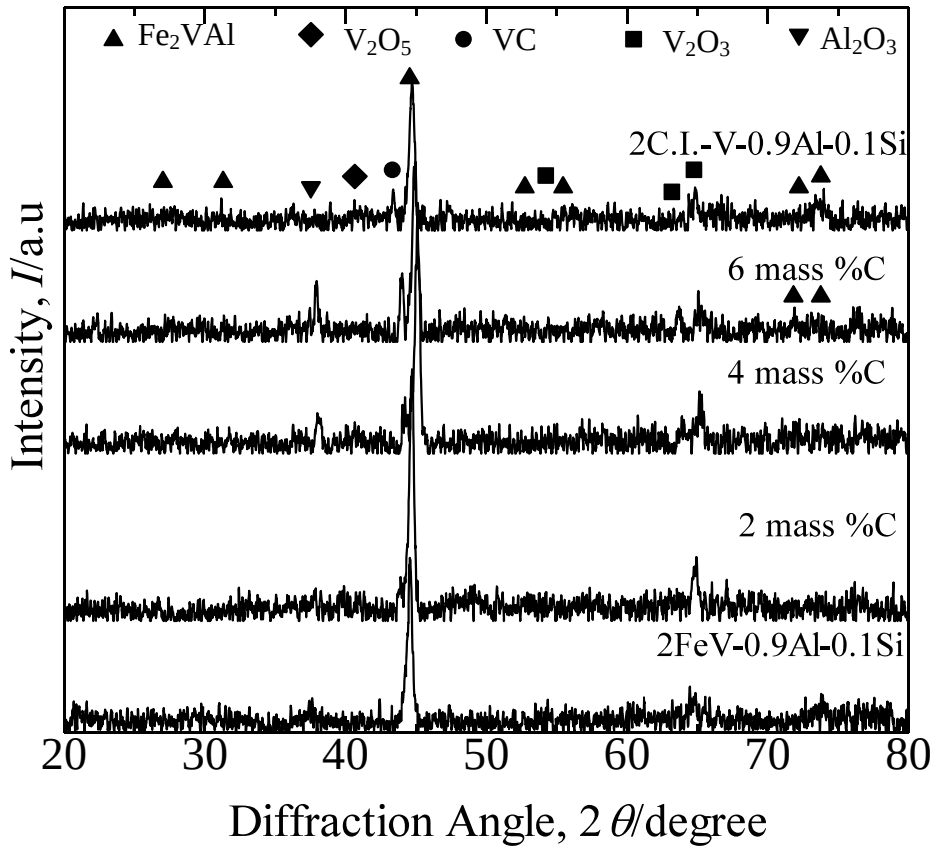

Figure 4.9 XRD patterns of the annealed Fe_2VAl samples with or without mass %C at 900°C for 2 d and 450°C for 6 h.

Figure 4.10 provides the SEM microstructures of experimentally prepared for annealed Fe_2VAl alloys prepared using pure Fe with 2, 4 and 6 mass% C and cast iron scrap chips, respectively. The SEM images of annealed Fe_2VAl with or without mass% C prepared from Fe and cast iron scrap chips show larger segregation of oxide, which are might be V_2O_3 or V_2O_5 phase. The pores size that could be observed from the SEM images were smaller than 10 µm in diameter.

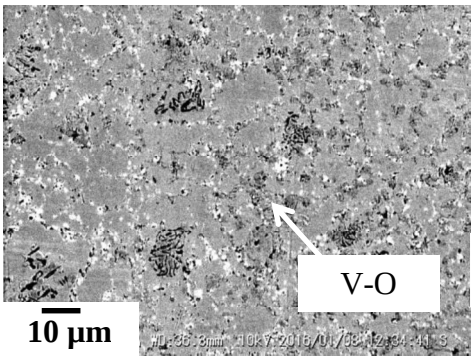

2Fe-V-0.9Al-0.1Si

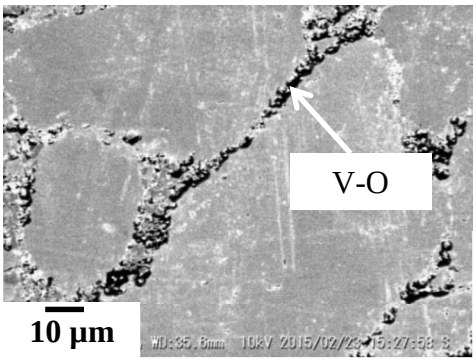

2C.I.-V-0.9Al-0.1Si

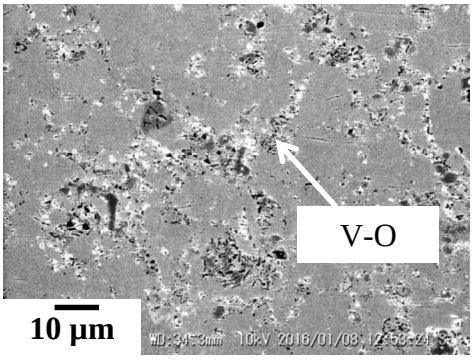

2Fe-V-0.9Al-0.1Si
with 2 mass% C

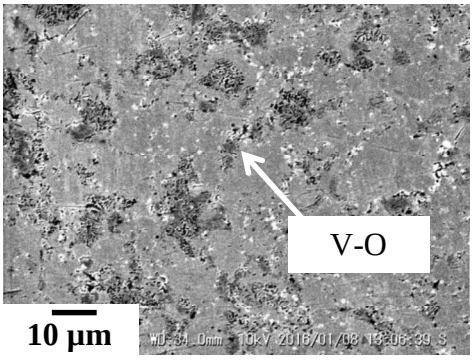

2Fe-V-0.9Al-0.1Si
with 4 mass% C

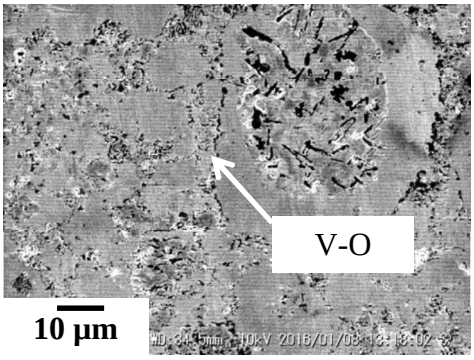

2Fe-V-0.9Al-0.1Si
with 6 mass% C

Figure 4.10 SEM microstructures of the annealed Fe_2VAl samples at 900°C for 2 d and 450°C for 6 h.

Figure 4.11 (a) shows the temperature dependence of Seebeck coefficient, *α*, for the annealed Fe_2VAl samples with or without mass% C at 900°C for 2 d and 450°C for 6 h. The 2Fe-V-0.9Al-0.1Si prepared using pure Fe added 2, 4 and 6 mass% C revealed same conduction type (p-type) compared to that 2C.I.-V-0.9Al-0.1Si specimen made from cast iron scrap chips. It means the estimating carbon contains in cast iron scrap chips is approximately 4 and 6 mass% C since the Seebeck coefficient and electrical conductivity results similar to that 2C.I.-V-0.9Al-0.1Si specimen made from cast iron scrap chips. In addition, from the thermoelectric properties results, it was confirmed that C affects the conduction type of 2C.I.-V-0.9Al-0.1Si specimen made from cast iron scrap chips.

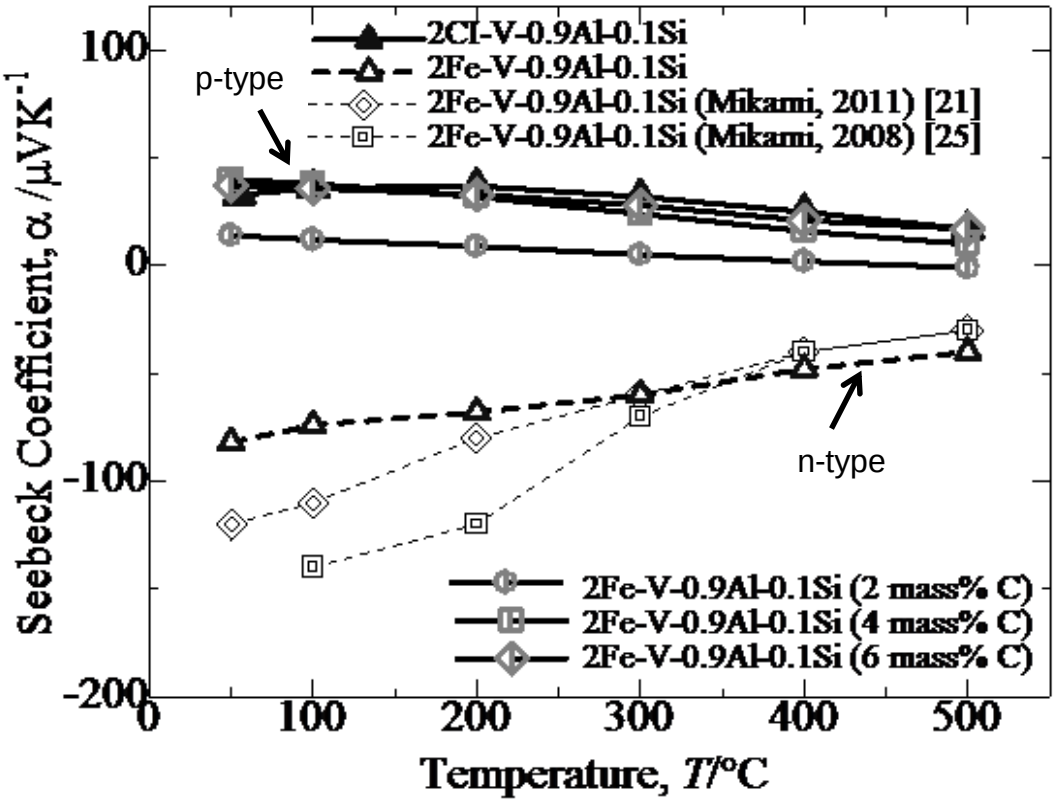

Figure 4.11 (a) Temperature dependence of Seebeck coefficient, *α*, for the annealed Fe_2VAl samples with or without mass% C at 900°C for 2 d and 450°C for 6 h.

Figure 4.11 (b) shows the temperature dependence of electrical conductivity, *σ* for the annealed Fe_2VAl samples with or without mass% C at 900°C for 2 d and 450°C for 6 h. The 2Fe-V-0.9Al-0.1Si added 6 mass% C specimen revealed the same

behavior with the 2C.I.-V-0.9Al-0.1Si specimen made from cast iron scrap chips. However, further investigation regarding the chemical analysis of 2Fe-V-0.9Al-0.1Si added 6 mass% C specimen is necessary in order to understand the position of graphite (C) in the specimen (substitution or interstitial to which element).

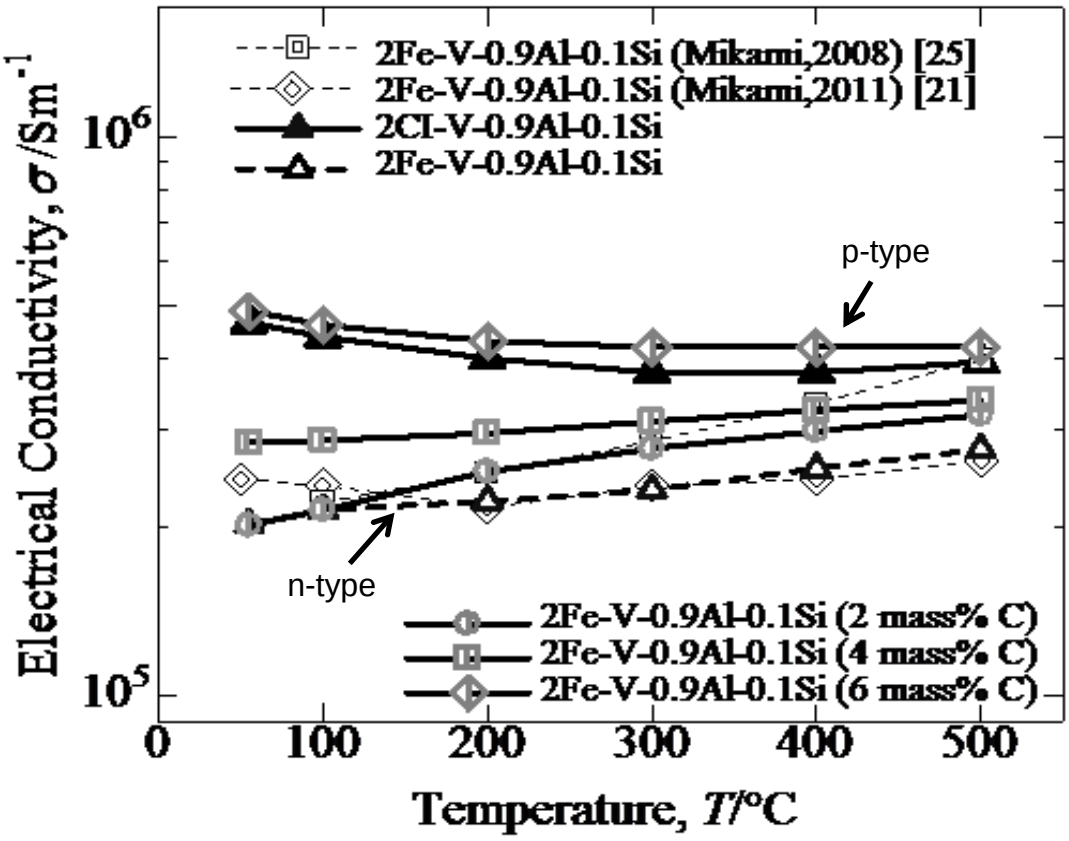

Figure 4.11 (b) Temperature dependence of electrical conductivity,σ, for the annealed Fe_2VAl samples with or without mass% C at 900°C for 2 d and 450°C for 6 h.

Figure 12 (a) shows the valence electron concentration (VEC) dependence Seebeck coefficient in previously [27] and currently reported Fe-based Heusley alloys [28]. The variation of valence electron concentration (VEC) due to the doping is the most important factor for a large enhancement in the Seebeck coefficient. Fe_2VAl has in total 24 valence electrons per formula unit, so that VEC = 6. The sign of the Seebeck coefficient has been always positive for the alloys with VEC ≤ 6 but becomes negative for VEC > 6. Thus the value of Seebeck coefficient including its sign varies most significantly in the vicinity of VEC = 6. From the experimental result of 2Fe-V-

0.9Al-0.1Si prepared using pure Fe added 4 mass% C, since the VC obtained from the sample as the V associated with C to produce VC, the V concentration in the system was reduced and influenced the Seebeck coefficient. Based on the VEC calculation of 2Fe-V-0.9Al-0.1Si prepared using pure Fe added 4 mass% C; (8x2) + ((5x0.7) since V lack in the system) + (3x0.9) + (4x0.1) + ((4x0.3) since the addition of 4 mass% C in the system) = 23.8/4 = 5.95 e/a shows the VEC ≤ 6 where the sign of the Seebeck coefficient has been always positive (p-type) for the alloys. When the V replacement is not sufficient in Fe_2VAl, Fe atoms supply the holes for conduction, because Fe has a lower valence than Al [7]. This qualitative explanation agrees with the compositional behavior of Seebeck coefficient. Therefore, a small deviation of VEC from the stoichiometric value of 6 always leads to a large enhancement in Seebeck coefficient. It is considered that, since the DOS within the pseudogap very small, even a small compositional change would result in an appreciable shift of the Fermi level from the central region in the pseudogap without modifying the band structure in any essential manner. Thus, it was confirmed that C affects the conduction type of 2C.I.-V-0.9Al-0.1Si specimen made from cast iron scrap chips since the pattern similar with 2Fe-V-0.9Al-0.1Si prepared using pure Fe added 4 mass% C.

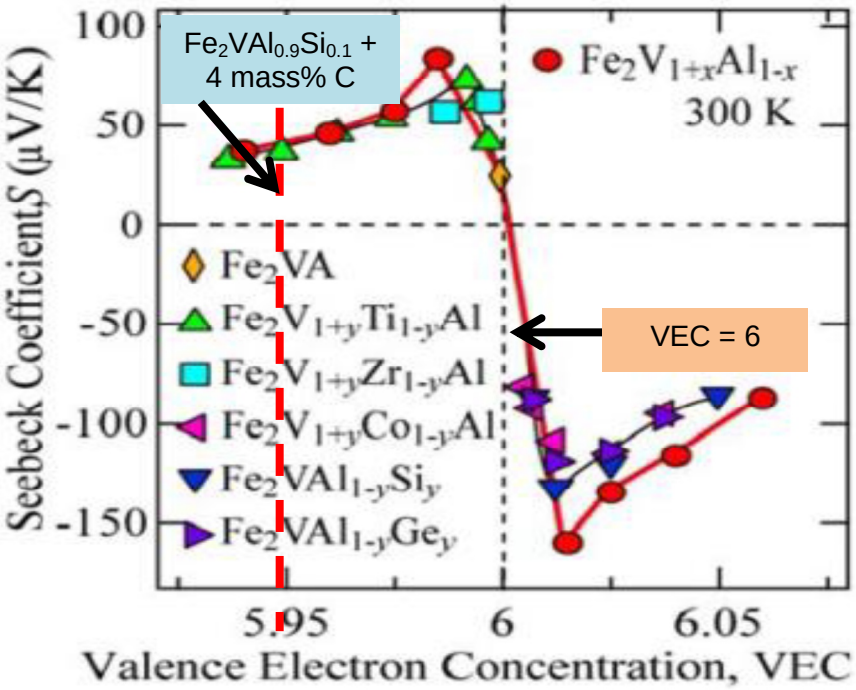

Figure 4.12 (a) Valence electron concentration (VEC) dependence of the experimental Seebeck coefficient at 300 K [28].

Figure 12 (b) shows the relationship between a (Al+Si) concentration and the Seebeck coeffiecient if the horizontal scale is the (Al+Si) concentration and the vertical scale is the Seebeck coefficient [29]. Referring to this figure, in the alloyed metal according to the invention, a p-type iron alloy thermoelectric material having the high Seebeck coefficient of more than 60 μV/K (up to 84 μV/K) can produced by adding the carbon and by adjusting the [V concentration – C concentration] to 20~24 at % as well as the [Al concentration + Si concentration] to 25~30 at %. Incidentally, in the invention, the vanadium carbides are separated out into the matrix by the addition of the carbon. So, according to the experimental result of 2Fe-V-0.9Al-0.1Si prepared using pure Fe added 4 mass% C, was similar to the reported patent [29]. Since the VC obtained from the sample as the V associated with C to produce VC, the V concentration in the system was reduced and influenced the Seebeck coefficient. Consequently, it was confirmed that C affects the conduction type of 2C.I.-V-0.9Al-0.1Si specimen made from cast iron scrap chips since the pattern similar with 2Fe-V-0.9Al-0.1Si prepared using pure Fe added 4 mass% C.

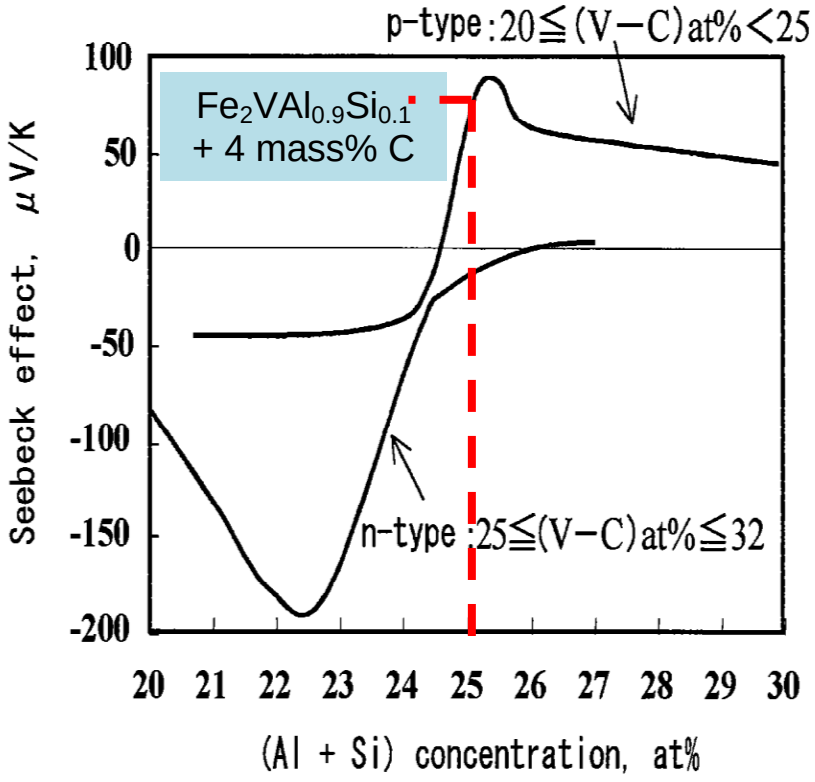

Figure 4.12 (b) A relationship between a (Al+Si) concentration and the Seebeck coefficient [29].

4.4.2 Oxide Phases

From the point of view of XRD, the traces of an impurity phase or secondary phase was observed such as the oxides of Al_2O_3, V_2O_5 and V_2O_3 as shown in Figure 4.13 It may influence the thermoelectric properties of Fe_2VAl samples made from cast iron scrap chips. As well, from the SEM microstructure and elemental mapping images, it can be seen clearly the presence of oxides in the matrix is considered to be caused by the easiest ability of Al or V element to be oxidized during sintering since the cast iron scrap chips are strongly oxidized by machining. This is most likely the oxidation of Fe_2VAl samples made from cast iron scrap chips were caused by impurity oxygen in the cast iron scrap chips used in the present study. Another possibility about the presence of oxide in the specimens is the size of V was 75 μm which was larger than that cast iron scrap chips (<100 μm but easy to break during the ball milling process), Fe (3-5 μm), Al (3 μm) and Ti (3 μm). This evidences that the inside of the product cannot be diffused completed. To obtain perfectly homogenized Fe_2VAl smaller size V and longer heat treatment will be needed [2].

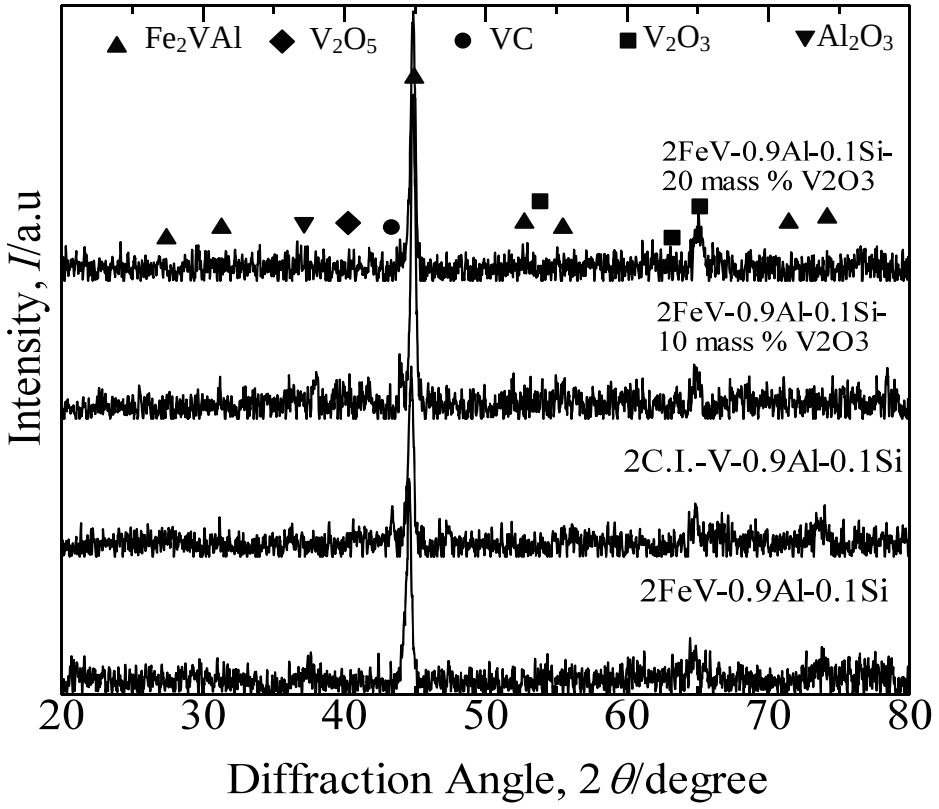

Figure 4.13 XRD patterns of the annealed Fe_2VAl samples with or without mass %V_2O_3 at 900°C for 2 d and 450°C for 6 h.

Figure 4.14 shows the Seebeck coefficient of the annealed Fe_2VAl samples with or without mass% V_2O_3 at 900°C for 2 d and 450°C for 6 h. The n-type Fe_2VAl samples with 10 and 20 mass% V_2O_3 obtained same conduction type (n-type) compared to that Fe_2VAl samples prepared from pure Fe. Figure 4.15 shows the temperature dependence of electrical conductivity, σ, for the annealed Fe_2VAl samples with or without mass% V_2O_3 at 900°C for 2 d and 450°C for 6 h. The annealed n-type Fe_2VAl samples with 10 and 20 mass% V_2O_3 prevailed similar behavior with n-type Fe_2VAl samples prepared from pure Fe. The V_2O_3 did not affect the conduction band type and shows less influence, especially to the microscopic electrical conductivity since it obtained at the grain boundary with very thin layer oxide phase. However, it might be attributed to the small difference in the off-stoichiometries of the specimen by impurity oxygen in cast iron scrap chips.

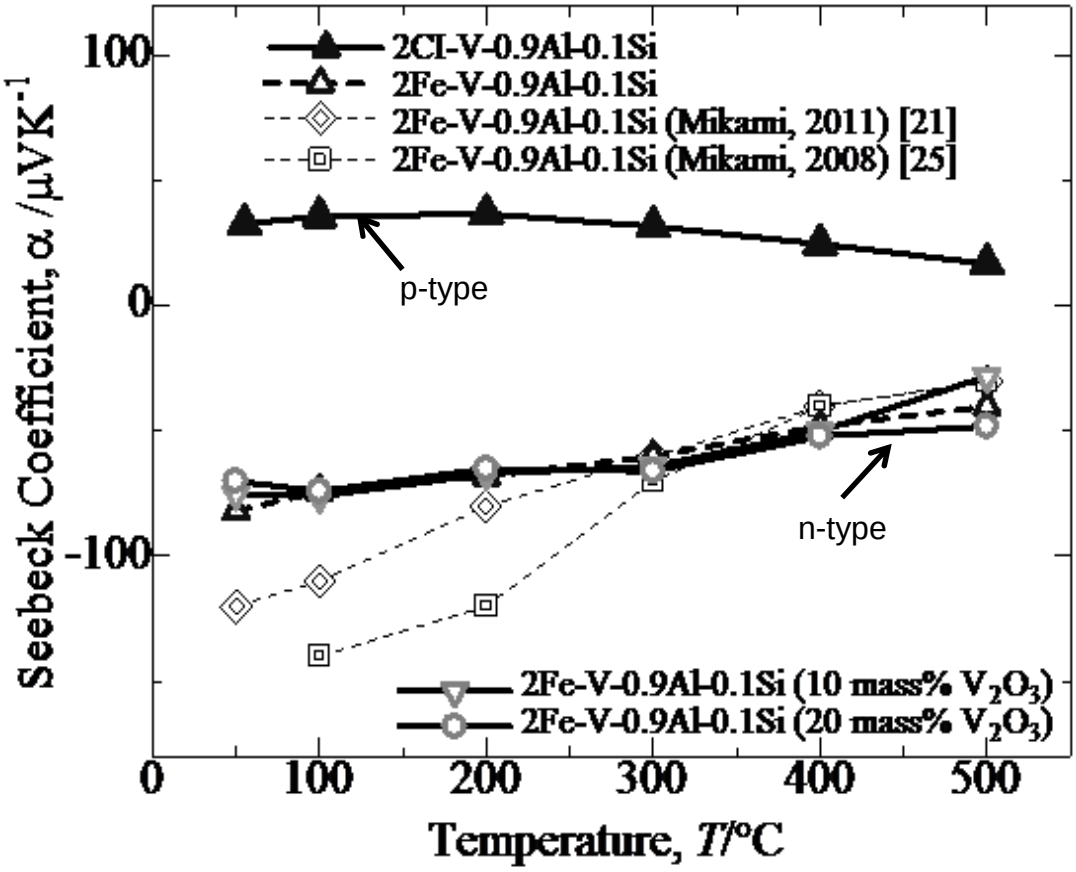

Figure 4.14 Temperature dependence of Seebeck coefficient, α, for the annealed Fe_2VAl samples with or without mass% V_2O_3 at 900°C for 2 d and 450°C for 6 h.

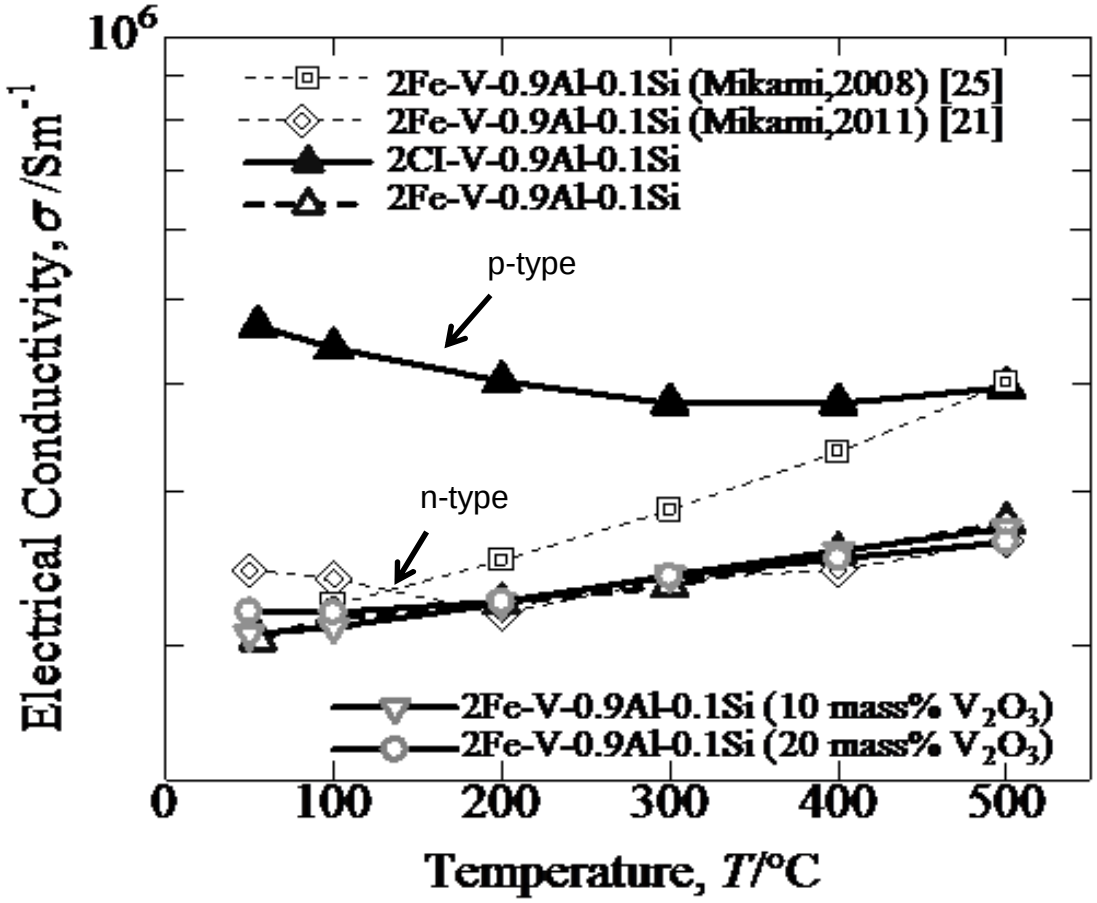

Figure 4.15 Temperature dependence of electrical conductivity, σ, for the annealed Fe_2VAl samples with or without mass% V_2O_3 at 900°C for 2 d and 450°C for 6 h.

4.5 Conclusion

The upgrade recycling of cast iron scrap chips shows promise as an eco-friendly and cost efficient production process for iron-based alloys. In the present study, the undoped and p-type Fe_2VAl specimens prepared using cast iron scrap chips have been successfully fabricated even though utilizing cast iron scrap chips as a starting material. The maximum power factor, *PF* value of p-type Fe_2VAl prepared using cast iron scrap chips was comparable than those previously reported [21,22] and possess *PF*= 1604 $\mu Wm^{-1}K^{-2}$ at 200°C, which is highest *PF* value at a certain temperature. Meanwhile, for the undoped Fe_2VAl prepared using cast iron scrap chips was prevailed approximately twice improved in power factor value, *PF*= 967 $\mu Wm^{-1}K^{-2}$ at 200°C, which is highest *PF*

value at a certain temperature as compared than those previously reported [23,24]. Thus, undoped and p-type Fe_2VAl prepared using cast iron scrap chips obtained positive impact in thermoelectric performance even utilized the cast iron scrap chips as a starting material. Nevertheless, in the present study, the n-type Fe_2VAl specimen made from cast iron scrap chips could not possible to fabricate due to the small difference in the off-stoichiometric of the specimen since the compositions of cast iron scrap chips contain some impurities such as Mn, C and Si. In addition, from the thermoelectric properties results, it was confirmed that C is considered to be an acceptor dopant and affect the conduction type of 2C.I.-V-0.9Al-0.1Si specimen made from cast iron scrap chips. Hence, it is further necessary to investigate the chemical analysis of C contains in cast iron scrap chips on the development of n-type Fe_2VAl alloy and further improvements in the thermoelectric performance are desired.

4.6 References

1. Mikami, M., & Ozaki, K. (2012). *Design for Innovative Value Towards a Sustainable Society (*pp. 513-516). Netherlands: Springer.
2. Kato, H., Kato, M., Nishino, Y., Mizutani, U., & Asano, S. (2001). Effect of silicon substitution on thermoelectric properties on Heusler-type Fe_2VAl alloy. *J. Jpn. Inst. Metals, 65*, 652-656.
3. Nishino, Y. (2001). Electronic Structure and Transport Properties of Pseudogap System Fe_2VAl. *Mater. Trans., 42* , 902-910.
4. Singh, D. J., & Mazin, I. I. (1998). *Phys. Rev., B57*, 14352/1-5.
5. Weht, R., & Pickett, W. E. (1998). *Phys. Rev., B 58*, 6855–6861.
6. Nishino, Y., Kato, H., Kato, M., & Mizutani, U. (2001). *Phys. Rev. B63*. 233303/1-4.
7. Hanada, Y., Suzuki, R. O., & Ono, K. (2001). Seebeck coefficient of $(Fe,V)_3Al$ alloys. *J. Alloy Comp., 329*, 63–68.
8. Lue, C. S., & Kuo, Y. K. (2002). *Phys. Rev. B66*. 085121/1-5.
9. Matsuura, H, Nishino, Y., Mizutani, U., & Asano, S. (2002). Doping effects on thermoelectric properties of the pseudogap Fe_2VAl system. *J. Jpn. Inst. Metals., 66*, 767–771.
10. Lu, W., Zhang, W., & Chen, L. (2009). *J. Alloy Comp., 484*, 812–815.

11. Nakayama, Ide. N., & Nishino, Y. (2008). Thermoelectric properties of p-type Heusler compounds $(Fe_{2-x}Co_x)(V_{1-y}Ti_y)$ Al. *Mater. Trans., 49*, 1858–1862.
12. Nishino, Y., Deguchi, S., & Mizutani, U. (2006). *Phys. Rev. B*, 115115/1-6.
13. Mori, T., Ide, N.,& Nishino, Y. (2008). *J. Jpn. Inst. Metal., 72* , 593–598.
14. Mikami, M., Matsumoto, A., & Kobayashi, K. (2008). Synthesis and thermoelectric properties of microstructural Heusler Fe_2VAl alloy. *J. Alloy Comp., 46*, 423–426.
15. Mikami, M., & Kobayashi, K. (2008). *J. Alloy Comp., 466*, 530–534.
16. Mikami, M., Tanaka, S., & Kobayashi, K. (2009). *J. Alloy Comp., 484,* 444–448.
17. Elbel, T., Senberger, J., Zadera, A., & Hampl, J. (2008). *International Scientific Journal, 33*, 111-116.
18. Laila, A., & Nanko, M. (2014), Characterization of Cast Iron Scrap Chips toward β-$FeSi_2$ Thermoelectric Materials. *Materials Science Forum, 804*, 3–6.
19. Laila, A., Nanko, M., & Takeda. M. (2014). Upgrade recycling of cast iron scrap chips towards β-$FeSi_2$ thermoelectric materials. *Materials, 7*, 6304–6316.
20. Laila, A., Nanko, M., & Takeda, M. (2016). Effect of Doping Elements in β-$FeSi_2$ Prepared Utilizing Cast Iron Scrap Chips. *Mater. Trans., 57 (3)*, 455-451.
21. Mikami, M., Kobayashi, K., & Tanka, S. (2011). *Mater. Trans, 52* (8), 1546-1548.
22. Mikami, M., Ozaki, K., Takazawa, H., Yamamoto, A., & Terazawa, Y. (2013). *J. Electronic. Mat., 42*, 1801-1806.
23. Mikami, M., Kinemuchi, Y., Ozaki, K., Terawa, Y., & Takeuchi, T. (2012). *J. App. Physics., 111,* 1-6.
24. Abe, K., Kikuchi, A., Okinaka, N., & Akiyama, T. (2014), Single thermite-type combustion synthesis of Fe_2VAl for thermoelectric applications from Fe, V 2 O 5 and Al powders. *J. Alloy. Comp., 611*, 319-323.
25. Mikami, M., & Kobayashi, K. (2008). *J. Alloy Comp., 466*, 530-534.
26. Nishino, Y., & Tamaka, Y. (2014). *J. App. Physics., 115*, 1-8.
27. Nishino, Y. (2005). *The Science of Complex Alloy Phases* (pp. 325). Warrendale, PA: TMS.
28. Miyazaki, H., Tanaka, Sugura., Ide, Naoki., Kazuo, Soda., & Nishino, Yoichi. (2014). *Materials Research Express, 1,* 1-9.
29. Suzuki, S., & Fujiki T. (2011). *United States Patent, US 7,906,044,B2*.

Chapter 5: General guidelines to highly valued intermetallic compounds towards upgrade recycling of cast iron scrap chips

5.1 Introduction

The scrap metal recycling industry encompasses a wide range of metals and alloys. Some of the most commonly recycled metals or alloys (by volume) are cast iron, steel, copper, aluminum, lead, zinc, and stainless steel. Scrap metals, in general, are divided into two basic categories: ferrous and nonferrous. Ferrous scrap is a metal or alloys that contain iron. Scrap chips of cast-iron consist primarily of iron with 2.1–4 mass% of carbon and 1–3 mass% of silicon. Cast iron scrap comes from sources such as: mill scrap (from primary processing), used construction beams, plates, pipes, tubes, wiring, and shot and automotive scraps. Therefore, the recycling of cast iron scrap chips is an interesting subject to explore because these chips are expected to be a good starting material for preparing iron-based intermetallic compound.

One example of the highly valid intermetallic compound is neodymium iron boron [1-4]. Magnet based on NdFeB alloys have been available for about 15 years. NdFeB is termed a rare earth magnet. The neodymium iron boron, NdFeB, magnets is made of an alloy primarily consisting of Neodymium, Iron and Boron and the alloy are chemically written as $Nd_2Fe_{14}B$. Up to 150°C, the Neodymium Iron Boron magnets are the strongest performers. The "Neo" magnets are a first choice for many applications as they offer the greatest performance with the smallest volume. Neodymium Iron Boron, NdFeB, magnets exists in a variety of grades. These grades not only variation in magnetic output performance, but they also vary with temperature rating. The maximum recommended temperature of operation for the “Neo” magnets is 200-230°C although the exact limit is actually dependent on the magnet shape and the total magnetic circuit. Therefore, the recycling of cast iron scrap chips is an interesting subject to explore because these chips can be preferable to used as a starting material for fabricating NdFeB. Considerably, in the future, this guideline could be applied to produce this material with good electrical and magnetic properties such as magnetic softness iron-based supercondcutors [5-8].

5.2 Limitation of alloying elements for fabrication of iron-based alloys prepared utilizing cast iron scrap chips

The general guidelines to highly valid intermetallic compounds towards upgrade recycling of cast iron scrap chips is described to achieve better upgrade recycling process in the future. Thus, this guideline could be applied to fabricate another highly valid intermetallic compound such as magnetic softness iron-based superconductor materials prepared using cast iron scrap chips or neodymium iron boron magnets made from cast iron scrap chips.

However, in the present work, there are some restrictions for the alloying elements in the β-$FeSi_2$ fabricated from cast iron scrap chips. For example, in order to improve the thermoelectric performance of the p-type β-$FeSi_2$ prepared utilizing cast iron scarp chips, Mn was chosen to replace Al as the dopant element for the p-type β-$FeSi_2$ specimen. In the case of the p-type specimen with Al doping, it is important to avoid any oxidation during sintering. For Mn doping, the oxidation is not as severe [9]. However, it is difficult to control Al doping as a result of oxidation, especially when using cast iron scrap chips as a starting material. This effect is caused by the high affinity of Al to oxygen compared to the Mn and Co. As described in the previous report [10-12], the Al doping element is not compatible with cast iron scrap chips because the ability to be more easier to oxidize during the preparation processes.

Therefore, it was decided from the above statement that the Al dopant is not preferable to use as an alloying element in the fabrication of iron-based made from cast iron scrap chips. Meanwhile, the optimization of high affinity dopant elements to oxygen could be considered for fabrication of iron-based made from cast iron scrap chips. On the other hand, oxidation of impurities from oxidized cast iron scrap chips might be reflected for manufacturing iron-based alloys prepared using cast iron scrap chips. This guideline could benefit to applying for producing another highly valid intermetallic compound in the future.

5.3 Influence of impurities contains in cast iron scrap chips towards preparation of iron-based alloys

Scrap chips of cast-iron were produced from the cutting and milling processes of cast-iron products, which consist primarily of iron with 2.1–4 mass% of carbon and 1–3 mass% of silicon. Thus, cast-iron scrap chips may be a suitable starting material for preparing iron-based materials. By considering the XRF and GDSM analysis of the cast iron bulk, the specimen already contained 2.1-2.2 mass% of silicon. For β-$FeSi_2$ specimen prepared from cast iron scrap chips, the optimization of the numerical chemical composition of Si in the cast iron scrap chips samples are considered. The ratio of powder mixture was reduced from C.I.:Si = 1:2 to C.I.:Si = 1:1.86 for lesser free silicon after sintering. It is necessary to control the composition ratio of C.I.:Si at approximately 1:1.86 to avoid the formation of ε-FeSi in the future. It was reported that the presence of ε-FeSi could arise from a deficiency of Si due to the oxidation during the powder preparation and/or the evaporation during sintering [13]. By reducing the numerical chemical composition of excess Si in the powder mixture of the C.I.-1.86Si β-$FeSi_2$ sample made from cast iron scrap chips, the thermoelectric performance was significantly enhanced for the C.I.-2Si sample compared to that of the sample prepared from pure Fe. These findings provide the following insights for future research that excess Si contains in cast iron scrap chips could influence in the properties of iron-based alloys made from cast iron scrap chips.

In the case of Fe_2VAl prepared using cast iron scrap chips, the n-type Fe_2VAl specimen made from cast iron scrap chips could not possible to fabricate due to the small difference in the off-stoichiometric of the specimen since the compositions of cast iron scrap chips contain some impurities such as Mn, C and Si. Based along the results from Fe_2VAl specimen made from cast iron scrap chips, there is sign showed the influence from the C contains in cast iron scrap chips. The VC peak was observed in the n-type Fe_2VAl specimen with 2, 4 and 6 mass% C as similar to the 2C.I.-V-0.9Al-0.1Si specimen. The 2Fe-V-0.9Al-0.1Si prepared using pure Fe added 2, 4 and 6 mass% C revealed same conduction type (p-type) compared to that 2C.I.-V-0.9Al-0.1Si specimen made from cast iron scrap chips. It means the estimating carbon contains in cast iron scrap chips is approximately 4 and 6 mass% C since the Seebeck coefficient and electrical conductivity results similar to that 2C.I.-V-0.9Al-0.1Si specimen made from

cast iron scrap chips. In addition, from the thermoelectric properties results, it was confirmed that affects the conduction type of 2C.I.-V-0.9Al-0.1Si specimen made from cast iron scrap chips. However, further investigation regarding the chemical analysis of 2Fe-V-0.9Al-0.1Si added 6 mass% C specimen is necessary in order to understand the position of graphite (C) in the specimen (substitution or interstitial to which element). Therefore, we can not neglect the influence of C for fabricating iron-based alloys made from cast iron scrap chips. Considerably on the above statement, this guideline could benefit.

5.4 Conclusion

In this chapter, the limitation of alloying elements for fabrication of iron-based alloys prepared utilizing cast iron scrap chips is discussed. Figure 5.1 shows the schematic illustration of the guidelines to highly valid intermetallic compounds towards upgrade recycling of cast iron scrap chips. Furthermore, the influence of impurities contains in cast iron scrap chips towards preparation of iron-based alloys are considered. This guideline has been suggested several courses of action for the fabrication of highly valued intermetallic compounds toward upgrade recycling of cast iron scrap chips in the future. It could benefit to applying for producing iron-based alloys made from cast iron scrap chips with good thermoelectric, magnetic performance and properties. This is an important issue for the future research. In the present study, we can conclude that we successfully fabricated iron-based thermoelectric β-$FeSi_2$ and Fe_2VAl prepared using cast iron scrap chips. This upgrade recycling material is considerable an effort to reducing the abundant waste towards eco-friendly and cost effective production process. Thus, this work revealed that the cast iron scrap chips can be optimum utilize as a starting material for fabricating iron based materials and prevailed comparable thermoelectric performance to that previously reported.

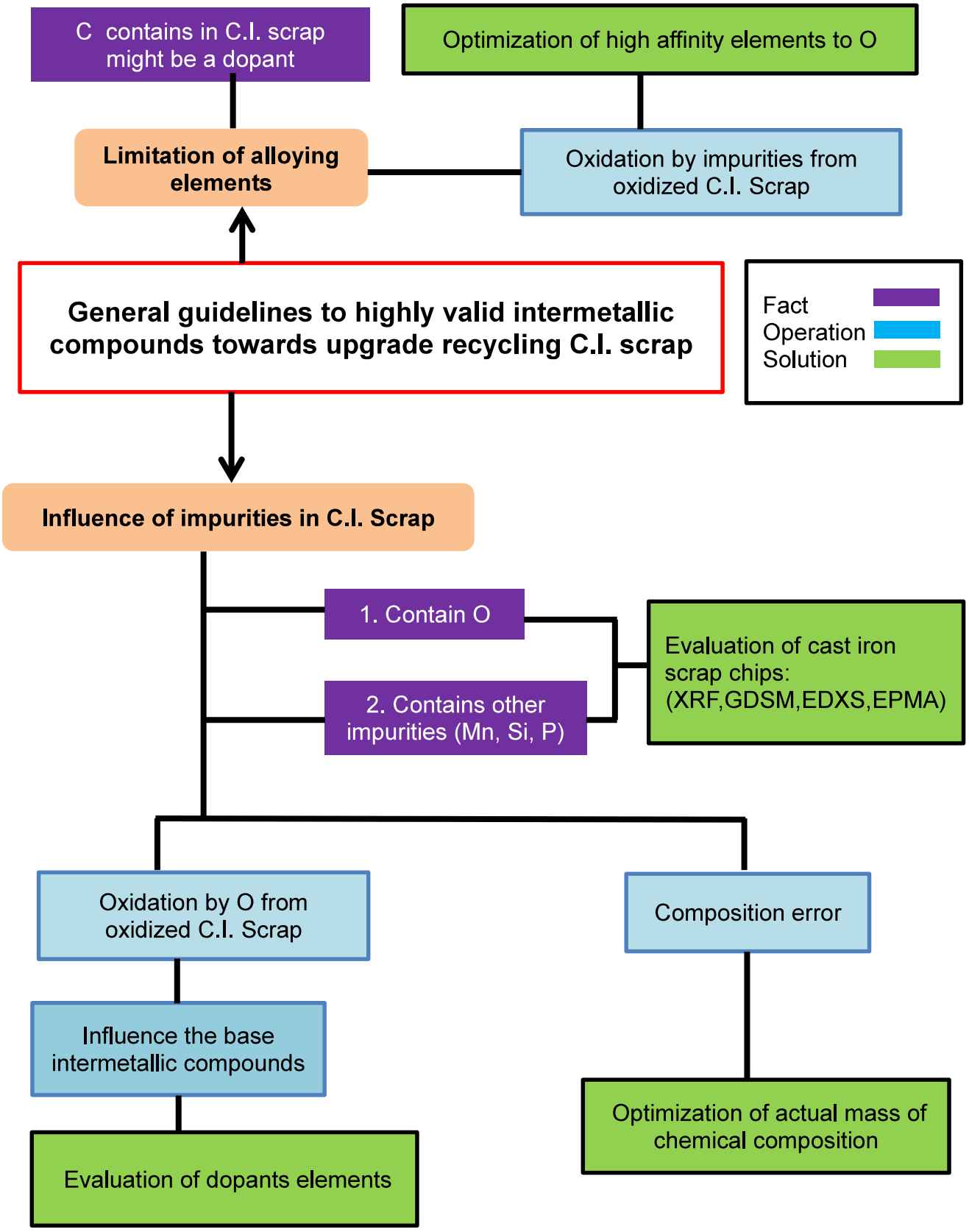

Figure 5.1 Schematic illustration of the guidelines to highly valid intermetallic compounds towards upgrade recycling of cast iron scrap chips.

5.5 References

1. Liu, W., Cao, L., Wu, J., & Li., T. (2003). Characterization of melt-spun NdFeB magnets prepared by explosive compaction. *J. Mat. Trans., 44*, 2094-2098.
2. Croat, J. J., Herbst, J. F., Lee, R. W., & Pinkerton, F. E. (1998). *J. Appl. Physics, 55* (6), 2078- 2082.
3. Sagawa, M., Fujimori, S., Togawa, M., Yamamoto, H., & Matsura, Y. (1998). *J. Appl. Physics, 55* (6), 2083-2087.
4. Koon, N. C., & Das, B. N. (1998). *J. Appl. Physics, 55* (6), 2063-2066.
5. Kamihara, Y., Watanabe, T., Hirano, M., & Hosono, H. (2008). Iron-based layered superconductor $La[O_{1-x}F_x]FeAs$ ($x = 0.05 - 0.12$) with $Tc = 26$ K. *J. Am. Chem. Soc., 130,* 3296.
6. Rotter, M., Tegel, M., & Johrendt, D. (2008). Superconductivity at 38 K in the iron arsenide $(Ba_{1-x}K_x)Fe_2As_2$. *Phys. Rev. Lett., 101,* 107006,.
7. Yeh, K. W., et al. (2008). Tellurium substitution effect on superconductivity of the α-phase iron selenide. *Europhys. Lett., 84*, 37002.
8. Guo, J., Jin, S., Wang, G., Wang, S., Zhu, K., Zhou, T., He, M., & Chen, X. (2010). Superconductivity in the iron selenide $K_xFe_2Se_2$ ($0 \leq x \leq 1.0$), *Phys. Rev., B82,* 180520(R).
9. Nishida, I. (1972). Study of semiconductors to metal transition in Mn-doped $FeSi_2$. *Phys Rev, B7,* 2710.
10. Laila, A., Nanko, M., & Takeda, M. (2014). Upgrade recycling of cast iron scrap chips towards β-$FeSi_2$ thermoelectric materials, *Materials, 7*, 6304–6316.
11. Laila, A., & Nanko, M. (2014), Characterization of Cast Iron Scrap Chips toward β-FeSi2 Thermoelectric Materials, *Materials Science Forum*, 804 (2015), 3–6.
12. Laila, A., Nanko, M., & Takeda, M. (2016). Effect of Doping Elements in β-FeSi2 Prepared Utilizing Cast Iron Scrap Chips. *Mater. Trans., 57 (3), 455-451.*
13. Cho, W. S., Choi, S. W., Park, K. W. S. (1999). Microstructure and thermoelectric properties of p-type $Fe_{0.9}Mn_{0.1}Si_2$ compounds prepared by pressure less sintering. *Mater. Sci. Eng., B68*, 116.

Chapter 6: Summary and general conclusions

In this work, the upgrade recycling of cast iron scrap chips towards iron-based thermo-electric materials are proposed and reported as an eco-friendly and cost-effective production process. Because cast iron consists mainly of iron with carbon and silicon, scrap chips of cast iron are expected to be a good starting material for preparing iron-based intermetallic compound with good thermoelectric properties such as β-$FeSi_2$ and Fe_2VAl. Firstly, the cast iron scrap chips were cleaned using ethanol in an ultrasonic bath over 4 cycles of 20 min and then dried in a fume chamber. The specimens were then characterized using X-ray fluorescence and energy dispersion X-ray spectroscopy for elemental and chemical analysis. Furthermore, for reconfirmation of chemical analysis, the concentration of impurities in the cast iron scrap chips was analyzed using glow discharge mass spectrometry. For GDMS synthesis, the evaluation of the cast iron scrap chip powders was performed by consolidation using a pulsed electric current sintering (PECS) technique. By reducing the numerical chemical composition of excess Si in the powder mixture of the C-Si1.86 sample made from cast iron scrap chips, the thermoelectric performance was significantly enhanced for the C-Si2 sample compared to that of the sample prepared from pure Fe as discussed deeply in chapter 3. Thus, the cast iron scrap chips could be preferable for use as a starting material to fabricate iron-based alloys (β-$FeSi_2$ and Fe_2VAl).

In iron-based materials, semiconducting iron disilicide (β-$FeSi_2$) is one of the useful thermoelectric materials at high temperatures. The achieved *ZT* is assumed to be comparatively the same for β-$FeSi_2$ thermoelectric materials made from pure Fe. The optimum value of *ZT* obtained in the present study is preferable for use as a starting material to produce β-$FeSi_2$ thermoelectric materials and showed promise as an eco-friendly and cost-effective production process for thermoelectric materials. We conclude that the cast iron scrap chips were successful at fabricating p-type 0.92C.I.-0.08 Mn-1.86Si (C.I.-Mn0.08) and n-type 0.94C.I.-0.06Co-1.86Si (C.I-Co0.06) β-$FeSi_2$ thermoelectric materials and that optimum thermoelectric performances were determined that were comparable with the previously reported results.

Thus, the thermocouple n-type and p-type β-$FeSi_2$ specimens prepared using cast iron scrap chips with optimum Co (C.I-Co0.06) and Mn (C.I.-Mn0.08) substitution concentration was successfully fabricated, yet when using cast iron scrap chips as a starting material. As well, the thermoelectric β-$FeSi_2$ prepared using cast iron scrap chips has probably a long lifetime at high temperature around 800°C in air and has excellent potential in high temperature stability for high temperature thermoelectric devices even when using cast iron scrap chips as a starting material. In addition, based on the results of CTE for n-type and p-type β-$FeSi_2$ samples prepared utilizing cast iron scrap chips showed the approximately CTE value highlights the less need for care in selecting interconnecting materials in the TE module to reduce the large stresses that can be induced by the thermal expansion mismatch. However, Al doping (0.09<Al<0.12) is not suitable for use with cast iron scrap chips as a starting material for β-$FeSi_2$ thermoelectric materials due to the tendency of the Al dopant (0.09<Al<0.12) to be oxidized during machining

Furthermore, the development of eco-friendly Fe_2VAl thermoelectric materials prepared using cast iron scrap chips is proposed and successfully achieved. The thermoelectric performance shows positive impact as the maximum power factor. In addition, it was prevailed that the *PF* values of undoped Fe_2VAl prepared using cast iron scrap chips was approximately twice improved as compared than those previously reported. Furthermore, the *PF* values of p-type Fe_2VAl prepared using cast iron scrap chips was about 10% smaller than those previously reported. Nevertheless, in the present study, the n-type Fe_2VAl specimen made from cast iron scrap chips could not possible to fabricate due to the small difference in the off-stoichiometric of the specimen since the compositions of cast iron scrap chips contain some impurities such as Mn, C and Si. Taking account of the XRD results and thermoelectric performance of sample n-type Fe_2VAl added in 2, 4, 6 mass% C, the results showed that samples have similar behavior with 2C.I-V-0.9Al-0.1Si sample. It means the C contains in cast iron scrap chips affect the conduction type by decreasing the V concentration when VC obtained in the specimen. Hence, it is further necessary to investigate the effect of impurities contains in cast iron scrap chips on the development of n-type Fe_2VAl alloy and further improvements in the thermoelectric performance are desired.

Ultimately, the general guidelines to highly valid intermetallic compounds towards upgrade recycling of cast iron scrap chips is discussed to achieve better upgrade recycling process. In the future study, this guideline could be applied to fabricate another intermetallic compound such as magnetic softness iron-based superconductor materials prepared using cast iron scrap chips or neodymium iron boron magnets made from cast iron scrap chips. In this chapter, the limitation of alloying elements for fabrication of iron-based alloys prepared utilizing cast iron scrap chips is discussed. Furthermore, the influence of impurities contains in cast iron scrap chips towards preparation of iron-based alloys are considered. From the above statements we can conclude that we successfully fabricated iron-based thermoelectric β-$FeSi_2$ and Fe_2VAl prepared using cast iron scrap chips. This upgrade recycling materials is considerable an effort to reducing the abundant waste towards eco-friendly and cost effective production process. Thus, this present study revealed that the cast iron scrap chips can be optimum utilize as a starting material for fabricating iron based materials and prevailed comparable thermoelectric performance to that previously reported.

Published Journals and Proceeding Papers

1. Laila, A., & Nanko, M. (2014). Characterization of Cast Iron Scrap Chips toward β-$FeSi_2$ Thermoelectric Materials. *Materials Science Forum 804*, 3-6.
2. Laila, A., Nanko, M., & Takeda, M. (2014). Upgrade Recycling of Cast Iron Scrap Chips towards β-$FeSi_2$ Thermoelectric Materials. *Materials 7* (9), 6304-6316.
3. Laila, A., Nanko, M., & Takeda, M. (2016). Effect of Doping Elements in β-$FeSi_2$ Prepared Utilizing Cast Iron Scrap Chips. *Journal of Materials Transactions 57 (3)*, 445-451.
4. Laila, A., Nanko, M., & Takeda, M. Eco-friendly Upgrade Recycling of Cast Iron Scrap Chips toward Fe_2VAl Thermoelectric Materials. (Submits to Journal of Alloys and Compound).

International and Domestic Conferences

1. The 32nd International Japan-Korea Seminar on Ceramic, Nagaoka Japan, Nov 2015.
2. 3rd International Conference on Powder Metallurgy in Asia, Kyoto Japan, Nov 2015.
3. Materials Science and Technology 2015, Ohio USA, Oct 2015.
4. Japanese Institute of Metal Conference JIM Shin-Etsu Branch Meeting, Niigata Japan, Dec 2014.
5. 1st Asian Workshop on High Temperature Oxidation and Corrosion, Tokyo Institute of Technology Japan, Tokyo Japan, Nov 2014.
6. Materials Science and Engineering Congress 2014 (MSE2014), Darmstard Germany, Sept 2014.
7. International Symposium On High-Temperature Oxidation And Corrosion 2014 (ISHOC 2014), Hakkodate Japan, June 2014.
8. 3rd International Gigaku Conference (GIGAKU2014), Nagaoka Japan, June 2014.
9. Japanese Institute of Metal Conference (JIM), Tokyo Institute of Technology Japan, Tokyo Japan, March 2014 .
10. International Symposium on Eco-materials Processing and Design (ISPED2014), Hanoi Vietnam, Jan 2014 .
11. Japanese Institute of Metal JIM Shin-Etsu Branch Meeting, Nagano Japan, Dec 2013.
12. Japanese Institute of Metal Conference (JIM), Kanazawa Japan, Sept 2013.

Acknowledgements

First and foremost, I would like to express my utmost gratitude to Allah S.W.T. for His guidance and His blessing that bestowed upon me. Without His love and guidance, surely I would not be able to complete this research and finally complete the dissertation which was physically and mentally challenging.

Warmest appreciation goes to my supervisor, Assoc. Prof. Makoto Nanko for accepting me in his laboratory as a Doctor student and also for his suggestions, discussions, advices and support that helped me to grow in my professional career and personal life. His encouragements always motivated me to give my best and I hope I have lived up to his expectations. A lot of knowledge and valuable experiences I have been obtained from him. This research would have never been accomplished according and successfully without his anticipation and assistance.

I would also want to acknowledge the Malaysia Ministry of Higher Education (MOHE) and International Islamic University of Malaysia (IIUM) for sponsoring my PhD study for 3 and half years. Furthermore, I also want to extend my gratitude to Assoc. Prof. Hanafi and Dr. Raihan for their support and assistance to come to Japan in order to pursue my doctoral studies and also for their kindly advices and suggestions during the earlier stage of my doctoral studies.

The author also wishes to express his gratitude to Prof. Masatoshi Takeda for his helpful discussion and suggestions in order to carry out the completion of this thesis and all the facilities provided for the use of thermoelectric apparatus in Takeda Lab. In addition, the feeling of gratitude is extended to all people from NUT who contribute in the development of this thesis especially for Prof. Uchitomi Naotaka, Prof. Kitagawa Hirouyuki and Assoc. Prof. Tomoyuki Homma for their helpful discussion and suggestions in order to carry out the completion of this thesis.

This author also would like to say thank you very much for all my friends from Malaysia and Japan for their support, time, funny and sad moments and unforgettable experiences that you share with me during my stay in Japan. Thank you very much especially to my best friend (Farhana Foudzi), Santiago, Mai Dung, Hayashi, Ishizaki, Abe, Kamoda, Hai, Hien, Isabel, Daniel, Onoda, Kurashige, Ito, Aizawa, Itaya, Kawamoto, Matsura, Dake, Takahashi, Ishikawa and other members of Nanko Lab and Takeda Lab. I also want to extend my gratitude to all foreign students from Sri Lanka, India, Thailand and Vietnam who gave me their friendship and share happy times with me.

Finally but not less important I want to express my full gratitude to those people who stay always next to me in the hard and happy moments of this work. Those people who give me the best inspiration, motivation and encourage me for being a better person day by day. Thank you very much for my parents because your lessons of life are the best thing that I could learn in my life. I also want to extend my full gratitude to my beloved husband (Mr. Zulhelmi) and my cute son (Alif Zaqwan) for their patience and effort during this time. Thank you for sharing with me happy and sad moments, for being that person who is the base of our family and thank you for suffer and rejoice with me.

Thank you to all of you for your patience, understanding and support. Without all of you I would never have been able to finish this work.

Terima kasih, ありがとうございます**, Cám ơn, Thank you**